1993

Accelerated aging of fiber composite bars and dowels

Eric A. Lorenz
Iowa State University

Accelerated aging of fiber composite bars and dowels

by

Eric A. Lorenz

A Thesis Submitted to the

Graduate Faculty in Partial Fulfillment of the

Requirements for the Degree of

MASTER OF SCIENCE

Department: Civil and Construction Engineering
Major: Civil Engineering (Structural Engineering)

Iowa State University
Ames, Iowa

1993

TABLE OF CONTENTS

LIST OF FIGURES

LIST OF TABLES

LIST OF SYMBOLS

a = the distance between the outer tension rods (in.)

A,B,C,D = constants used to represent the solution for deflection of the dowel bar

A_1 = area of the bearing contact surface (in^2)

A_2 = area of the lower base of a right pyramid or cone formed by extending the sides of the bearing area at a 2 to 1 slope (in^2)

A_{FC} = Area of the FC rebar found in Table 3.3 (in^2)

A_{flat} = surface area of the flat part of the truncated pyramid in Figure 4.1 (in^2)

A_{slope} = surface area of the 45° slope sides of the truncated pyramid in Figure 4.1 (in^2)

AF = unitless acceleration factor

b = the distance between the inner tension rods (in.)

c = distance from neutral axis to extreme fiber (in.)

d = diameter of the dowel bar (in.)

d_c = $5 - (d_d/4)$

d_d = diameter of the dowel (in.)

d_{sp} = diameter of specimen in the split cylinder test (in.)

DEFL1= deflection at Point 1 in Figure 3.15 (in.)

DEFL2= deflection at Point 2 in Figure 3.15 (in.)

DEFL3= deflection at Point 3 in Figure 3.15 (in.)

DEFL4= deflection at Point 4 in Figure 3.15 (in.)

e_1 = error or standard deviation for L_c

e_2 = error or standard deviation for d_c

e_3 = error or standard deviation for f'_{cd}

E = tensile modulus of elasticity for the FC rebar found in Table 3.3 (psi)

E_d = apparent modulus of elasticity for the FC dowel (psi)

E_s = modulus of elasticity of the dowel bar (psi)

EI_z = flexural rigidity of the dowel (lb-in^2)

f_b = allowable flexural stress from Table 3.4 (psi)

f'_c = concrete compressive strength (psi)

f'_{cd} = concrete strength used to develop the dowel model (psi)

F_A = force on the outer tension rods (lbs)

F_B = force on the inner tension rods (lbs)

I = moment of inertia from Table 3.4 (in^4)

I_s = moment of inertia for the dowel bar (in^4)

k_o = modulus of dowel support (pci)

ℓ_{sp} = length of test specimen in the split cylinder test (in.)

L_b = length of the rebar not bonded to the concrete that is under tension (in.)

L_c = length of initial crack in dowel specimens (in.)

L_e = depth of concrete in tension (in.)

L_s = simply supported span length equal to 16 (in.)

MAT = mean annual temperature in °C

M_s = bending moment caused by curvature in the dowel (in-lb)

I_s = moment of inertia for the dowel bar (in^4)

P = load applied to the center of the dowel (lbs)

P_c = the nominal tensile strength of the concrete pyramidal elements (lbs)

P_d = load causing a split cylinder failure mode in dowel specimens (lbs)

P_L = load applied to the dowel specimen (lbs)

P_{sp} = maximum load applied in the split cylinder test (lbs)

P_t = load applied to the FC specimen (lbs)

T = the temperature of the aging solution (°F)

U = average bond strength (lbs)

W = width of the flat portion in Figure 4.1 (in.)

x = distance along dowel from the face of the joint (in.)

X = 1000/[(50°C+(MAT-10.4°F))+273]

y = deflection of dowel (in.)

y_o = deflection at the center of dowel (in.)

Y = length of the flat portion in Figure 4.1 (in.)

ß = term used for mathematical expediency (in^{-1})

ϕ = radius of curvature (in.)

ϵ_m = maximum normal strain (in/in)

δ = tensile elongation (deflection) of the FC rebar (in.)

δ_U = loss in deflection due to bond forces (in.)

Δ = deflection at the center of the dowel (in.)

μ = factor specifying the type of concrete (ie., 1.0 for normal weight, 0.85 for sand-lightweight, and 0.75 for all-lightweight)

PREFACE

This thesis is the second part of a final report submitted to the Iowa Department of Transportation. Part 1 contained a comparison of unaged fiber composite and steel dowels and derivation of the appropriate theoretical model for analyzing the results. Part 2 of this final report (this thesis) covers the theoretical and experimental models for accelerated aging of fiber composite reinforcing bars and dowels cast in a concrete environment.

This thesis contains results from testing of unaged and aged fiber composite dowels and steel dowels, in addition to unaged and aged fiber composite reinforcing bars. Additional tests have been performed on unaged dowels (both steel and fiber composite) to verify results from Part 1 and to keep the testing program consistent. Slight modifications have been made to the dowel specimens presented in Part 1. These modifications are noted in the Section 3.4 of this report.

The flexural modulus of elasticity for the FC dowel bar given in Part 1 of the final report (Table 3.2) was for the incorrect structural shape (non-circular cross section). The value is corrected and given in this thesis (Table 3.4 for the modulus of elasticity supplied by the manufacturer, and Tables 3.5 and 3.6 for experimentally determined modulus of

elasticities). The value in Part 1 was not used for any analysis of the FC dowel bars.

ABSTRACT

The introduction of new materials into industry requires that both the unaged load-carrying capabilities and a knowledge of the long term effects of aging must be determined before comparisons can actually be made between these new materials and materials that have been in use for decades. Studying the effects of aging in a natural real weather environment can be unrealistic if the life expectancy of this material is greater than a few years. The life expectancy of fiber composite materials can span over many tens of years, therefore, this report presents a method of accelerated aging to predict the long term capabilities of fiber composite materials. This report also looks at the possibility of using fiber composite reinforcing bars and dowels as a viable alternative to steel as concrete reinforcement.

Accelerated aging entails submersion of fiber composite materials (these fiber composite materials are cast in a concrete system) in a water solution at an elevated temperature. Two theories have been suggested for the loss in strength of fiber composite materials. First, the hot, wet environment accelerates the reaction between the glass fibers and the alkali in the concrete. A hydration product is deposited between the individual glass fibers causing them

to become brittle. Second, direct attack by the alkali in the cement on the glass fibers, results in etching and pitting of the glass fibers and loss of tensile capacity. This process of strength loss (due to accelerated aging) has been compared to strength loss in real weather aging in the natural environment. Accelerated aging was used by Pilkington Brothers Limited of the United Kingdom and further testing by other experimenters has verified that accelerated aging can be used to approximate real weather aging of fiber composite materials. The results of accelerated aging on glass fibers embedded in a mortar environment (strand-in-cement test) and glass fiber reinforced concrete (GFRC) were used to predict long term aging of these glass fibers.

The effects of accelerated aging on fiber composite reinforcing bars and dowel bars composed of E-glass fibers encapsulated in a vinyl ester resin matrix are presented in this report. These fiber composite specimens were cast in concrete and exposed to three different aging bath solutions (water, lime, and salt) at an elevated temperature of 140°F for nine weeks. Control (unaged) specimens were compared with aged specimens, and the affects of aging could then be observed. The aged fiber composite reinforcing bars cast in concrete specimens were tested in direct tension to determine the degradation, if any, in bond between the concrete and fiber composite material. The aged fiber composite dowel

bars in concrete specimens were tested in direct shear to find the effects of accelerated aging on the shear capacity.

Degradation of uncoated E-glass fibers has been proven by other researchers to be extensive in a mortar environment due to alkali attack. Vinyl ester resin has been tested by Dow Chemical and proven to be highly resistant to chemical attack. The E-glass/vinyl ester resin fiber composite (both dowels and reinforcing bars) have been shown through testing at Iowa State University to be highly resistant to the detrimental affects of accelerated aging and can be considered a potential substitute for steel.

CHAPTER 1. INTRODUCTION

The presentation of the final report to the Iowa Department of Transportation has been submitted in two parts (this thesis being Part 2). Part 1 presented a comparison between steel and fiber composite dowels both theoretically and experimentally. This thesis contains results from aging studies on fiber composite reinforcing bars and dowel bars. For convenience, the overall objectives and scope requirements for the entire project are covered in both parts of the final report.

1.1. Experimental and Analytical Investigation

The use of fiber composites (FC) as an alternative to steel in reinforcing bars and dowel bars requires a knowledge of the effects of long term aging on fiber composite materials. The experimental aging portions of the project focused on developing a model (based on previous work done by Pilkington Brothers Limited [1]) to approximate the real weather aging of fiber composite materials in a relatively short period of time.

The investigation described herein was conducted at Iowa State University (ISU) in coordination with the Iowa Department of Transportation (IDOT). This work was conducted

at the ISU Structural Engineering Laboratory under the auspices of the Engineering Research Institute (ERI) with research funds as recommended by the Iowa Highway Research Board and as provided by the IDOT.

1.1.1. Objective

The objectives of this research project were to determine the following:

1. Shear behavior and strength of FC dowel bars without aging,
2. Shear behavior and strength of FC dowel bars with aging, and
3. Potential aging effects on bond of FC reinforcing bars.

1.1.2. Scope

The scope of this research project included:

1. Selecting an appropriate theoretical model for analyzing the results,
2. Design and construction of experimental tests for Objectives 1 and 2,
3. Testing the dowel-shear specimens both aged and unaged,
4. Analyzing the dowel shear testing results,
5. Design and construction of the test specimen details for examining the aging effects on bond behavior of FC reinforcing bars in concrete, and
6. Conducting experiments and analyze results for FC reinforcing bars.

1.2. Literature Review

1.2.1. Accelerated aging of composite materials

An extensive reference search was conducted on accelerated aging of fiber composite materials. The material covered, in depth, the accelerated aging of glass fiber reinforced composites (GFRC) but did not deal with the accelerated aging of glass fibers coated with a vinyl ester resin. The fiber composites (FC) being investigated at ISU were composed of E-glass fibers, encapsulated in a vinyl ester resin matrix. Three different types of FC materials were investigated; two types of three-eighths-inch diameter reinforcing bars and one type of one-and-one quarter-inch diameter dowel bar.

The degradation of E-glass fibers exposed to an alkali environment (within a concrete system) occurs due to chemical etching and pitting of the glass fibers or deposition of hydration product (namely calcium) between the individual glass fibers. As explained in References 1 through 8, the process of chemical degradation and deposition of hydration product is accelerated between the concrete and FC material if this system is exposed to water at an elevated temperature. Based on work done by Pilkington Brothers Inc. given in References 1 and 3, a temperature-aging criteria was

developed to indicate the accelerated aging of FC materials. According to References 1 and 3 this temperature-aging criteria should be adjusted to account for the differences in the mean annual temperature (MAT). Once the temperature-aging criteria was developed and adjusted for the MAT, the number of days aged per day, in the aging tanks at an elevated temperature, could be determined. The FC material was aged 50 years based on this criteria in a little over two months.

Problems may develop during accelerated aging tests as presented in References 9 through 15. These problems include; alkali-silica reactivity, corrosion of steel (spalling), and sulfate attack. Accelerated aging involves submersing a fiber composite specimen in a water solution at an elevated temperature. The hot, wet environment may be conducive to the previously listed problems and accelerate their detrimental affects.

References 16, 17, 18, and 19 cover the composition of the vinyl ester resin and E-glass fibers that make up the fiber composite materials currently being tested at ISU. The material properties of the E-glass fibers and the vinyl ester resin are listed in this report.

1.2.2. Testing to determine the affects of accelerated aging

Aged and unaged reinforcing bars cast in concrete were tested in direct tension and the relative bond was monitored to determine any (if any) degradation to the bond capacity due to accelerated aging. The testing apparatus was based on a common pullout testing procedure.

Aged and unaged FC dowel bars cast in concrete were tested in direct shear. Based on the Iosipescu shear test in Reference 20, a modified ISU direct shear test apparatus was constructed to determine if any degradation to the FC materials shear capacity occurred during accelerated aging.

1.2.3. Theoretical model for pullout and dowel specimens

The deflections for the pullout specimens were approximated very closely using the following equation (that can be found in any mechanics book):

$$\delta = \frac{P_t L_b}{E A_{FC}}$$

where:

δ = tensile elongation (deflection) of the FC rebar (in.)
P_t = load applied to the FC specimen (lbs)
L_b = length of the rebar not bonded to the concrete that is under tension (in.)

E = tensile modulus of elasticity for the FC rebar found in Table 3.3 (psi)
A_{FC} = Area of the FC rebar found in Table 3.3 (in^2)

This equation gives the approximate tensile elongation of the reinforcing bars used in this experiment. This equation also verified the values of area (A) and modulus of elasticity (E) used in this report.

A theoretical model was developed for the dowel specimens based on References 21 and 22. An equation was developed for a truncated pyramid failure mode (based on work in Reference 22) that is a possible failure mode for the dowels. The splitting of the concrete was modeled using the split cylinder test equation (found in Reference 21). This model accounted for the initial concrete failure that was exhibited by the dowel specimens.

Dowel analysis based on Timoshenko's finite beam on an elastic foundation (using References 23 and 24) was developed in Part 1 of the final report. In this thesis the theoretical moment diagram was verified for the 1.5-inch steel dowel specimens using strain gages. The strain gage analysis was based on Reference 25.

The aforementioned models are developed and utilized further in this thesis and will be shown in more detail with each associated test discussion.

CHAPTER 2. ACCELERATED AGING

2.1. Introduction

With the introduction of fiber composites into industry, the knowledge of how long term aging affects the strength behavior of this material must be understood. One approach would involve exposing fiber composites to real weather conditions for a long period of time, while another method would entail subjecting this material to accelerated aging (this process involves casting the fiber composite material in a concrete system and submersing this system in a hot, wet, aggressive environment [1]), reflecting the real weathering capabilities of fiber composites over a shorter time period. Due to the recent interest in fiber composites, the latter approach (accelerated aging) has helped play an important role in understanding the long term strength of fiber composite materials. This chapter will introduce the reader to the analysis involved in determining the effects of accelerated aging on fiber composite materials.

The information obtained from the references, used to determine accelerated aging properties of composite materials in this thesis, was based on the "strand-in-cement" test. The strand-in-cement test is used to determined the alkali resistance of glass fibers in a concrete environment. The

data in this thesis was obtained from tensile, bond, and shear tests of fiber composite materials composed of E-glass fibers encapsulated in a vinyl ester resin matrix and cast in a concrete specimen. Obtaining the true aging of a specific fiber composite material can only be accomplished through natural aging under normal environmental conditions. The use of accelerated aging on fiber composites is considered to be a good approximation to real weather aging.

2.2. Accelerated Aging Compared with Real Weather Aging

The process of comparing accelerated aging with natural weathering of composite materials was determined in References 2 and 3 as follows:

- determining the tensile strength of alkali resistant (AR) glass fibers in a mortar mix (see Section 2.2.1) that have been exposed to accelerated aging,
- determining the strength of glass fiber reinforced concrete (GFRC) composites that have been exposed to similar accelerated aging process (see Section 2.2.2), and
- comparison of the tensile strengths obtained from above to similar composites exposed to real weather aging in different regions.

The two subsections to follow give details of these above-mentioned comparison processes.

2.2.1. Strand-in-cement test

An understanding of the effects of accelerated aging on composite materials can be directly related to the effects on the individual alkali resistant (AR) glass fibers making up those composites [1,3]. The development of the strand-in-cement (SIC) test has been used extensively to study the effects of accelerated aging on glass fibers. The SIC test specimen is shown in Figure 2.1.

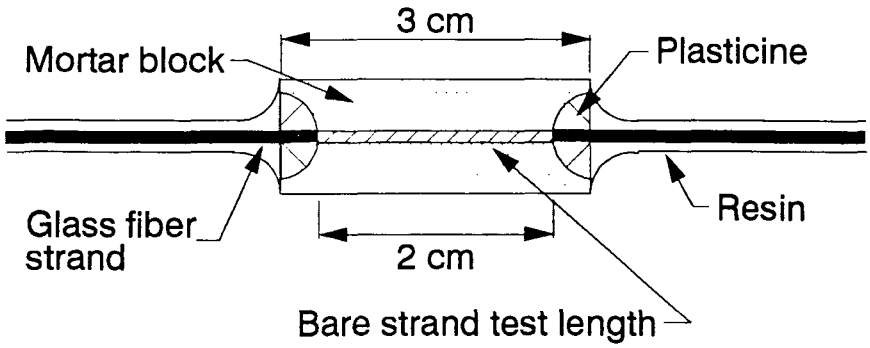

a) Tensile strength specimen

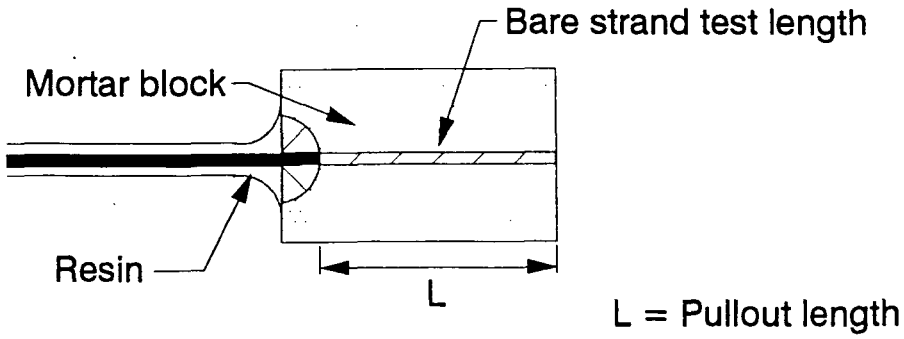

b) Pullout specimen for bond strength

Figure 2.1. Strand-in-cement specimens [1,3]

The SIC specimens are submersed in water at elevated temperatures and subsequently tested in direct tension. The test was used to determine the effects of aging on the AR glass fibers when exposed to different mortar environments and alkaline solutions and to make a strength comparison between glass fibers and composite materials [3]. The bare strand test length (see Figure 2.1) is exposed to the concrete, which is a highly alkaline material with pH of 12.5-13.0 [4]. The elevated temperature of the aging solution is used to speed up the cement hydration process and accelerate the reactions occurring between the glass fibers and the concrete [5]. Figure 2.1a determines the degradation in tensile capacity due to aging of a glass material. Figure 2.1b is used to determine the effects of aging on the bond of a glass material.

Strength comparisons between accelerated aging and real weather aging have shown that one chemical reaction was occurring over the entire range of accelerated temperatures (20°C to 80°C) and that long term aging predictions, made over a very short period of time, at higher temperatures are possible [1,3]. This chemical reaction occurring between the mortar and glass fibers is due to an alkaline attack and creates pits in glass fibers reducing the effective area [3]. Reduction of this alkaline attack by use of protective coating (such as alkali resistant (AR) glass fibers or

possibly vinyl ester resin in composites) results in greater strength retention of the glass fibers [1].

References 1, 6, and 7 state that the activation energy for the strength loss reaction occurring in glass composites during accelerated aging tests remains unchanged for different glass compositions (AR, E-glass, etc.) and surface coatings (poly vinyl chloride, etc.) used to protect the glass fibers. The strength loss reaction affects certain glasses more severely due to the differences in glass surface chemistry [8].

2.2.2. Accelerated aging of fiber composite materials

Accelerated aging of composite materials involves submersing these materials in water at different elevated temperatures ranging from 4°C to 80°C (39°F to 176°F) for various periods of time and relating the strength loss to similar composite materials aged in real weather conditions [1,3]. The real weather aging effects have been determined for different climates around the world.

These aging studies show that the composite materials, when subjected to accelerated aging, exhibit two distinct regions as shown in Figure 2.2 [3]. Figure 2.2 compares the flexural strength of fiber composite sheets (5% to 6% AR glass fibers by weight in a 150 mm long by 50 mm wide by 6-8

mm thick concrete sheet) against the log of time in the accelerated aging baths [3]. Two curves with different aging bath temperatures are shown for comparison, as well as a curve for composites aged in real weather conditions. Region 1 (see Figure 2.2) shows the initial loss in flexural strength (where this flexural strength loss is directly proportional to the fiber SIC strength). The initial rate of strength loss is dependent on the temperature of the aging solution and occurs more rapidly at higher temperatures. Similar strength losses occur at lower temperatures (the

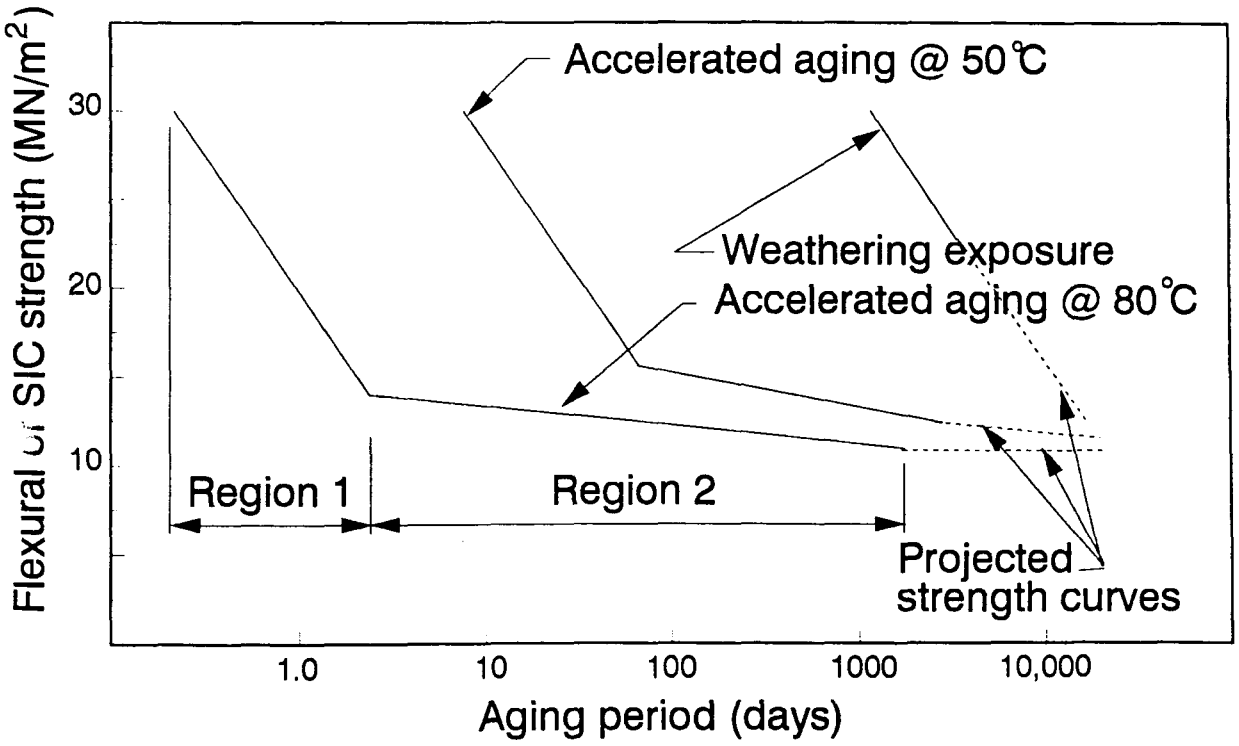

Figure 2.2. Strength of GFRC composites in water and weather

initial strength losses are parallel in Figure 2.2) but at a slower rate. The initial strength loss region is followed by Region 2 (see Figure 2.2) which shows a constant or nearly constant strength region for the remainder of the accelerated aging period [1,3].

According to Litherland et al [3;p.461]:

> "thus it seems reasonable and conservative (or cautious) to assume that, over a very long period, the strengths at these lower temperatures will ultimately reach the level indicated from the constant strength regions of the higher temperature curves".

This statement gives a good indication that accelerated aging of composite material (in water at a higher temperature) can be used to predict long term aging effects in a relatively short time. Put another way, the constant strength region shown in Figure 2.2 (Region 2) will be obtained from various accelerated aging test temperatures and the results of long term strength is not dependent on temperature. Therefore, the long term aging (greater than 50 years) of composites will ultimately reach the same level of constant strength whether aging occurs in natural real weather or artificial accelerated conditions.

The temperature-time dependence exhibited by composite materials has been covered extensively in Reference 1. The general slopes of the lines in Figure 2.2 are not affected by changes in climate (i.e., rainfall, humidity, periods of heat

and cold) but rather depend on the mean annual temperature (MAT) occurring in a particular climate [1,3]. The rate of decrease in strength occurs more rapidly for a warmer MAT than for a cooler MAT (the same dependence exhibited by accelerated aging). This indicates that one set of temperature-time criteria for an accelerated aging test can not be used for two different climates (with different MAT's). Based on the MAT for a given climate, acceleration factors (AF) are used to adjust the temperature-time criteria and provide a way of estimating the real weather aging of composite materials. The accelerated aging temperature-time criteria's dependence on the MAT is covered in Section 3.5 of this thesis.

The accelerated aging studies in References 1 and 3 are based on one type of composite material (5% to 6% glass fibers by weight). But according to Proctor et al [1;p.177]:

> "research to date on a variety of fibers indicates that the procedure, and possibly even the actual acceleration factors, should be applicable across a range of glass compositions".

2.3. Effects of Accelerated Aging on Concrete

The process of accelerated aging increases the aging effects on composite materials, and may also intensify the problems associated with concrete aging. In the absence of

these problems concrete is known to increase in compressive strength indefinitely (however the additional deposition of hydration product occurs at a slower and slower rate) with exposure to a wet environment. The concrete durability may be subject to a wide range of problems that could occur over a short period of time in a hot, wet aggressive environment (accelerated aging). The most common problems associated with concrete durability (that could effect the results of accelerated aging tests) are [9]:

1. alkali-silica reactivity,
2. corrosion of steel (spalling),
3. sulfate attack,
4. freezing and thawing, and
5. scaling.

Both Items 4 and 5 will not effect an accelerated aging test due to the absence of alternating freezing and thawing action. They are listed for completeness and may affect the natural aging of concrete in real weather conditions.

2.3.1. Alkali-silica reactivity

Alkali-silica reactivity (ASR) occurring in concrete may cause cracking and expansion that would ultimately reduce the concrete strength and the bond between the concrete and reinforcement. ASR can be shown by the following two-step reaction [10]:

Alkali + Silica = Gel reaction product
Gel reaction product + Moisture = Expansion Eqn. 2.1

The three main products in Equation 2.1 will be present in all concrete mixes, but the quantity of each product may vary. The alkali (sodium and potassium) comes from the cement, the silica (reactive form) comes from the aggregate and sand, the moisture adds strength to the concrete through hydration [10].

The accelerated aging solutions create a wet environment that can be conducive to ASR if a reactive form of silica aggregate is used in the concrete mix. The problem of ASR that would occur over months or years in the real weather could again be accelerated in a hot, wet environment.

Cements in concrete can be classified into three ranges of alkali content expressed as percent Sodium Oxide (NaO_2); low alkali cements, 0.60% or less, intermediate alkali cements, 0.61% to 0.75%, and normal alkali contents, 0.76% to 0.85% [11]. The use of cement with a low alkali content (0.60% or less of total alkalies) and the use of fly ash (which reacts chemically with the lime to produce further hydration product) have been used to reduce or even eliminate the problem of ASR [11].

2.3.2. Corrosion of steel

The use of deicing salts on bridge decks, in particular, has shortened their working life due to the corrosion of the reinforcing steel [12]. The dowel bars used in concrete pavement joints are also exposed to similar deicing salts and subject to corrosion. This process of corrosion due to deicing salts is shown in Figure 2.3.

In the presence of chloride and sufficient oxygen, carbonation will corrode steel [9]. Sodium and calcium chlorides, if present, can move through the concrete cover (by means of a crack in the concrete or concrete permeability) and corrode the reinforcing steel. With presence of moisture and air, corrosion of steel produces a red rust, which expands in volume and creates internal forces on the concrete [12,13]. The rust formed from the corrosion of steel can occupy twice the volume as the original steel

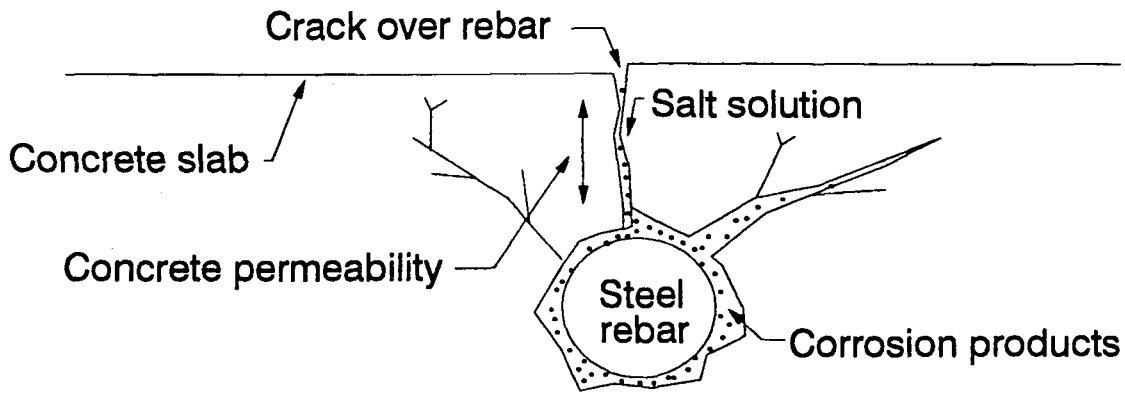

Figure 2.3. Corrosion of steel [12]

material applying a force of as much as 4,700 psi on the concrete, exceeding the concrete tensile capacity [13].

2.3.3. Sulfate attack

Sulfate attack requires that an external source of sulfate reacts with the cement paste [9]. The external source comes from soil or water that contains the sulphate and magnesium ions [14]. Also, the use of deicing salts on highways contributes to the problems of increased sulphate. The expansion due to sulphate attack can result in deterioration of concrete.

Examples of structures that can be affected by sulphate attack include canals, pipelines, transmission tower footings, and highway pavement [15]. The problem with sulphate attack lies in locating areas where sulfates are in high concentrations [15]. These high concentrations may effect only certain portions of a structure, requiring repair of the damaged areas.

Certain aggregates used in concrete may contain quantities of sulphate [15]. When exposed to moisture these aggregates may expand and cause damage to the concrete. This leads the author to believe that an accelerated aging bath can be conducive to sulphate attack by exposing concrete to a hot, wet environment (accelerated aging).

Sulphate attack is prevalent in only 10% of concrete structures built in the United States [15]. This low probability, along with testing for sulfates and use of sulphate resistant concrete (ASTM Type V) have reduced the chances of a problem associated with sulphate attack [15].

2.4. Composites Used in ISU Research

The fiber composite specimens used in this research program (pullout and dowel) contain E-glass fibers that are susceptible to degradation from aging. To reduce this degradation, the E-glass fibers are coated with a vinyl ester resin. The vinyl ester resin/E-glass composite is under investigation at ISU to determine its resistance to aging in harsh chemical environments. Properties of the vinyl ester resin and the composition of the E-glass fibers are given in Section 3.4 of this report.

2.4.1. Effects of accelerated aging on E-glass fibers

Aging studies were performed in Reference 8 on glass fiber reinforced cement (GFRC) composites containing four different glass fibers, one of which was the E-glass fiber. The performance of each glass fiber varied but the embrittlement of the glass fibers resulted from hydration

product (calcium) deposited between the glass fibers and not from chemical attack [8].

The GFRC composites were exposed to water solutions at 20°C (68°F) for two months. With scanning electron microscopes (SEM) the glass fibers were observed after aging. The E-glass fibers exhibited both chemical attack (etching of the glass fiber) and deposition of hydration product between the glass fibers. The embrittlement of the composites by either chemical attack or hydration product was not determined [8].

A glass fiber filament is around 10 microns (micro meters) in diameter and approximately 204 of these individual glass fibers make up a glass fiber bundle [5]. The space between the glass fibers is two to three microns, whereas the cement is 30 microns in diameter. Accelerated aging can result in formation of hydration product between the individual glass fibers. Since the diameter of cement is greater than the space between the glass fibers, cement particles will not fill the voids between the glass fibers and stop the formation of hydration product [5].

The use of E-glass fibers, therefore, requires a durable alkali-resistant coating to reduce or eliminate their degradation caused by aging. This cover protects the E-glass fibers against the high pH in concrete and adds strength to composite material.

2.4.2. Effects of accelerated aging on vinyl ester resin

Vinyl ester resin was used in lieu of AR glass fibers to coat and protect the glass fibers from harsh environments, and provides many advantages over steel or polyester materials, including [16]:

- binds the fibers together,
- transfer forces from fiber to fiber,
- resistance to corrosion from many different chemicals,
- impact resistance,
- fatigue resistance,
- high strength to weight ratios, and
- high electrical and thermal insulation properties.

The vinyl ester resin also exhibits excellent bonding with the glass fibers that produces the high strength in fiber composite materials.

DERAKANE[1] 411-45 vinyl ester resin used to coat the E-glass fibers has been tested extensively by Dow Chemical for corrosion resistance to over 600 different chemicals [16]. The corrosion resistance to both alkalies and acids have resulted in a very durable coating for glass fibers. The accelerated aging studies conducted at ISU on the vinyl ester resin/E-glass fiber composite will be used to determine this fiber composite's resistance to a high pH environment.

The accelerated aging studies conducted at ISU entails

---

[1] The name DERAKANE is a trademark used by The Dow Chemical Company

subjecting the fiber composite specimens to a high alkali environment (inside the concrete) at an elevated temperature of 140°F (60°C) for nine weeks. Three different aging solutions were used and include water, lime and salt. Reference 16 suggests that the maximum recommended service temperature versus chemical environment for the DERAKANE 411-45 resin should be; water - 180°F (82°C), lime ($Ca(OH)_2$) - 210°F (99°C), salt (sea water) - 180°F (82°C). Therefore, the selected aging solution temperature of 140°F (used in this study) falls well below these maximum values and should not effect the results of the accelerated aging tests due to temperature degradation.

The chemical makeup of the vinyl ester resins consists of molecular chains made up of carbon-to-carbon double bonds and ester groups or linkages [16]. The chemical degradation of the vinyl ester resins occur as a result of decomposition of the ester groups through splitting and addition of water elements (organic compounds) or by splitting of the carbon-to-carbon double bonds through combination with a halogen (chlorine, fluorine, etc.) or loss of electrons (oxidation) [16]. In the DERAKANE vinyl ester resins, the carbon-to-carbon double bonds react completely to form continuous units which increase the chemical resistance [16].

CHAPTER 3. EXPERIMENTAL INVESTIGATION

3.1. Introduction

The experimental investigation described herein was conducted at ISU in coordination with the Iowa Department of Transportation (IDOT). This section repeats a brief description of the objectives and scope given in Sections 1.1.1 and 1.1.2, respectively, which focused on:

1) determining the effects of accelerated aging on the bond strength of fiber composite (FC) reinforcing bars (rebars) embedded in concrete, and
2) the suitability of substituting FC dowels for steel dowels.

3.2. Objective

The objectives of this research project are stated in Section 1.1.1 of this thesis and focused on a direct comparison between FC and steel dowel bars and a direct comparison between two types of FC rebars. The objectives consequently entailed testing of two specimen types; namely, pullout and dowel. Dowel-specimen types included FC dowels from Supplier A[2] and steel dowels. Pullout-specimen types

[2] Each type of FC supplier is identified by a letter, omitting the name of the supplying company, to avoid direct comparison.

included Supplier's B and C FC rebars. Both specimen type objectives were accomplished by studying the effects of accelerated aging on specimens (either pullout or dowel) and comparing these effects with control (reference) specimens that were not exposed to accelerated aging (unaged).

The objective of the pullout testing portion of the research program was to determine the FC rebar's relative bond performance with concrete over the design life of a structure. The pullout tests were conducted for the purpose of a performance comparison of aging parameters and were not used to determine the explicit development length per se. Another important point was to observe if a significant degradation of the FC rebars pullout tensile strength occurred.

The objective of the dowel testing portion was to determine the suitability of substituting FC dowel bars for steel pavement dowels, which are currently used in practice. The important point of this portion of the research was to determine the effects in the FC dowel's shear capacity due to accelerated aging.

3.3. Scope

The scope of the research included experimental testing of 40 pullout specimens (including Suppliers B and C FC

rebars) subjected to axial tension and 40 dowel specimens (including Supplier A FC dowels and steel dowels) subjected to direct shear. The test matrix for the 40 pullout and 40 dowel-shear specimens was developed by ISU in coordination with the IDOT and can be found in Table 3.1. The test matrix is shown in two different subtables, designated Series 1 and 2. Series 1 shows the rebar type, the supplier designation and the number of test specimens for the pullout tests. Series 2 shows the dowel type, the supplier designation and the number of test specimens for the dowel-shear tests. The

Table 3.1. Test matrix

Series 1 (pullout specimens):

Rebar type	Supplier	Number of test specimens			
		Unaged (air)	Aged in Water	Aged in lime	Aged in salt
FC	B	5	5	5	5
FC	C	5	5	5	5

Series 2 (dowel specimens):

Dowel type	Supplier	Number of test specimens			
		Unaged (air)	Aged in water	Aged in lime	Aged in salt
FC	A	5	5	5	5
steel	O	5	5	5	5

solutions used in the accelerated natural aging process are indicated in Table 3.1 and include air (unaged), water, lime and salt.

3.4. Materials and Specimens

Pullout specimens were constructed as shown in Figure 3.1. The three-eights-inch FC rebars were embedded into the concrete a certain length (depending on the specimen type) on both sides of the gap (shown in Figure 3.1). Specimens containing Suppliers B and C FC rebar had out-to-out dimensions of 10 by 10 by 23 inches and 10 by 10 by 17 inches, respectively. These embedment lengths used in this research project were significantly less than the development length of the rebar to insure a pullout failure of the rebar and preempt a tensile failure (that did not exhibit any bond failure). The proportion decided upon, without specifically testing for it, was roughly two-thirds of the development length of the individual rebars. Due to the surface texture (Supplier B was without surface roughness) each rebar had different embedment lengths. A three-inch gap (refer to Figure 3.1) was constructed in the center of the specimens in order to expose the rebar to the effects of the accelerated aging process and provide a way to monitor the bond failure. One-half inch of the rebar was exposed on either side of the

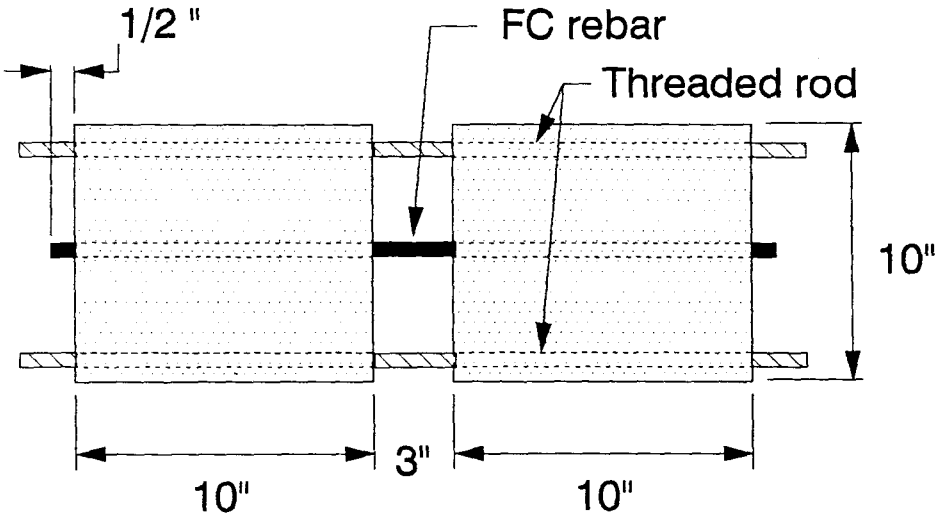

Supplier B

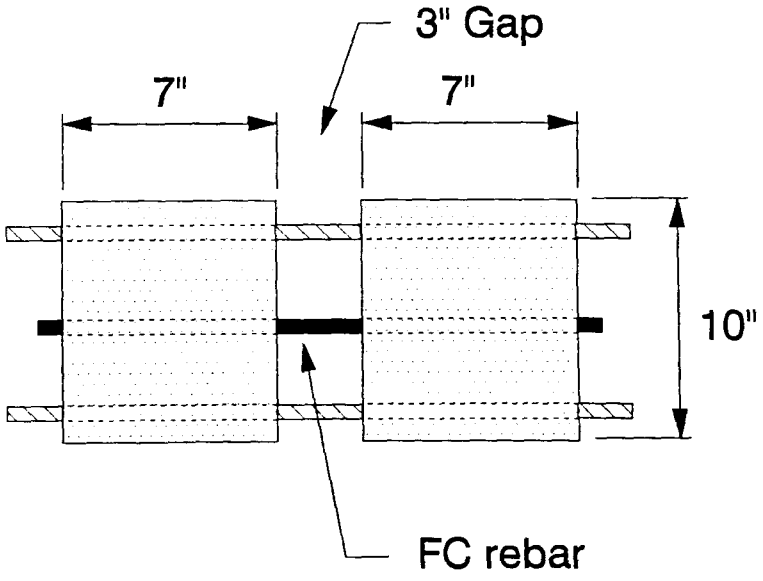

Supplier C

Figure 3.1. Test assemblies for pullout specimens

specimen (see Figure 3.1) providing a way to monitor the bond failure.

The gap in the pullout specimens was formed using three-inch Styrofoam[3] pieces. Three-eighths-inch diameter threaded rods were cast in each corner of the pullout specimens (see Figure 3.1.) in the longitudinal direction to eliminate twisting or flexing of the FC rebar during handling. The threaded rods were kept in the specimens until testing.

Dowel-shear specimens were constructed as shown in Figure 3.2. These specimens consisted of a 10- by 10- by 23-inch concrete member (Part 1 of the final report used a 10- by 10- by 24-inch concrete member) with a pavement dowel centered in the concrete (1.25-inch FC dowels or 1.50-inch steel dowels). A gap in the specimen (see Figure 3.2) helped insure that no force was transferred by aggregate interlock, and that all of the force was transferred through the dowel being tested. To keep the specimen close to field conditions a gap of approximately one-eighth inch was used.

The gap in the dowel-shear specimens was constructed using two half-sheets of plexiglass approximately one-eighth-inch thick. The plexiglass was removed after curing of the specimens and before placement in the aging tanks.

During the testing of the dowel bars, four possible

---

[3] Styrofoam is a registered trademark of the Dow Chemical Company

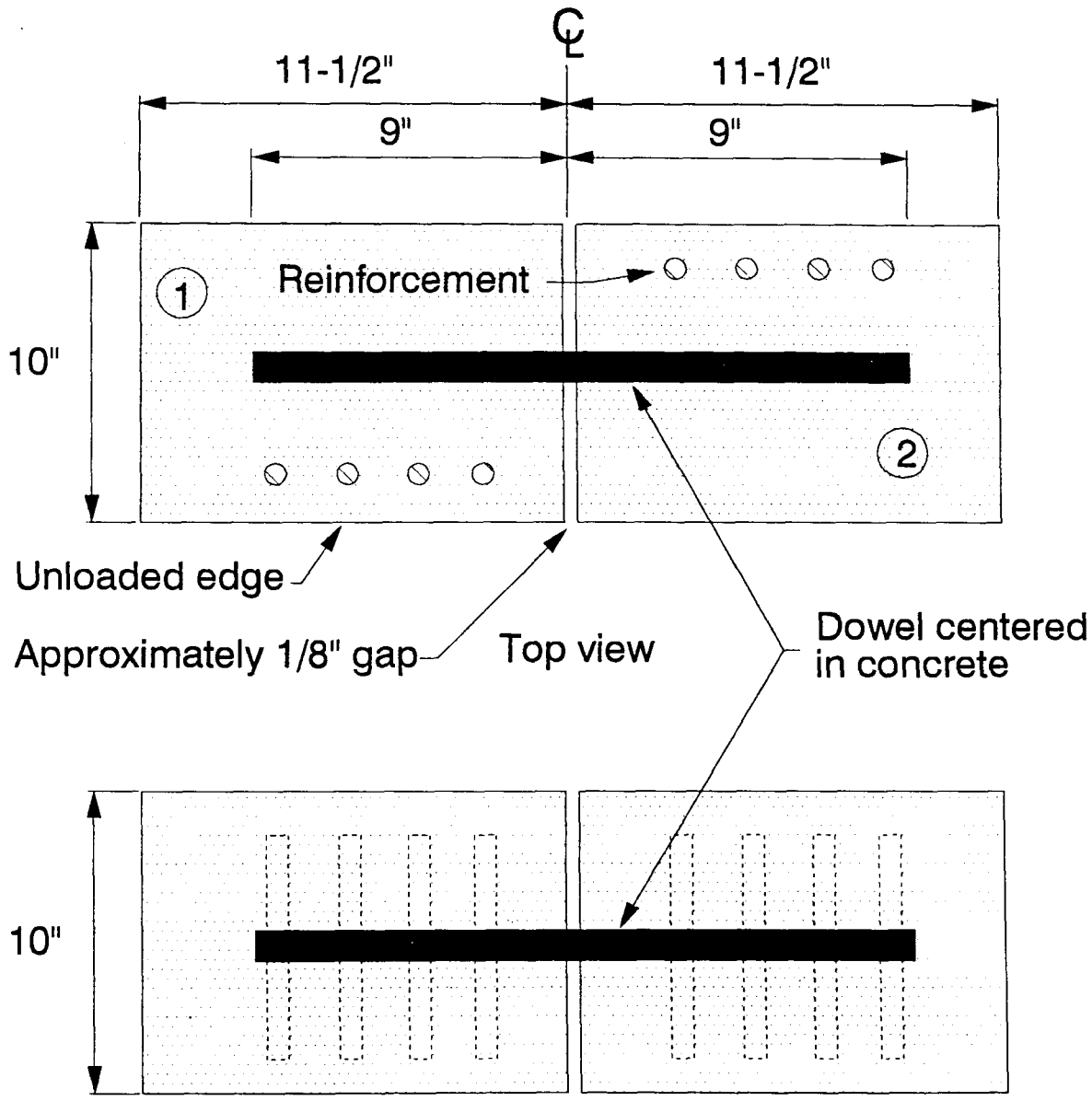

FC and steel assemblies

Figure 3.2. Dowel specimens

modes of failure may occur in the specimens:

- shear failure of the dowel bar,
- bearing failure of the concrete beneath the dowel bar,
- bending failure of the dowel bar, and
- a vertical shear of the concrete surrounding the dowel bar.

These four failure modes are depicted in Figure 3.3. Vertical shear also named splitting of the concrete is presented in Section 4.3 of this report. All of the failure modes, with the exception of the vertical shear mode, can occur to dowel bars in pavement, as well as in test specimens. A vertical shear mode is possible only in test specimens because of the limitations put on the specimens length (a shorter length made testing more practical). In the test specimens, the length of the pavement needed to resist the vertical shear mode is half of the specimen length; in a pavement slab, the length able to resist the vertical shear is the distance between the joints in the pavement. Due to this relatively large length of concrete between the joint, a vertical shear is not a possible failure mode in the pavement [17]. Reinforcement was positioned in the dowel specimens near the unloaded edge (refer to Figure 3.2.) to reduce the effects of vertical shear. Number five rebar with two-inch spacing and two inches of cover were used (dowel specimens used in Part 1 contained no vertical reinforcement).

The specimens were constructed using steel prefabricated

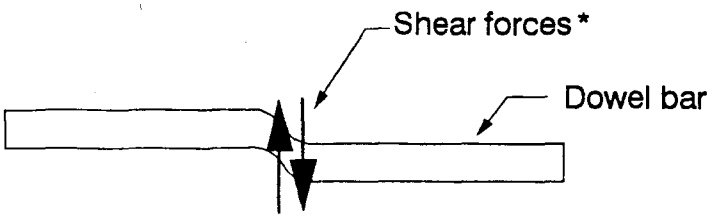

(a) shear failure of dowel

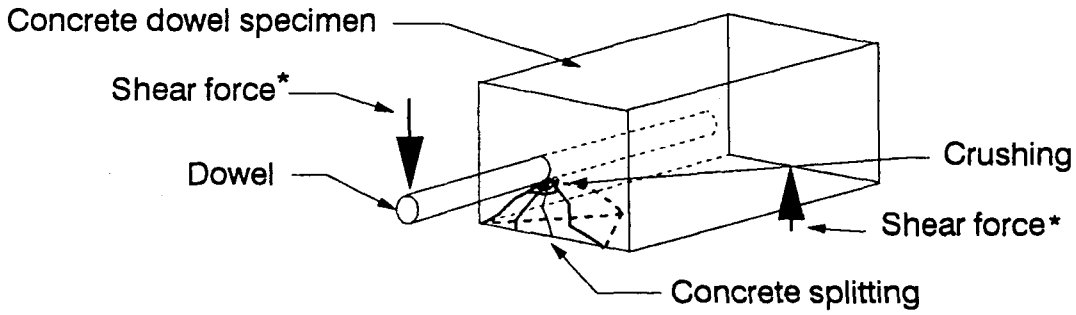

(b) bearing failure of concrete

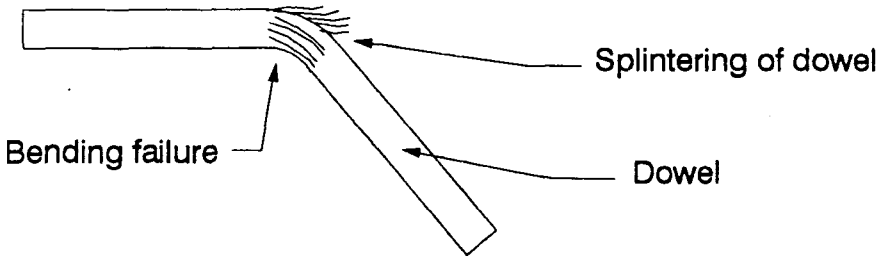

(c) bending failure of dowel

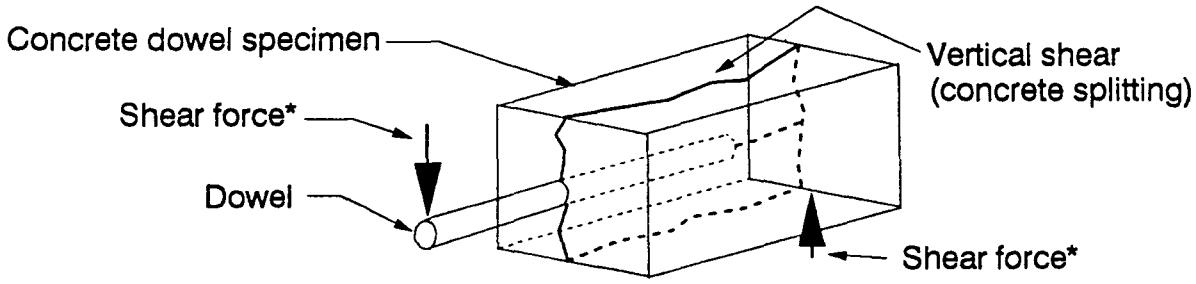

(d) vertical shear of the concrete

* Only applied forces shown, equilibrium forces from test apparatus are ommitted for clarity.

Figure 3.3. Failure modes in dowel specimens

forms. A standard 28-day nominal 5000 psi concrete mix, with a specified six-inch slump, no air, plasticizer or fly ash, was ordered from a local manufacturer. The specimens were cast in two separate pours, dowel and pullout. Sand used in casting the concrete specimens was shipped from the Mississippi River to help eliminate the possibility of ASR.

The average concrete compressive strength was determined (see Table 3.2) for pullout and dowel specimens by testing at least three standard 6- by 12-inch cylinders. Table 3.2 exhibits average concrete strengths for aged specimens prior to aging and after aging and unaged (control) specimens. Table 3.2 is shown divided in two subtables (pullout and dowel specimens) for clarity.

Table 3.3 exhibits the unaged properties of FC and steel rebars (steel rebars were listed for comparative purposes only). The values in Table 3.3 are the average diameter, area, and apparent modulus of at least five rebar specimens. The diameters were measured by taking the diameter at two points perpendicular to each other on the rebar and averaging them. The areas were determined by submersing the rebars in water and weighing the water (in grams) displaced by the rebar. Using a conversion factor, 1.0 gram equals 1.0 cubic centimeter, this weight in grams is equivalent to the same volume in cubic centimeters. The volume was converted to cubic inches and then divided by the specimen length (in

Table 3.2. Concrete strengths

Pullout specimens:

Rebar type	Supplier	Average compressive strength (psi)				
		Aged specimens				Unaged specimens
		Before aging	Aged in water	Aged in lime	Aged in salt	
FC	B	7286	7324	7102	7423	7149
FC	C	7286	7057	7339	7254	7149

Dowel specimens:

Dowel type	Supplier	Average compressive strength (psi)				
		Aged specimens				Unaged specimens
		Before aging	Aged in water	Aged in lime	Aged in salt	
FC	A	7191	7856	7943	7660	7090
Steel	O	7191	7856	7943	7660	7090

inches) to obtain the average area of the rebar. These values were verified with other research (the use of Autocad and volume measurements) at ISU by Mr. Kent Fish [18]. The apparent modulus of the rebars was determined by applying a tensile load and monitoring the strain near the center of the rebar. The apparent modulus of elasticities listed in Table 3.3 are the average of at least three FC rebars from each

Table 3.3. Unaged properties of 3/8-in. FC and steel rebars

Rebar type	Supplier	Measured diameter (in.)	Area (in^2)	Apparent modulus of Elasticity (psi)*
Steel**	O	0.375	0.110	28.85×10^6
FC	B	0.364	0.096***	4.72×10^6
FC	C	0.416	0.117***	6.05×10^6

* These values were determined through tensile testing.
** The steel rebar is shown here for comparison purpose only.
*** These areas were determined by submerging the rebar in water and measuring the weight of water displaced and dividing by the length.

supplier. To diminish any compressive forces that would damage the rebars due to clamping from the testing machine, each end of the FC rebar was cast in copper tube using epoxy. Then these copper tubes were clamped by the testing frame and a tensile load was applied. A strain measuring device (extensometer) was mounted at the center of the span and strains were recorded at every 50-pound intervals. All FC rebars were loaded to 60 percent of ultimate tensile capacity to insure no failure of the FC rebar (failure would damage the instrumentation). The tensile loads were divided by the area of the rebar and a corresponding stress was determined. The strain was plotted against the stress, and the slope of the stress-strain diagram gave the apparent tensile modulus of elasticity.

At least three FC dowel bars were placed in different

aging solutions for the specified nine-week aging period. The dowels were not cast in concrete and were exposed to the water, lime, and salt solutions at an elevated temperature of 140°F (60°F). This process was used to determine the effects of a hot, wet environment on the modulus of elasticity of the dowel bars. Table 3.4 exhibits typical mechanical properties

Table 3.4. Typical properties of 1.25 in. FC dowel bars [19]

Allowable tensile stress (psi)	100,000
Tensile modulus (psi)	6.0×10^6
Allowable flexural stress (psi)	100,000
Coefficient of thermal expansion (in/in/°F) *	3.0×10^{-6}
Flexural modulus (psi) **	6.0×10^6
Area (A) (in^2)	1.24
Moment of inertia (I) (in^4)	0.120

* The average coefficient of thermal expansion for concrete is 5.5×10^{-6} in/in/°F and for steel is 6.0×10^{-6} in/in/°F [21]. The use of a material as reinforcement in concrete with a significantly different value of thermal expansion may be detrimental to the concrete. The coefficient of thermal expansion listed in Table 3.4 is a published value and may not reflect the actual value. The value for the thermal expansion was determined at ISU to be around 6.0×10^{-6}.

** This value of flexural modulus has been changed from the value in Part 1 of this report. 6.0×10^6 is the correct value.

of unaged 1.25-inch diameter vinyl ester dowel bars used in this research project as supplied by the manufacturers.

Values in Table 3.4 (allowable flexural stress and moment of inertia) were used to determine apparent flexural modulus of elasticities for aged and unaged dowel bars. A simple beam procedure was used to collect the load-deflection data for modulus of elasticity calculations. A point load was applied to the center (eight inches from either end) of a simply supported dowel bar having a 16-inch span. The dowels were loaded to about 50 percent of the maximum allowable load (this procedure was used so that the instrumentation was not damaged) based on flexure. The maximum allowable load was calculated using Equation 3.1.

$$f_b = \frac{MC}{I} \quad where \quad M = \frac{PL_s}{4} \qquad \text{Eqn. 3.1}$$

where:

f_b = allowable flexural stress from Table 3.4 (psi)
P = load applied to the center of the dowel (lbs)
L_s = simply supported span length equal to 16 (in.)
c = distance from neutral axis to extreme fiber (in.)
I = moment of inertia from Table 3.4 (in^4)

Solving Equation 3.1 for P gives the maximum load allowed on the 16-inch dowel span based on flexure. The maximum load was reduced by about 50 percent to ensure that no failure of the dowel bar and no damage to the deflection

instrumentation would occur. Load-deflection data was recorded every 50 pounds up to 2,500 pounds. Equation 3.2 was used to determine the apparent modulus of elasticity for the dowels.

$$\Delta = \frac{PL_s^3}{48E_dI} \qquad \text{Eqn. 3.2}$$

where:

Δ = deflection at the center of the dowel (in.)
E_d = apparent modulus of elasticity for the FC dowel (psi)

Equation 3.2 can be solved for E_d (apparent flexural modulus of elasticity) by using the load and corresponding deflection data point along with the moment of inertia from Table 3.4. The E_d between each data point was calculated. The average of these values (apparent flexural modulus of elasticity) is listed in Table 3.5 for unaged dowel specimens. The apparent flexural modulus of elasticity for the aged dowel specimens was calculated using the same procedure and is presented in Table 3.6.

The FC materials consist of E-glass fibers which determine some of the mechanical properties (tensile strength, etc.), vinyl ester resin which establishes electrical, chemical, and thermal properties, and additives which contribute special properties (such as cost reduction).

Table 3.5. Unaged properties of FC and steel dowel bars

Dowel type	Supplier	Measured diameter (in.)	Area (in^2)	Apparent modulus of elasticity (psi)*
FC	A	1.250	1.227	$6.93x10^6$
Steel	O	1.500	1.767	$28.0x10^6$

* These values were determined through flexural testing.

Table 3.6. Aged apparent modulus of 1.25-in. FC dowel bars

Dowel type	Supplier	Aging solution	Apparent Modulus of Elasticity (psi)*
FC	A	water	$6.95x10^6$
FC	A	lime	$6.91x10^6$
FC	A	salt	$6.87x10^6$

* These values were determined through flexural testing.

This thesis will present some basic properties of both the vinyl ester resin and E-glass fibers. These properties are listed in Tables 3.7, 3.8, and 3.9.

Standard burn-down tests were performed on all FC materials, used in this investigation, to determine the percent of E-glass fibers by weight as shown in Table 3.7. The burn down tests were conducted similar to ASTM D2584-68 specification [26] and performed by the Materials Analysis and Research Laboratory at ISU. These values were the average of at least three samples from each fiber composite

specimen. The specimen weight varied from 3 to 6 grams (see initial weight in Table 3.7). Each sample was ignited in a crucible and burned until only ash and carbon were left (the vinyl ester resin was removed). The remaining residue was further reduced by heating in a muffle furnace at 565°F overnight, allowed to cool, and finally weighed (see final FC material weight in Table 3.7).

The results from Table 3.7 indicate that the FC

Table 3.7. Percent of E-glass fibers by weight

Supplier	Initial weight of FC material (grams)			Final weight of FC material (grams)			Average Percent of E-glass fibers by weight (%)
	1	2	3	1	2	3	
A (dowel)	4.10	3.41	4.23	3.25	2.70	3.37	79.3
B (rebar)	3.94	3.57	4.30	2.83	2.55	3.11	71.9
C (rebar)	4.77	4.90	5.12	3.62	3.74	3.89	75.9

Table 3.8. Typical properties of E-glass fibers [5]

Specific gravity	2.54
Tensile strength (psi)	500×10^3
Strain at break, %	4.8
Modulus of elasticity (psi)	10.4×10^6

Table 3.9. Properties of DERAKANE 411-45 resin [16]

Tensile strength (psi)	11-12,000
Tensile modulus (psi)	4.9×10^{-5}
Elongation (%)	5.0-8.0
Flexural strength (psi)	16-18,000
Flexural modulus (psi)	4.5×10^{-5}
Coefficient of linear expansion (in/in/°F)	$17\text{-}23 \times 10^{-6}$

materials are composed of a high percentage of E-glass fibers by weight and only 20 to 30 percent vinyl ester resin (other compounds may be present, but their weights were not considered). Therefore, the majority of tensile strength provided by the FC materials is due to the E-glass fibers. Table 3.8 exhibits some properties of individual E-glass fibers. The values listed in Table 3.8 are taken from Reference 5 and not determined at ISU. Table 3.9 lists some typical properties (not used as specifications) for the DERAKANE 411-45 resin coating the E-glass fibers in the FC specimens. These values in Table 3.9 were taken from Reference 16 and not determined through testing at ISU.

Composition by weight of the E-glass fibers making up the FC materials is shown in Table 3.10. These composition

values expressed as percent by weight were determined through testing at ISU's Materials Analysis and Research Laboratory. X-ray fluorescence was used to determine the percent by weight of each compound and is given as an oxide in Table 3.10. The equipment used includes; a Siemens SR 200 sequential spectrometer, CR tube operated at 50 kV and 50 MA, spectrometer operated in vacuum mode, and fully computer controlled.

Table 3.10. Composition of the E-glass fibers

Composition	Pullout specimens		Dowel specimens
	Supplier B	Supplier C	Supplier A
	weight (%)	weight (%)	weight (%)
Silica (SiO_2)	53.9	53.9	54.3
Calcium oxide (CaO)	21.8	21.8	21.9
Alumina (Al_2O_3)	14.4	14.2	15.1
Boron oxide (B_2O_3)	5-10*	5-10*	5-10*
Magnesia (MgO)	0.5	0.4	0.5
Alkali oxides (Na_2O and K_2O)	1.0	1.2	0.8
Titanium dioxide (TiO_2)	0.9	0.9	0.7
Ferric oxide (Fe_2O_3)	0.3	0.2	0.2
Fluorine (F_2 as CaF_2)	0-1*	0-1*	0-1*
Bare glass	100	100	100

* These values were not specifically obtained from analysis.

3.5. Accelerated Aging Conducted at ISU

The process of accelerated aging as mentioned previously involves submersing the fiber composite specimens in a solution at an elevated temperature. The temperature of the aging solution and the mean annual temperature (MAT) can be used to determine the rate of aging (accelerated aging) occurring in the tanks.

To age the specimens in a solution at an elevated temperature, tanks had to be built that were large enough to hold the specimens. Three 1000-gallon wooden tanks with dimensions 4 by 4 by 8 feet were constructed as shown in Figure 3.4. The tanks were insulated on all sides by styrofoam to reduce heat loss. The bottom and sides of the tanks were lined with a fiberglass coating to protect the wood framing against the harsh solutions in the tanks. A immersion heater was mounted in the tanks to regulate and maintain the temperature.

Prior to the start of accelerated aging, all FC specimens were stored at room temperature (60°F to 65°F) for a standard 28-day curing period. On the 28th day the specimens were separated and placed in three temperature-controlled baths. Each tank contained two layers of specimens; pullout and dowel. The bottom layer (dowel specimens) was placed on the floor of the tanks while the second layer (pullout

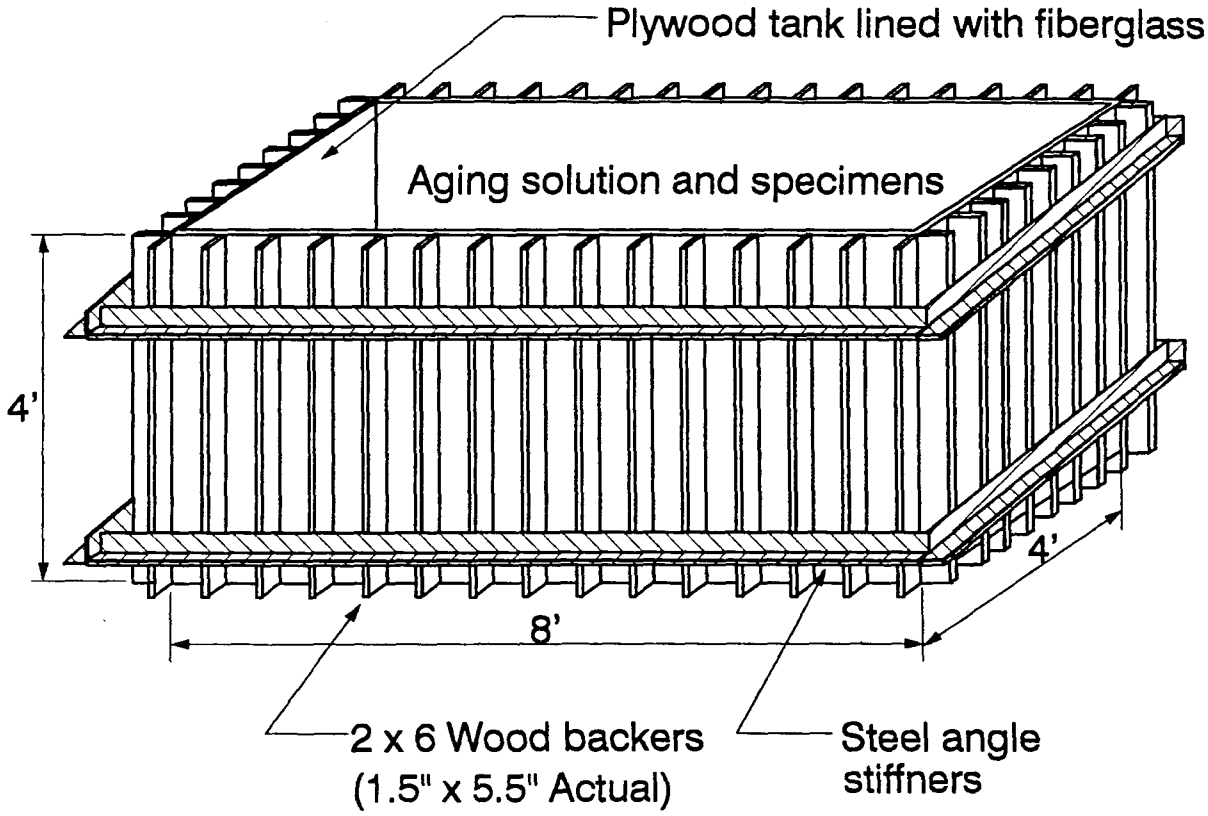

Figure 3.4. Aging tanks

specimens) was placed on a support rack. This support rack kept the two layers of specimens separate and allowed the aging solutions to affect the specimens equally and to eliminate pre-loading of the specimens in the tanks.

The IDOT suggested that the following three solutions should be used in the accelerated aging process of the specimens:

- water,
- lime, and
- salt.

Unaged (air) specimens were used as reference. The water solution was ordinary tap water. The lime solution contained reagent grade calcium hydroxide ($Ca(OH)_2$). A sufficient amount of $Ca(OH)_2$ was added to create a basic solution with a pH of 11-12 that was maintained throughout the aging process. The salt solution contained three-percent sodium chloride salt (NaCl) by weight and was maintained throughout the aging process. The salt water solution had the same concentrations of salt as that of sea water. The tanks were stirred on a regular basis to keep the lime and salt in solution and to prevent stagnation of the aging baths.

The temperature-aging criteria was selected based on work done by Pilkington Brothers Ltd. [1]. Using a temperature-time relationship, four-data points were given in Reference 1 for composite materials aged in a water solution. These values are shown in Table 3.11.

The data points given in Table 3.11 relate the temperature of the aging solution to the number of days aged for every day the FC specimens remain in the aging solution. These data points were established for a mean annual temperature (MAT) of 10.4°C (50.72°F). The process of aging in real weather is dependent on the MAT, where the rate of decrease in strength of FC materials occurs more rapidly in

Table 3.11. Temperature-time data

Temperature of aging solution °C (°F)	Number of days aged per day (days/day)
50 (122)	101*
60 (140)	272*
70 (158)	693*
80 (176)	1672*

* These time criteria values are based on a MAT of 10.4°C 50.72°F).

warmer climates (higher MAT) than in cooler climates (lower MAT) [3].

The process of accelerated aging is based on real weather aging in the United Kingdom (UK) environment (MAT = 10.4°C). If the MAT changes, such as in some other environment, the rate of natural aging would change. Since accelerated aging is related to aging in the real environment (UK), accelerated aging must also change in relation to the MAT. With a MAT less than 10.4°C, for the same temperatures given in Table 3.11, the number of days aged per day will increase by some factor and for a MAT greater than 10.4°C the number of days aged per day will decrease by some factor. In other words, the colder the climate (less than 10.4°C) the more aggressive the affects of accelerated aging, which causes the number of days aged per day to increase by a factor. This factor, called the acceleration factor (AF),

has been established as shown by an approximate-exponential curve in Figure 3.5. Figure 3.5 shows the AF (given for several different climates in Reference 1; United Kingdom, Montreal, New York, Tokyo, Johannesburg, and Miami) versus the inverse of absolute temperature. The equation for the absolute temperature, T°K, that takes into account the change in MAT for different environments, was developed at ISU (based on data from Reference 1) as follows:

1. Use the standard acceleration temperature of 50°C (the aging data from different environments, with different MAT's, was based on accelerated aging bath temperatures of 50°C),
2. Add the quantity (MAT - 10.4°C), which accounts for the difference in MAT (a lower MAT decreases the standard acceleration temperature and a higher MAT increases the standard acceleration temperature),
3. Convert it to absolute (°K) by adding 273, and
4. Take the inverse of T°K (therefore, a lower MAT will increase the value of 1/T°K and a higher MAT will decrease the value of 1/T°K).

The inverse of T°K multiplied by 1000 can be conveniently used in Equation 3.3, for X, to determine the AF.

$$AF = 2.986E\text{-}19e^{13.783X} \qquad \text{Eqn. 3.3}$$

AF = unitless acceleration factor
X = 1000/[(50°C+(MAT-10.4°C))+273]
MAT = mean annual temperature in °C.

Using Equation 3.3 the time values given in Table 3.11 can be adjusted for any MAT to develop approximate real weather aging effects on FC materials. The MAT for central Iowa over the past 35 years is given as 9.87°C (49.77°F)

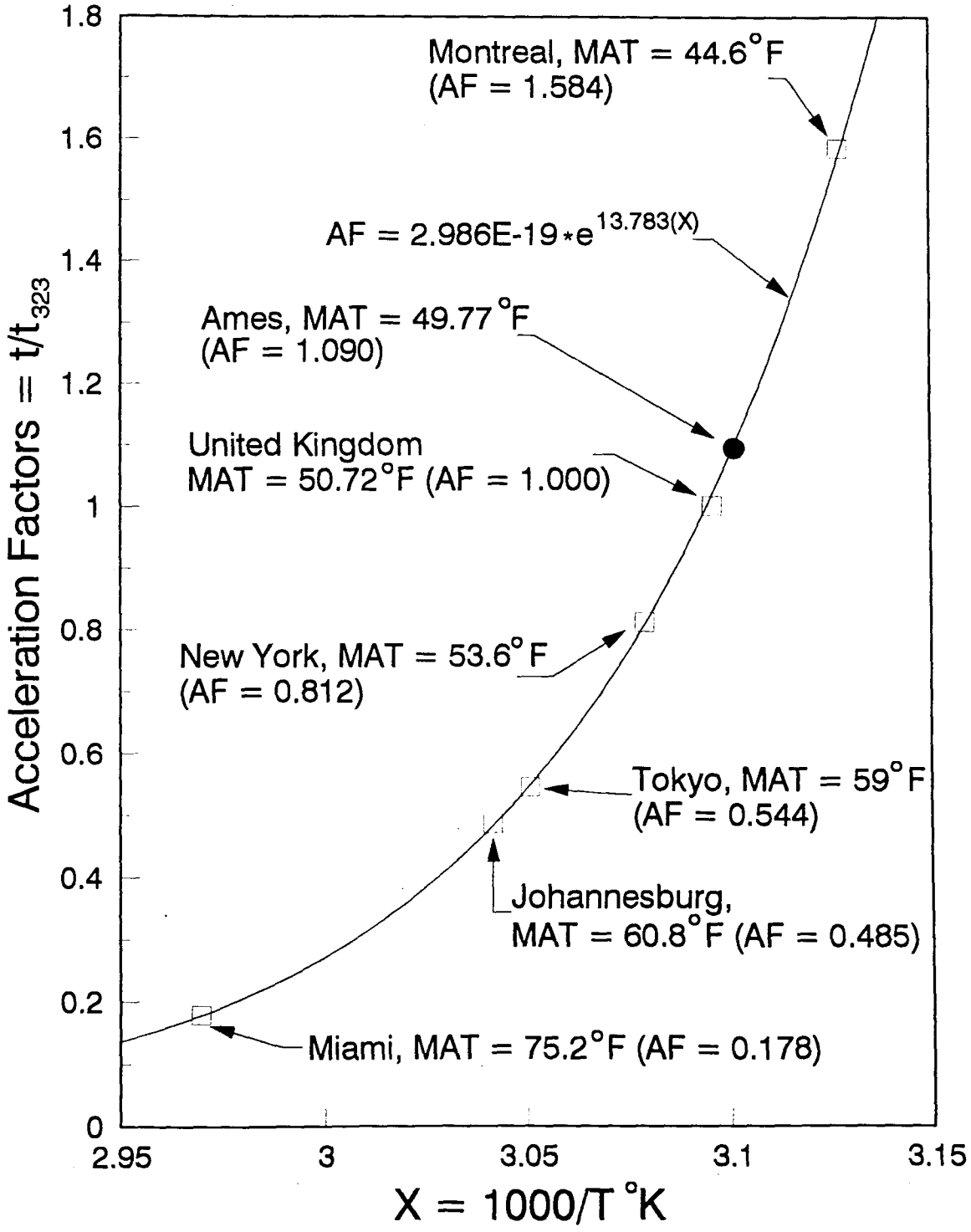

Figure 3.5. Acceleration factor curve

[27,28]. Using Equation 3.3 the AF for this climate can be established as 1.09. This AF is then applied to the number of days aged per day in Table 3.11 and a new set of temperature-time data is determined for central Iowa as shown in Table 3.12.

Table 3.12. Adjusted temperature-time data for central Iowa

Temperature of aging solution °C (°F)	Number of days aged per day (days/day)
50 (122)	1.09(101) = 110*
60 (140)	1.09(272) = 296*
70 (158)	1.09(693) = 755*
80 (176)	1.09(1672) = 1822*

* These time criteria values are based on a MAT of 9.87°C (49.77°F).

The data points given in Tables 3.11 and 3.12 are plotted using best fit approximated-exponential curves in Figure 3.6 (Curves A and Curve B exhibit data from Tables 3.11 and 3.12, respectively). These curves help establish temperature-time criteria for aging solution temperatures other than those stated in Tables 3.11 and 3.12. Accelerated aging effects have been studied for elevated temperatures as high as 80°C (176°F) with good correlation of results compared with real weather aging [1]. Use of higher temperatures than 80°C requires extrapolation of data and is not

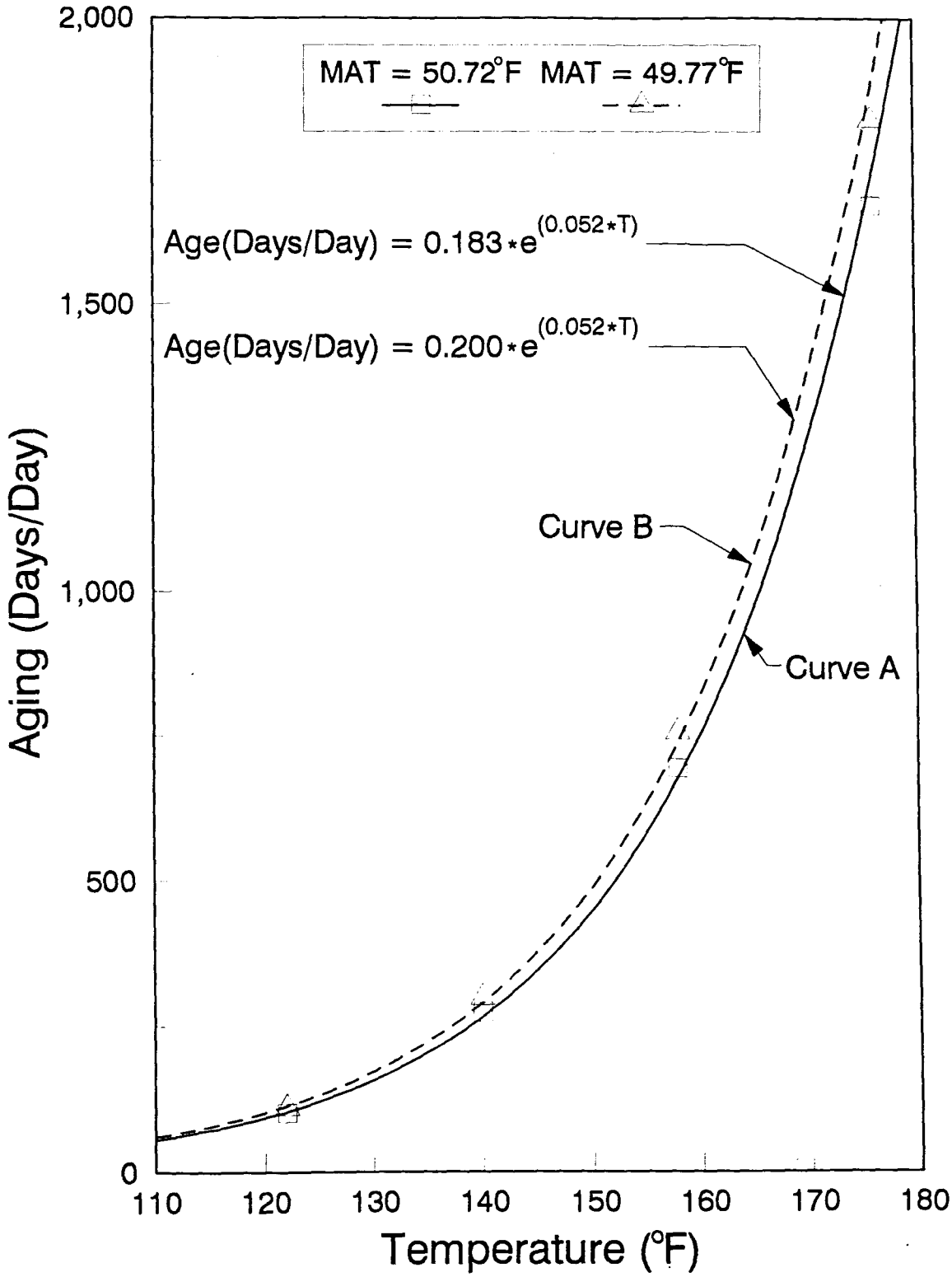

Figure 3.6. Temperature-time criteria curve

recommended.

The equations developed from the data in Tables 3.11 and 3.12 are given by Equations 3.4 and 3.5, respectively.

$$Age\left(\frac{days}{day}\right) = 0.183 * e^{(0.052*T)} \qquad \text{Eqn. 3.4}$$

$$Age\left(\frac{days}{day}\right) = 0.200 * e^{(0.052*T)} \qquad \text{Eqn. 3.5}$$

where:

T = the temperature of the aging solution (°F).

Equations 3.3 through 3.5 were developed by ISU researchers based upon data given in Reference 1. Equation 3.4 should be used for a MAT of 10.4°C (50.72°F) and Equation 3.5 was used to determine the temperature-time criteria for central Iowa (Ames). The temperature-time curve in Figure 3.6 (see Curve B) relates the temperature (in Fahrenheit) of the aging solution to the number of days aged per day. For example, a specimen in a solution at 130°F will age approximately 171.5 days for every day it remains in the solution (i.e., a specimen left in a solution at 130°F for 10 days will age approximately 1715 days or 4.7 years).

The solutions in all three tanks were maintained at a constant temperature of 140°F. Using Equation 3.6, with T equal to 140°F, the equivalent number of days aged per day

was determined as 288.4. The specimens were aged 50 years (as suggested by the IDOT) which is equivalent to 18262.5 days (including 12.5 days for leap year). Therefore, an accelerated aging period of 63.3 days at an elevated temperature of 140°F in the solutions was equivalent to 50 years in the Ames environment.

Upon completion of the accelerated aging tests, the solutions in the tanks were allowed to cool and samples were taken for chemical analysis (see the Section 3.7.2 of this thesis). The tanks were drained and the specimens allowed to dry for one day. The specimens were tested and an observation of both aged and unaged FC rebars and dowels was made under a scanning electron microscope (see the Section 3.7.1 of this thesis).

3.6. Testing Procedure

Two testing procedures were utilized in this investigation based upon pullout and dowel-shear specimens. Both procedures used the same testing frame with modifications made to accommodate either axial tension (pullout specimens, see Figure 3.7) or direct shear (dowel specimens, see Figure 3.8).

The first testing procedure was developed to determine the pullout capacity of both aged and unaged FC rebars

embedded in concrete (refer to Figure 3.1). The pullout capacity was related directly to the bond strength and reflected the effects of aging on the specimens. The use of conventional test grips on the specimens was determined as inadequate. The high transverse-compressive forces generated in a conventional method of gripping tend to restrict pullout of the rebar. To alleviate this problem threaded rods were placed as shown in Figure 3.1 and a special grip was developed for the test frame. The threaded rods were used to grip the specimen on both ends (see Figure 3.7). As explained in Section 3.4, threaded rods were cast through the entire length of the specimens to eliminate twisting of the FC rebar during handling. The threaded rods were cut prior to testing. A tensile force was applied by a hydraulic-load ram (see Figure 3.7) through the center of the test specimen.

Bond slip was monitored on both ends (refer to Points 1 and 2 in Figure 3.7) and is discussed in the Section 3.7.3 of this thesis. The graphs in the Appendix, for the pullout specimens, reflect load versus deflection monitored at Points 3 and 4 in Figure 3.7 (the behavior of the graphs will be discussed later in the Section 3.7.3).

The second testing procedure was developed to determine the shear capacity of both aged and unaged FC and steel dowel bars embedded in concrete (refer to Figures 3.2 and 3.8). The testing frame shown in Figure 3.8 is based upon the

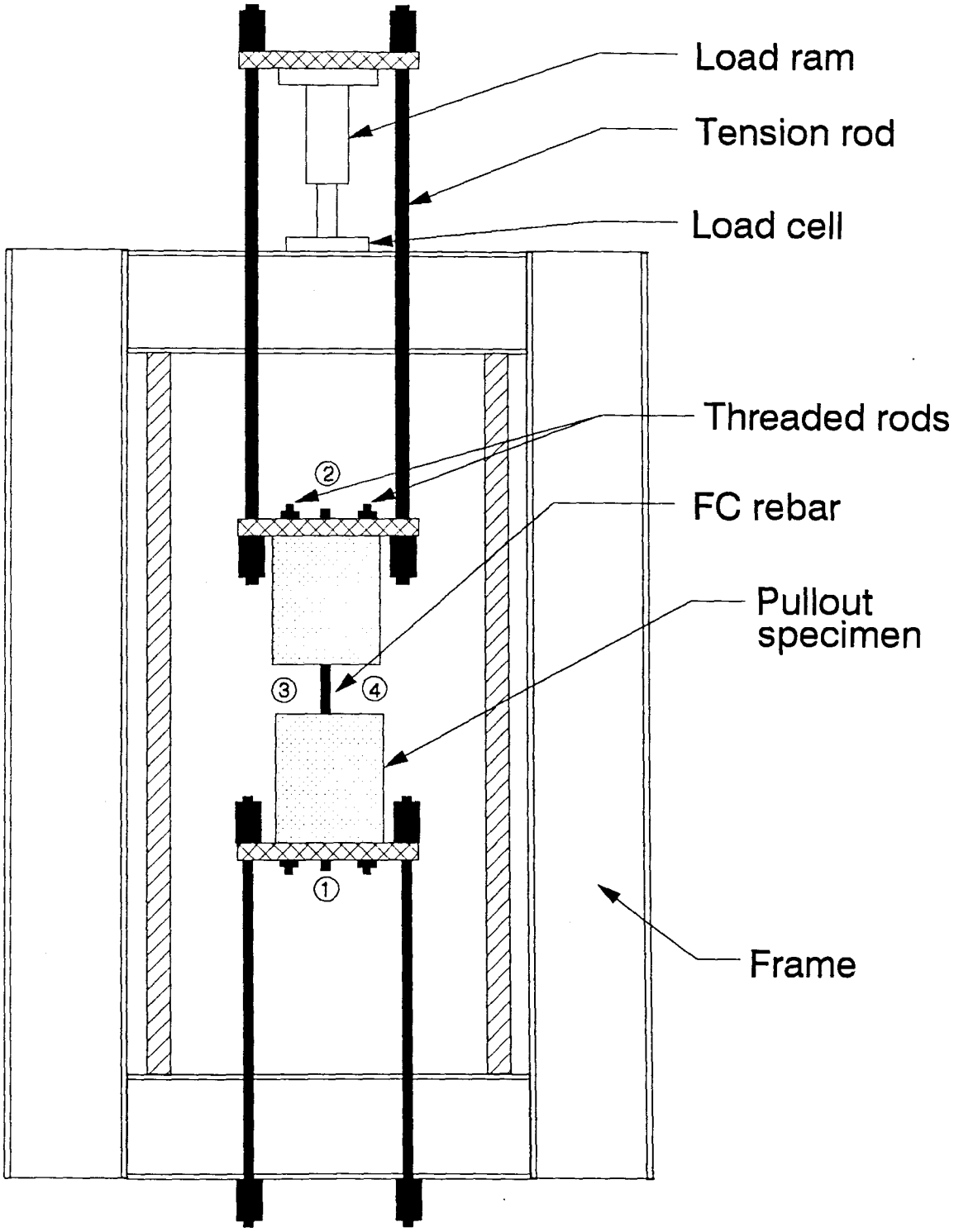

Figure 3.7. Pullout frame

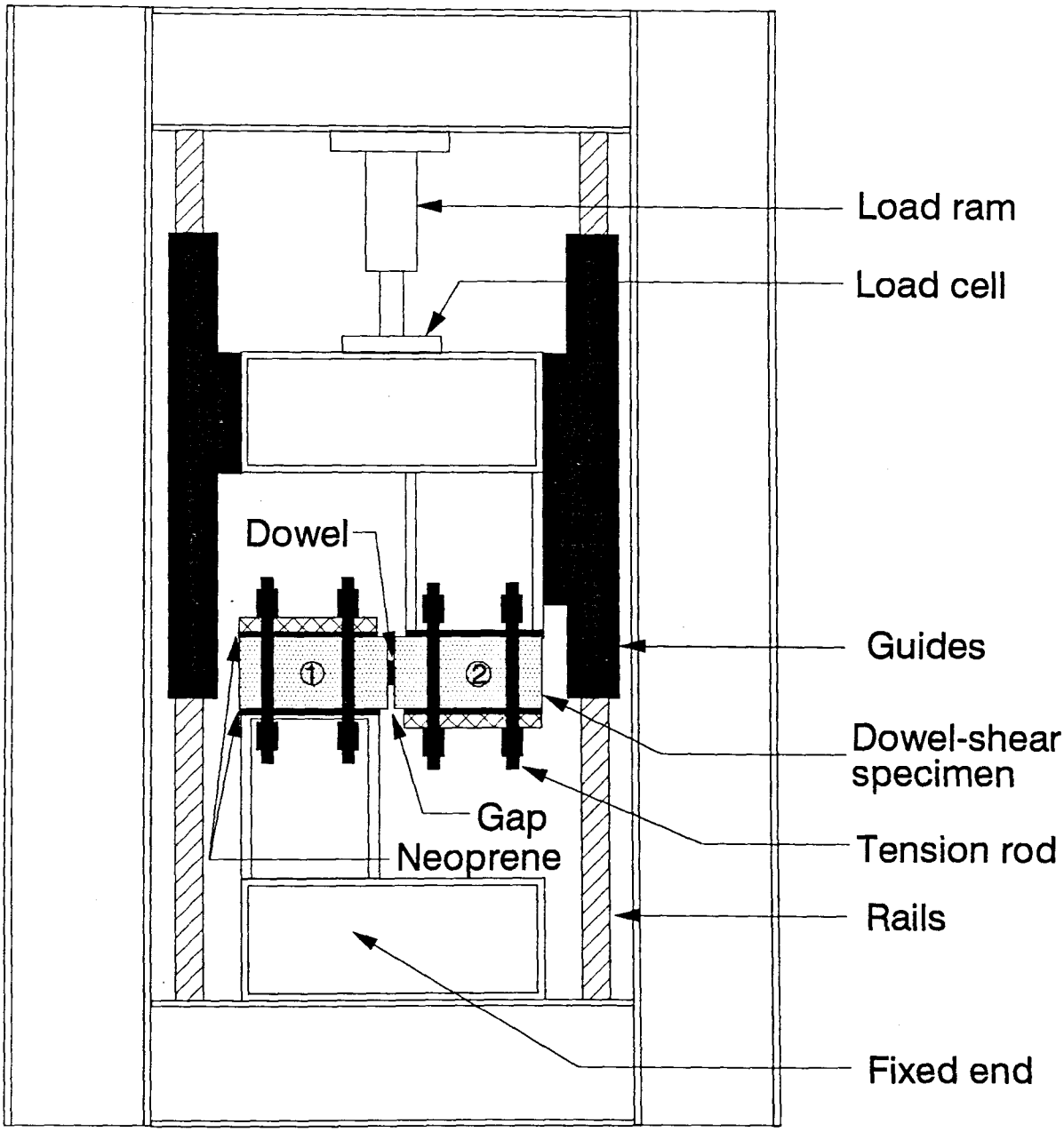

Figure 3.8. Dowel-shear frame

Iosipescu shear test [20]. The Iosipescu shear procedure was chosen as the more appropriate test method for the dowels as explained in Part 1 of this report. The testing method is similar to the way dowels are used in common practice. The dowel-shear specimen was held securely by tension rods (refer to Figure 3.8) to minimize bending and rotation of the assembly during testing. One half of the specimen (designated by Side 1 in Figures 3.2 and 3.8) was anchored to the fixed end of the frame while the force (applied by a hydraulic ram) was transferred through the other side (designated by Side 2 in Figure 3.2 and 3.8) resulting in direct shear of the dowel bar. Neoprene was used as shown in Figure 3.8 to transfer the load evenly across the face of the dowel specimen. The graphs in the Appendix, for the dowel-shear specimens, reflect the differential deflection between Sides 1 and 2 (see Figure 3.8) versus load.

3.7. Results

A description of the specimen identification system used for each test series is depicted in Figure 3.9. This identification system indicates the supplier, specimen type, specimen designation, and aging solution.

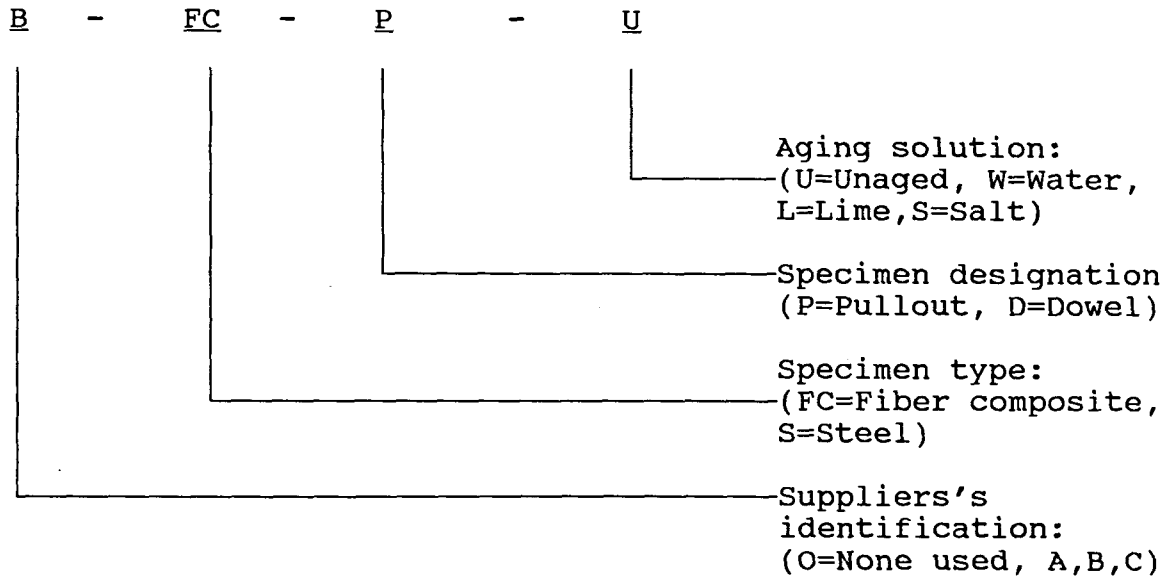

Figure 3.9. Specimen identification system

3.7.1. FC specimens under scanning electron microscope

Samples of FC rebars and dowels taken from all three aging tanks were observed under a scanning electron microscope (SEM). The concrete was split to expose the FC rebar that was in contact with the concrete. FC rebars failing in both tension and bond were examined for any etching of the glass fibers or deposition of hydration product between the glass fibers. Also a surface analysis was made to determine any degradation of the vinyl ester resin coating.

Specimens that were not tested and not aged (not exposed to concrete) were used as reference. The outer surface of an

unaged and untested FC rebar from Supplier B is shown parallel to the glass strands and magnified 500 times in Figure 3.10. The outer surface of an unaged and untested FC rebar from Supplier C is shown parallel to long direction of the rebar and magnified 100 times in Figure 3.11. A difference in glass fiber orientation between the two FC rebars is depicted in Figures 3.10 and 3.11.

Figure 3.12 shows the magnified surface (100 times) of a sample length of rebar taken from C-FC-P-L specimen that exhibited a bond failure with slight fraying of the rebar. Figure 3.12 exhibits a dense formation of hydration product (namely calcium and carbon) that covers the surface of the FC rebar.

Figure 3.12 was typical of the rest of the aged specimens and represented the surface aging of FC reinforcing bars. No etching of the glass fibers or deposition hydration product between the individual glass fibers was observed under the SEM. Therefore, the vinyl ester resin was a very effective protection for the glass fibers and aging effects exhibited by uncoated E-glass fibers (in the published references) was not present. Further studies on the affect that the hydration product (shown in Figure 3.12) had on the bond of the FC pullout specimens is presented in Section 3.7.3.

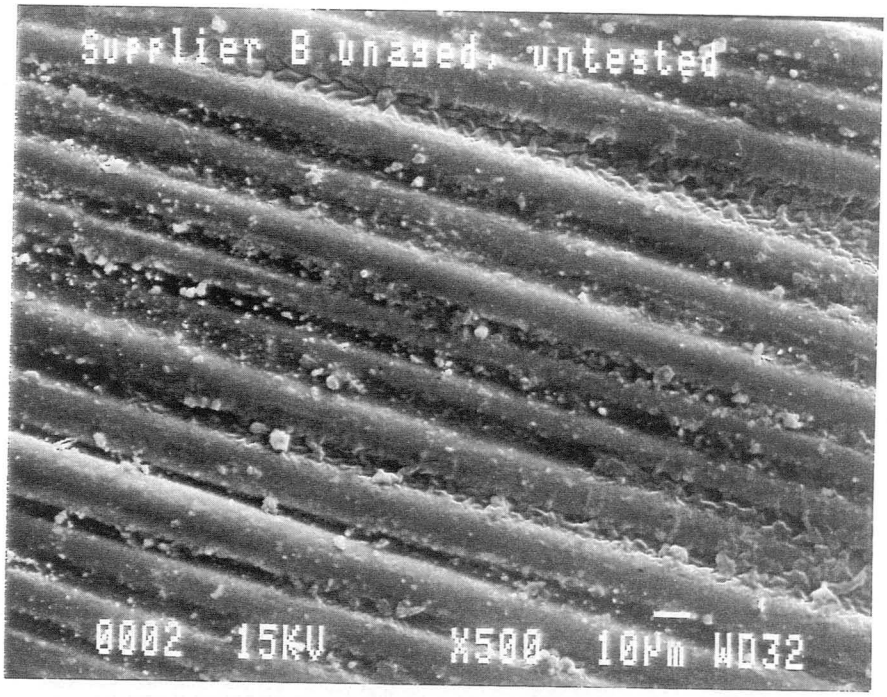

Figure 3.10. Surface microstructure of an unaged and untested B-FC-P rebar parallel to the long direction

Figure 3.11. Surface microstructure of an unaged and untested C-FC-P rebar parallel to the long direction

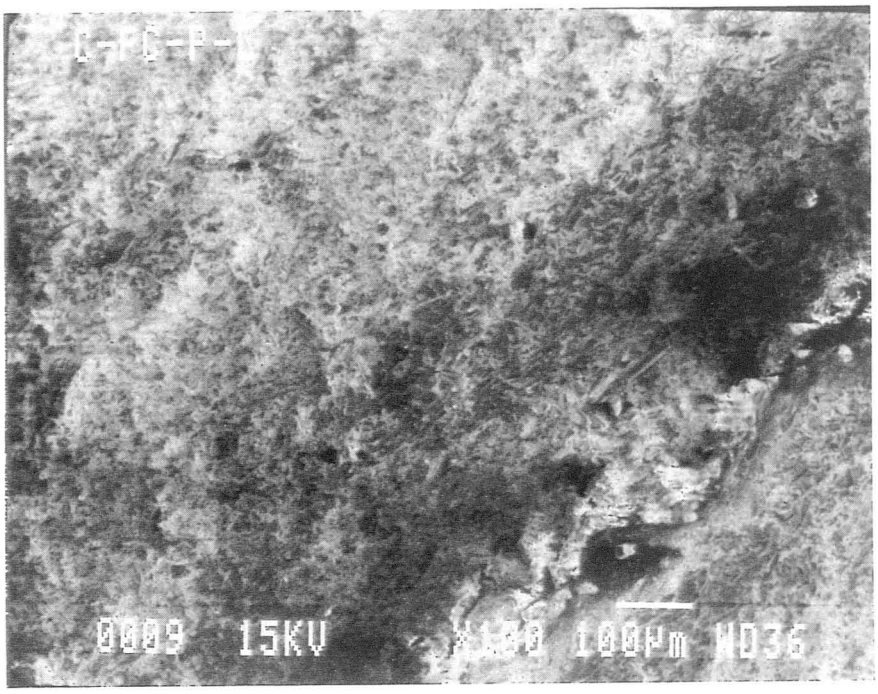

Figure 3.12. Surface microstructure of C-FC-P-L rebar

3.7.2. Chemical analysis of aging solutions

Chemical analysis was used to determine certain elements in each aging solution. The samples were taken from the baths after cooling one day. The chemical analysis was performed at the Analytical Services Laboratory at ISU. Table 3.13 exhibits the chemical composition of the each aging solution including pH, sodium, potassium, chloride, and sulphate concentrations. The pH presented in Table 3.13, for water and salt, is slightly basic (greater than 7.0) due to

possible leaching of lime from the concrete specimens. The salt solution exhibits high quantities of sodium and chloride from the reagent grade NaCl used in the aging process. For comparison purposes, Table 3.14 shows typical values of pH, sodium, potassium, chloride, and sulphate for surface water and ground water. Results from Saylorville lake and Red Rock Wells near Ames, as determined by the Analytical Services Laboratory at ISU, is presented in Table 3.14. The variability in each compound is due the change in runoff and land surface usage.

No detrimental quantities of the any compounds in Table 3.13 were present in the aging solutions (such as sulfates) that would cause problems with the concrete specimens. Potassium in ground and surface water was much less than in the aging solutions, due again to possible leaching effects.

Table 3.13. Chemical composition of aging solutions

Aging solution	water	lime	salt
pH ($-\log H^+$)	8.24	10.54	8.83
Sodium (mg/l as Na)	165	240	1980
Potassium (mg/l as K)	176	252	198
Chloride (mg/l as Cl^-)	47.4	67.5	2780
Sulphate (mg/l as SO_4^-)	37.8	53.4	68.0

Table 3.14. Chemical composition of surface and ground water

Sample location	Saylorville lake surface water	Red Rock wells groundwater
pH ($-\log H^+$])	7.0	6.66 - 7.38
Sodium (mg/l as Na)	10 - 20	10.4 - 16.9
Potassium (mg/l as K)	2.2 - 2.8	0.58 - 2.95
Chloride (mg/l as Cl^-)	28 - 36	21.3 - 26.2
Sulphate (mg/l as $SO_4^=$)	50 - 100	73.0 - 684

3.7.3. Pullout specimen results

Results of both aged and unaged tests on FC pullout specimens are presented in this section. Table 3.15 exhibits the peak loads for both aged and unaged pullout specimens. Figures 3.13 and 3.14 show a comparison of aged and unaged pullout specimens for both Suppliers A and B, respectively.

The pullout specimens (from both suppliers) exhibited some pullout (bond failure) up until the peak load. This was followed by either a final pullout of the FC rebar or a tensile failure of the rebar. The load and deflection data was similar for both final failure modes (pullout and

tensile). Aging did not alter the failure mode for the pullout specimens.

The comparisons of the B-FC-P assemblies given in Figure 3.13 depicts an increase in peak load (see Table 3.15) after aging although the deflections stay relatively the same (a slight decrease is noticed). This indicates that something other than degradation of the glass fibers is occurring. This could possibly be due to expansion of the FC rebars during the aging process.

The comparisons of the C-FC-P assemblies given in Figure 3.14 shows a slight decrease in average peak (see Table 3.15) load due to aging for lime and salt solutions but shows a significant decrease in strength due to aging in water. Also, slight decreases in deflections at peak load are observed. The general shape of the curves remained relatively the same within a particular aging solution.

While observing Supplier C's FC rebars, that were aged in water, under the SEM there was no noticeable degradation of the individual glass fibers. Hydration product seemed to be relatively dense on the surface, but was not observed within the glass fibers.

Figure 3.11 shows very random orientation of fibers for Supplier C as opposed to Supplier B. Perhaps this randomness could possibly be associated with a corresponding lack of complete glass fiber coating protection, such as would be

Table 3.15. Peak loads for pullout specimens

Assembly	Trial 1 peak load (lbs)	Trial 2 peak load (lbs)	Trial 3 peak load (lbs)	Trial 4 peak load (lbs)	Trial 5 peak load (lbs)	Avg. peak load (lbs)
B-FC-P-U (mode)	5968 (PF)	7865 (PF)	6955 (TF)	6668 (TF)	6398 (PF)	6771 (NA)
B-FC-P-W (mode)	9896 (PF)	10331 (PF)	10071 (PF)	10629 (TF)	10000 (PF)	10185 (NA)
B-FC-P-L (mode)	9165 (TF)	9232 (PF)	8530 (PF)	10267 (TF)	7836 (PF)	9006 (NA)
B-FC-P-S (mode)	10138 (PF)	8152 (PF)	10093 (TF)	* (NA)	* (NA)	9461 (NA)
C-FC-P-U (mode)	12117 (TF)	12275 (PF)	9940 (PF)	10969 (PF)	11115 (PF)	11283 (NA)
C-FC-P-W (mode)	6698 (PF)	7512 (TF)	4767 (PF)	5931 (PF)	6293 (TF)	6240 (NA)
C-FC-P-L (mode)	7888 (TF)	8779 (TF)	12132 (PF)	12398 (PF)	10206 (PF)	10281 (NA)
C-FC-P-S (mode)	12388 (PF)	8995 (TF)	9767 (TF)	10382 (TF)	11061 (PF)	10519 (NA)

found in the uniform, straight fiber orientation. Thus, this possible lack of coating protection for Supplier C's rebar may be a hypothetical reason for the significant deterioration in strength due to aging in the bath solution for the C-FC-P series. Also, note that test results for the series aged in the water bath have divergent results possibly reinforcing this hypothesis of possible random aging of some exposed fibers.

Table 3.15 also exhibits the failure mode for the

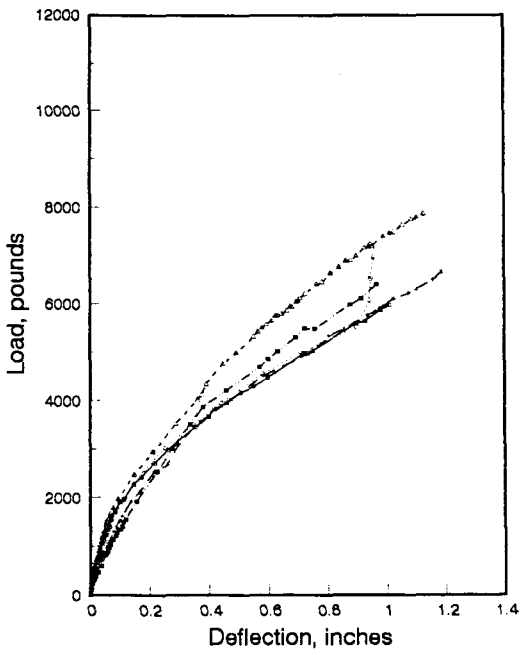

Unaged

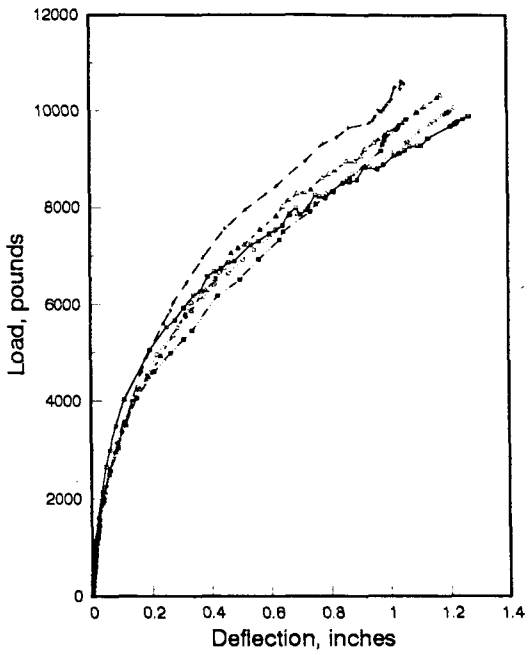

Aged in water

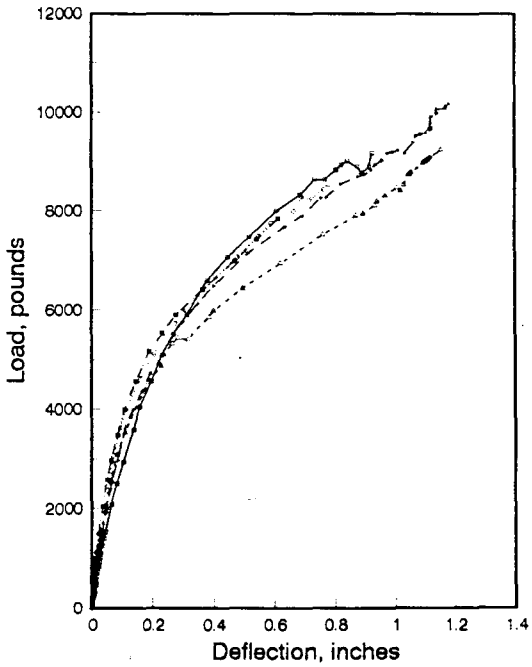

Aged in lime

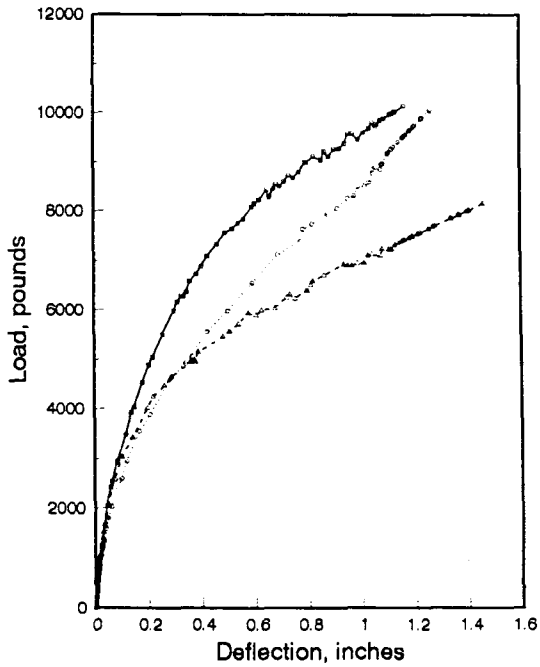

Aged in salt

Figure 3.13. Comparison of aged and unaged B-FC-P assemblies

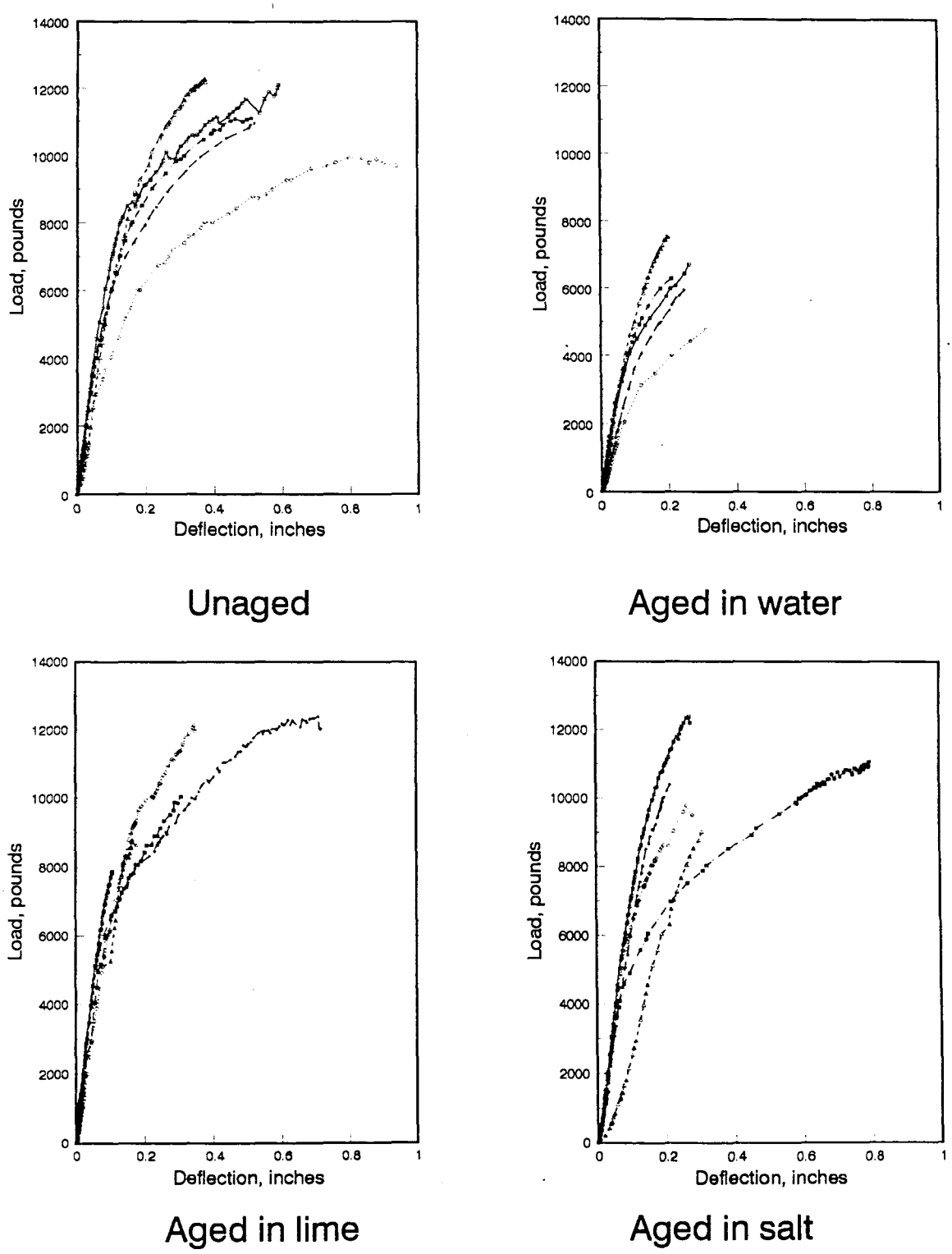

Figure 3.14. Comparison of aged and unaged C-FC-P assemblies

pullout specimens. Either a pullout failure or a tensile failure was observed in the pullout tests. TF indicates a tensile failure and PF indicates a pullout failure, as presented in Table 3.15.

A pullout specimen is shown in Figure 3.15. The load versus deflection data given in the Appendix for the pullout specimens (as explained previously in Section 3.6) is a result of load applied to the pullout specimen, and an average deflection at the gap (Points 3 and 4 in Figures 3.7 and 3.15). The bond slip was monitored at the ends of the pullout specimens (Points 1 and 2 in Figures 3.7 and 3.15).

The deflection at the gap is the sum of bond slip (at Points 1 and 2 in Figure 3.15) and tensile elongation of the FC reinforcing bar. The theoretical relationship for the tensile elongation of the reinforcing bars is given by Equation 3.6.

$$\delta = \frac{P_t L_b}{E A_{FC}} \qquad \text{Eqn. 3.6}$$

where:

- δ = tensile elongation (deflection) of the FC rebar (in.)
- P_t = load applied to the FC specimen (lbs)
- L_b = length of the rebar not bonded to the concrete that is under tension (in.)
- E = tensile modulus of elasticity for the FC rebar found in Table 3.3 (psi)
- A_{FC} = Area of the FC rebar found in Table 3.3 (in^2)

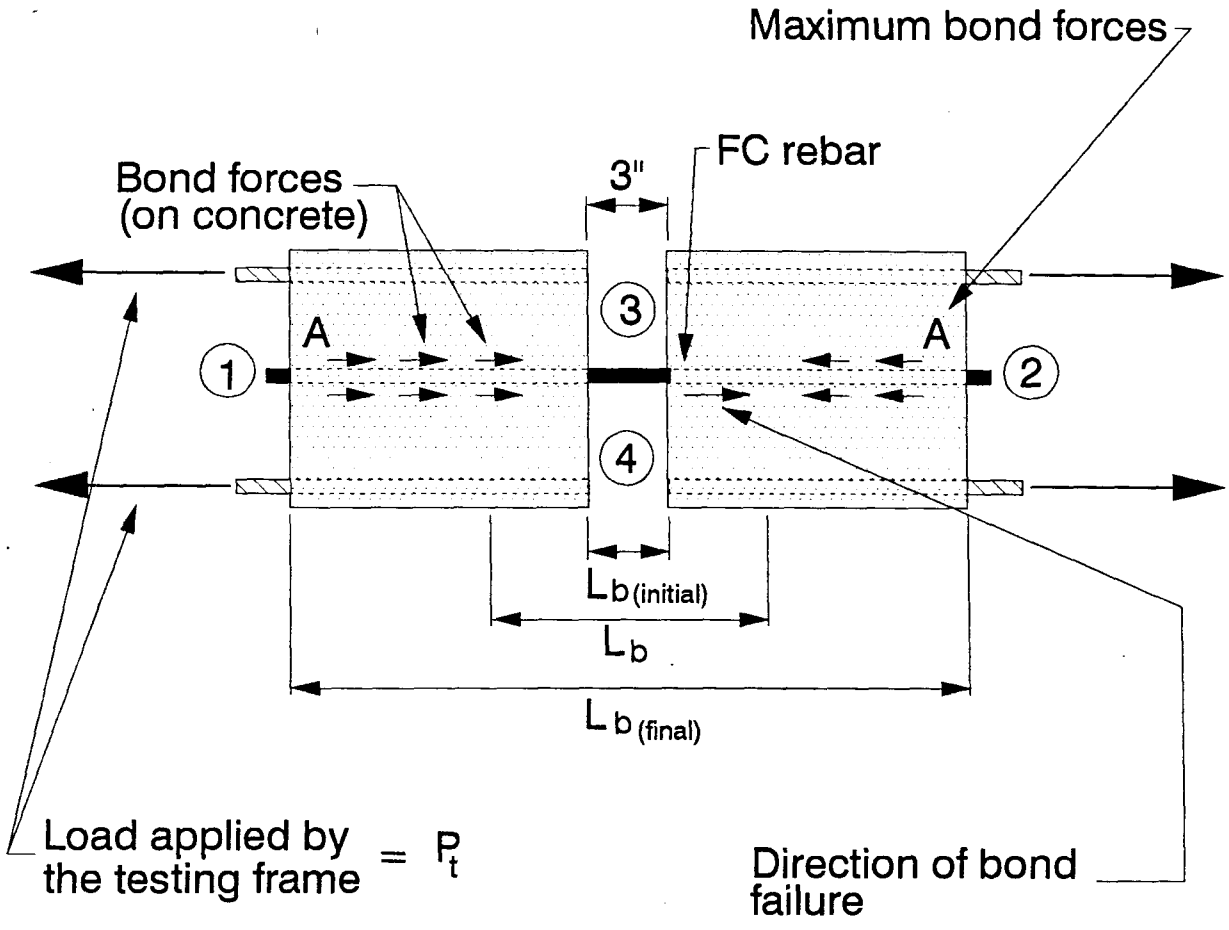

Deflection of pullout specimens:

$$\frac{③ + ④}{2} = \text{Gap deflection}$$

$$\frac{P_t L_b}{E A_{FC}} + ① + ② = \text{Approximate gap deflection}$$

$$\frac{U L_b}{E A_{FC}} = \text{Loss in deflection due to bond}$$

Figure 3.15. Bond failure for the pullout specimens

The value of L_b (see Figure 3.15) increases throughout the test as the load P_t is increased. Length, L_b is initially equal for both Suppliers B and C rebars (3-inch gap length). As the load increases, bond continues to fail from the gap (center of the specimen) outward (see Figure 3.15). The bond did not fail at equal rates on both sides of the specimen. Therefore, the actual value was not known during the test. The length, L_b (length of rebar in tension), could be initially approximated as three inches (the gap dimension in Figure 3.15). As the bond failure progressed, the value of L_b increased on both sides of the specimen (certain specimens exhibited bond failure on only one side). When end slip was noticed at one end of the specimen (the bond had failed over the entire length of the specimen side) the length (L_b) could be approximated as 13 inches for Supplier B and 10 inches for Supplier C. Finally, when end slip was noticed on both sides of the specimen the length could be approximated as 23 inches for Supplier B and 17 inches for Supplier C.

When end slip is noticed on one side of the specimen, the value of L_b assumes that the surface of the rebar is completely free from bonding to the concrete except for all but a small portion shown at Point A in Figure 3.15. Therefore, the value of L_b (the length of the rebar in tension) can be taken as the gap length plus the length of one side of the pullout specimen. When end slip is noticed

both sides of the specimen, L_b can be approximated as the gap length plus the length of rebar on both sides of the pullout specimen.

Using these values of L_b in Equation 3.6, a deflection due to tensile forces could be determined. This added to the deflection at Points 1 and 2 gave an approximated total deflection at the gap.

The approximated deflection versus load is plotted with the actual deflection versus load in Figures 3.16 and 3.17. These are typical curves for unaged pullout specimens, both Suppliers B and C. The approximated curve (Curve B, in Figures 3.16 and 3.17) exhibits good correlation to the actual curve (Curve A, in Figures 3.16 and 3.17). Typical curves for pullout specimens aged in water, lime, and salt are shown in the Appendix (Figures A23 through A28).

There is only slight variation in Figure 3.16 between the approximated deflection and actual deflection for the B-FC-P-U assembly (measured at the gap). The trend for the aged B-FC-P specimens in the Appendix (Figures A23 through A25) is for the approximated load-deflection values to exceed the actual load-deflection values. The author feels that this is due to increased mechanical anchorage (where L_b is not equal to the entire rebar length in tension). The increased mechanical anchorage may account for the increased deflections at peak load in Figure 3.13 (due to aging) and

may be caused by the dense formation of hydration product on the surface of rebar as shown in Figure 3.12. The surface texture is relatively smooth for unaged rebars from Supplier B, but the formation of hydration product created a rough surface, therefore, increasing the bond.

The opposite effect is exhibited by the C-FC-P assemblies. A slight decrease in peak load and deflections at peak load due to aging (as shown in Figure 3.14) for the salt and lime bathes can be observed and a corresponding significant decrease in load is shown for the water bath. As shown in Figure 3.17 and the Appendix (Figures A26 through A28), the trend is towards a slight decrease in mechanical anchorage due to aging effects (curves move closer together). The surface texture (see Figure 3.11) is relatively rough for an unaged specimen but the possible aging in the water for random orientation of fibers near the surface as discussed in Section 3.7.3, may have completely offset any potential surface roughness benefits.

The value of the average bond strength is given by U in Equation 3.7. The average bond strength can be determined by integrating the bond stresses over the length of the rebar in concrete. Equation 3.7 in Figure 3.15 could be used to obtain an approximation of the loss in deflection due to bond forces.

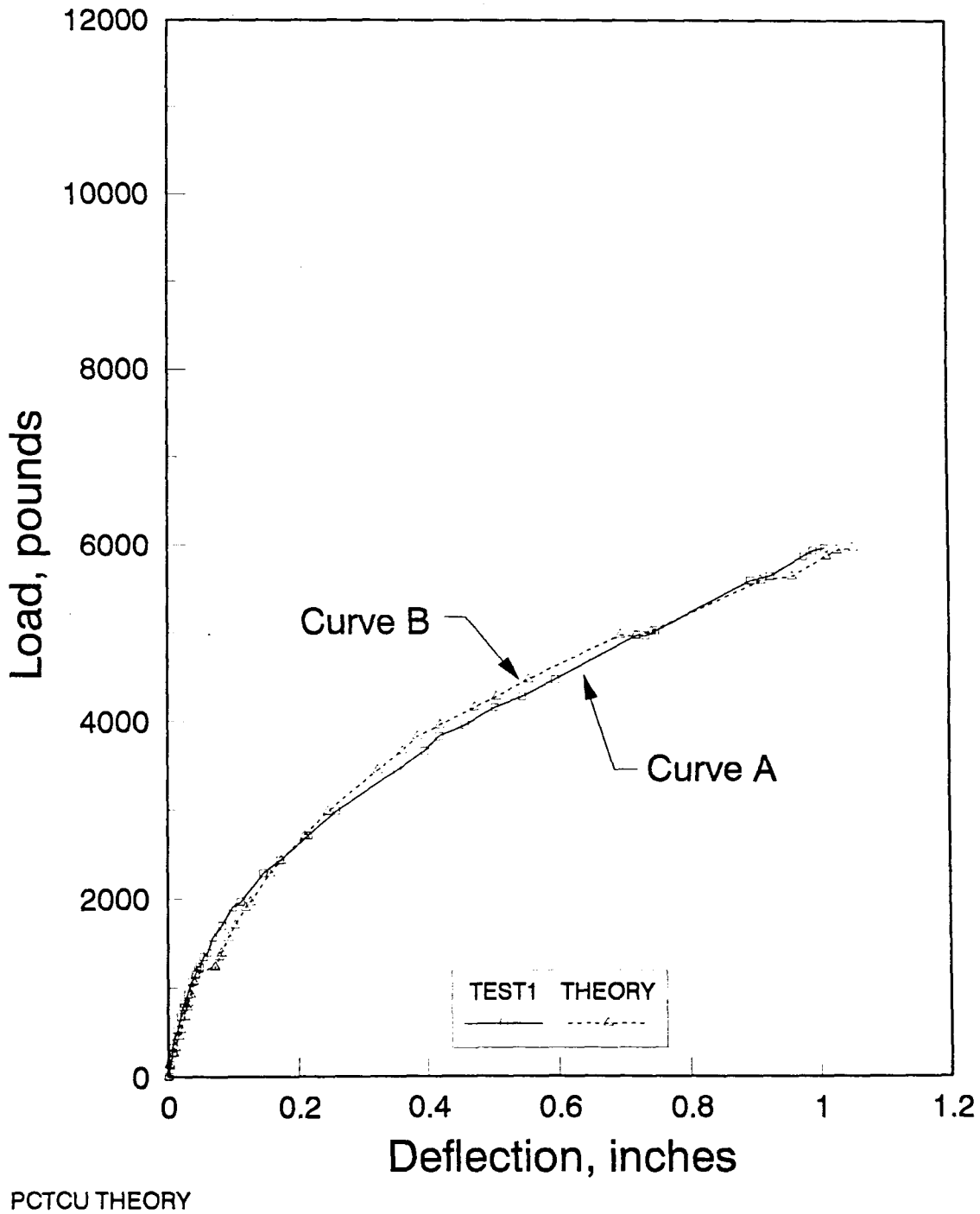

Figure 3.16. Comparison of approximated and experimental load-deflection curves for B-FC-P-U assembly

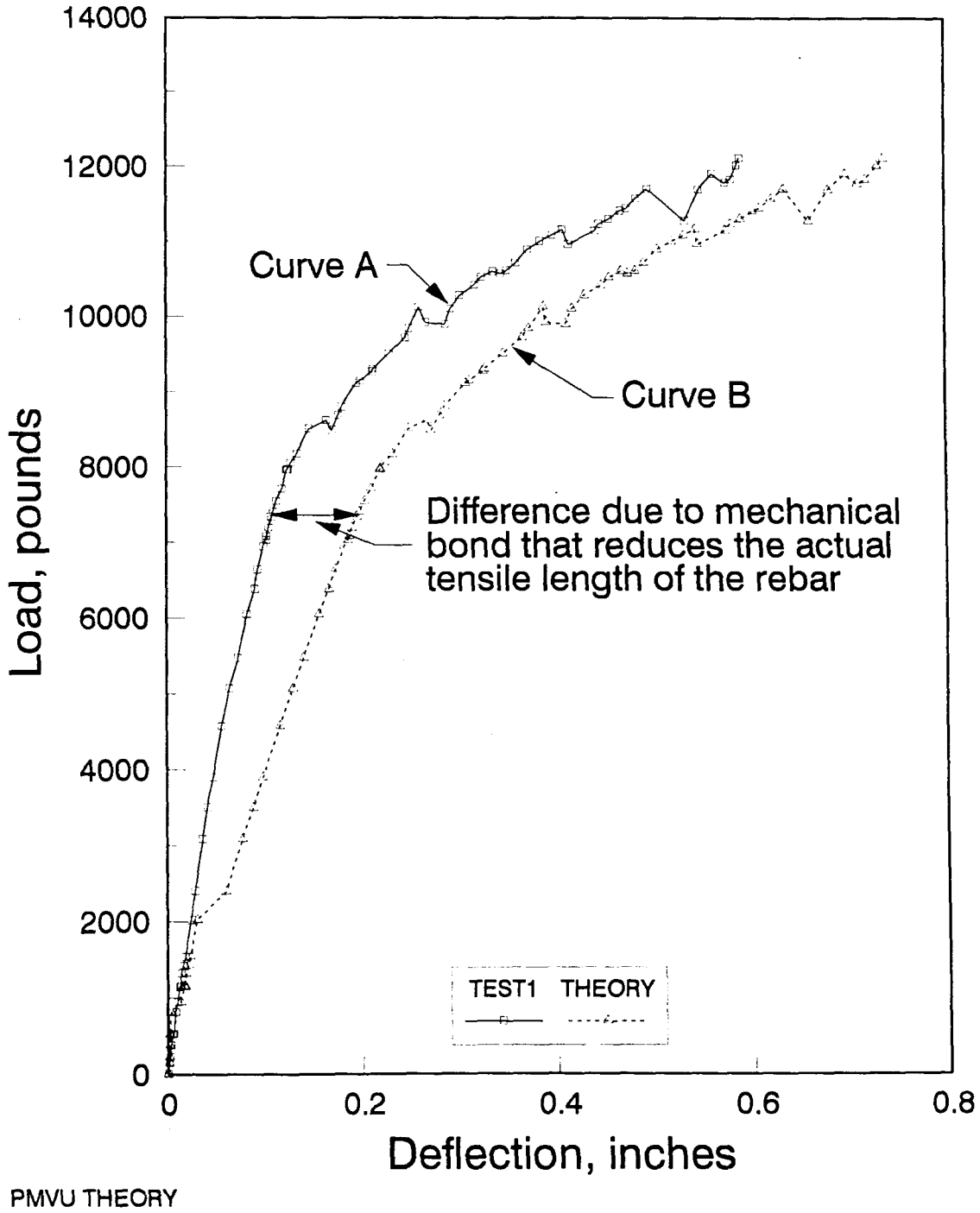

Figure 3.17. Comparison of approximated and experimental load-deflection curves for C-FC-P-U assembly

$$\delta_U = \frac{UL_b}{EA_{fc}} \qquad \text{Eqn. 3.7}$$

where:

δ_u = loss in deflection due to bond forces (in.)
U = average bond strength (lbs)

In Figure 3.17, the "Curve A" is found by Equation 3.8:

$$\frac{DEFL3 + DEFL4}{2} \qquad \text{Eqn. 3.8}$$

where:

DEFL3 = deflection at Point 3 in Figure 3.15 (in.)
DEFL4 = deflection at Point 4 in Figure 3.15 (in.)

whereas, the "Curve B" is found by Equation 3.9:

$$\frac{P_t L_b}{EA_{FC}} + DEFL1 + DEFL2 \qquad \text{Eqn. 3.9}$$

where:

DEFL1 = deflection at Point 1 in Figure 3.15 (in.)
DEFL2 = deflection at Point 2 in Figure 3.15 (in.)

The difference in these values reflect the contribution by Equation 3.7. Therefore, the total approximated deflection at the gap can be given by Equation 3.10.

$$\frac{DEFL3 + DEFL4}{2} = \frac{P_t L_b}{EA_{FC}} - \frac{UL_b}{EA_{FC}} + DEFL1 + DEFL2 \qquad \text{Eqn. 3.10}$$

The value of average bond strength will increase as the mechanical anchorage increases. Therefore, a higher bond strength will decrease the approximated deflection in Equation 3.9. This would cause the approximated curve to more closely represent the actual curve in Figure 3.17 (for an unaged specimens).

Additional approximated curves for the aged pullout specimens are very representative of the actual curves - see the Appendix. Therefore, no apparent degradation in the FC's tensile modulus of elasticity (E) was observed. This comparison procedure also verifies the areas and modulus of elasticities given in Tables 3.3 that were used in Equation 3.6.

3.7.4. Dowel specimen results

The peak loads were considered to be the maximum load obtained during testing. This peak load was considered as not representing an ultimate load for the dowel specimens. The Reasonably Expected Elastic Loads (REEL) are taken from the graphs in the Appendix. The REEL values indicate the end of the elastic region (initial straight line portion of the graph) and the start of the inelastic region. As will be discussed in Section 5.0, the REEL load marked the beginning of the concrete cracking. This concrete failure was

restrained by the clamping forces applied by the testing frame, and an increase in load was observed. The REEL loads will therefore be taken as the maximum usable loads.

Table 3.16 exhibits REEL load data for aged and unaged FC and steel dowel specimens. The failure modes observed during testing are shown in Figure 3.18. These failure modes occurred at or near the REEL load for both steel and FC dowel specimens. The crack propagation (see Figure 3.18) started at the gap in the dowel specimen on the compressive sides of the dowels. The length (given as L_c in Figure 3.18) of the initial crack was different for steel and FC dowels. The measured average L_c was 3.0 inches for the FC dowels and 5.5

Table 3.16. REEL loads for dowel specimens

Assembly	Trial 1 REEL load (lbs)	Trial 2 REEL load (lbs)	Trial 3 REEL load (lbs)	Trial 4 REEL load (lbs)	Trial 5 REEL load (lbs)	Avg. REEL load (lbs)
A-FC-D-U	13106	11035	11822	11925	13036	12185
A-FC-D-W	12061	11902	12038	11274	*	11819
A-FC-D-L	11461	13442	11662	12373	10643	11916
A-FC-D-S	12519	12872	12758	14367	13177	13139
O-S-D-U	20328	19985	23556	25433	24155	22691
O-S-D-W	21447	21185	23376	22210	26299	22903
O-S-D-L	24078	19532	25319	20769	22064	22352
O-S-D-S	25754	21102	23953	19335	22150	22459

inches for the steel dowels.

The REEL loads given in Table 3.16 are for 1.25-inch FC and 1.50-inch steel dowel bars cast in concrete. Therefore, a direct comparison can not be made between the FC and steel dowels due to the different diameter. A possible adjustment can be made to the 1.25-inch FC dowels that would scale the REEL load up to an equivalent 1.50-inch diameter FC dowel.

Figures 3.19 and 3.20 give a comparison between aged and unaged FC and steel dowels, respectively. The FC dowel specimens exhibited a very slight decrease in average REEL load due to aging in both water and lime but increased slightly in the salt aging solution. The slight increase in concrete compressive strengths for the aged dowel specimens (see Table 3.2) may have helped maintain the REEL loads after aging. Figure 3.19 shows the trend towards a smaller increase in load after the initial drop in load. As shown in Figure 3.20, the steel dowel specimens exhibited almost no change in REEL load. Overall, the accelerated aging solutions of water, lime, and salt apparently had little or no affect on any of the dowel bar series.

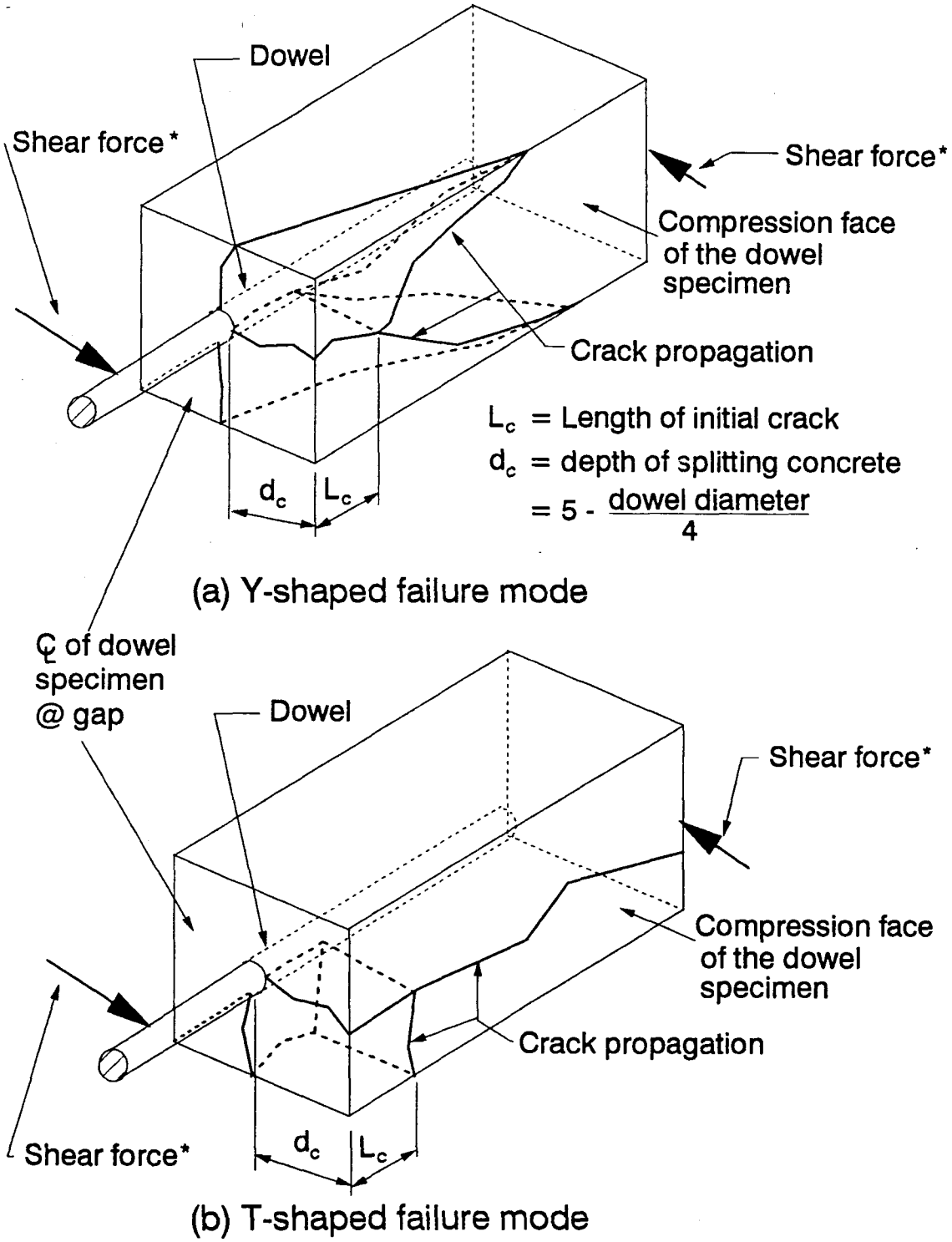

* Only applied forces shown, equilibrium forces from test apparatus are ommitted for clarity.

Figure 3.18. Splitting failure modes for the dowel specimens

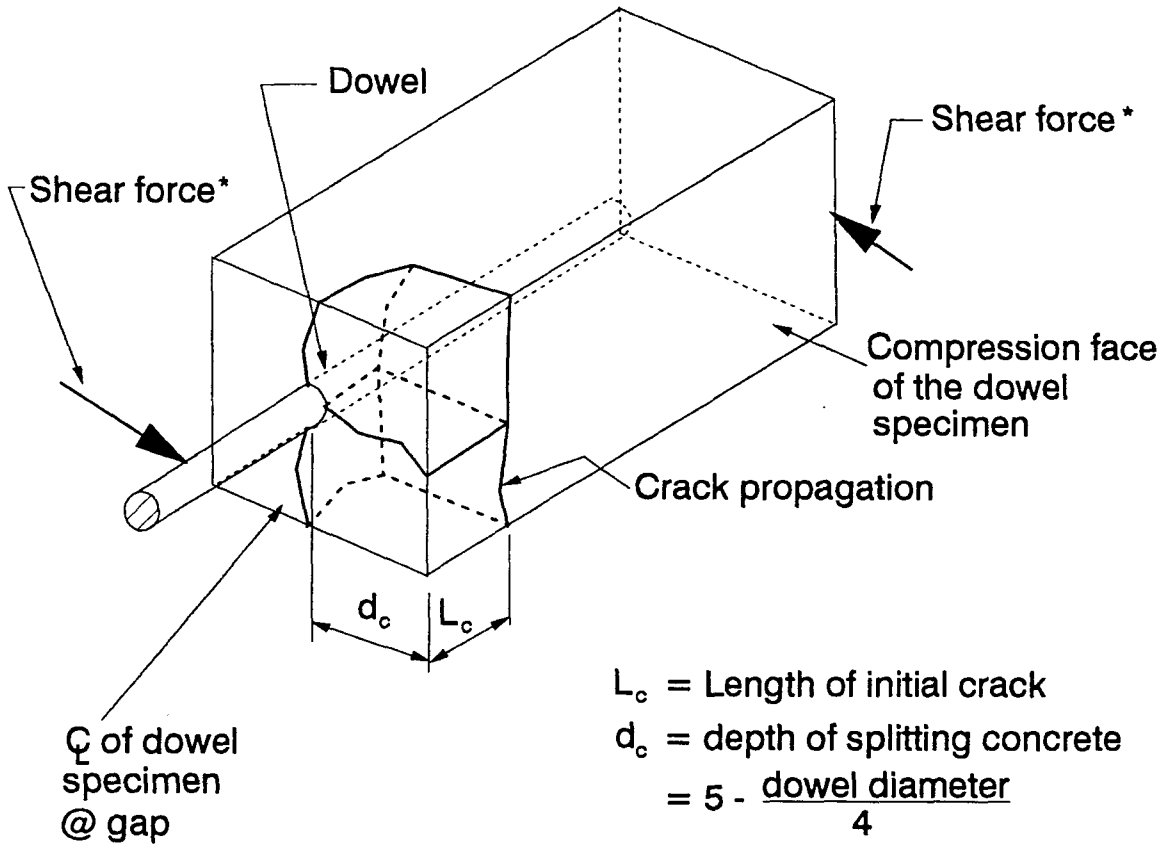

(c) Block-shaped failure mode

* Only applied forces shown, equilibrium forces from test apparatus are ommitted for clarity.

Figure 3.18. Continued

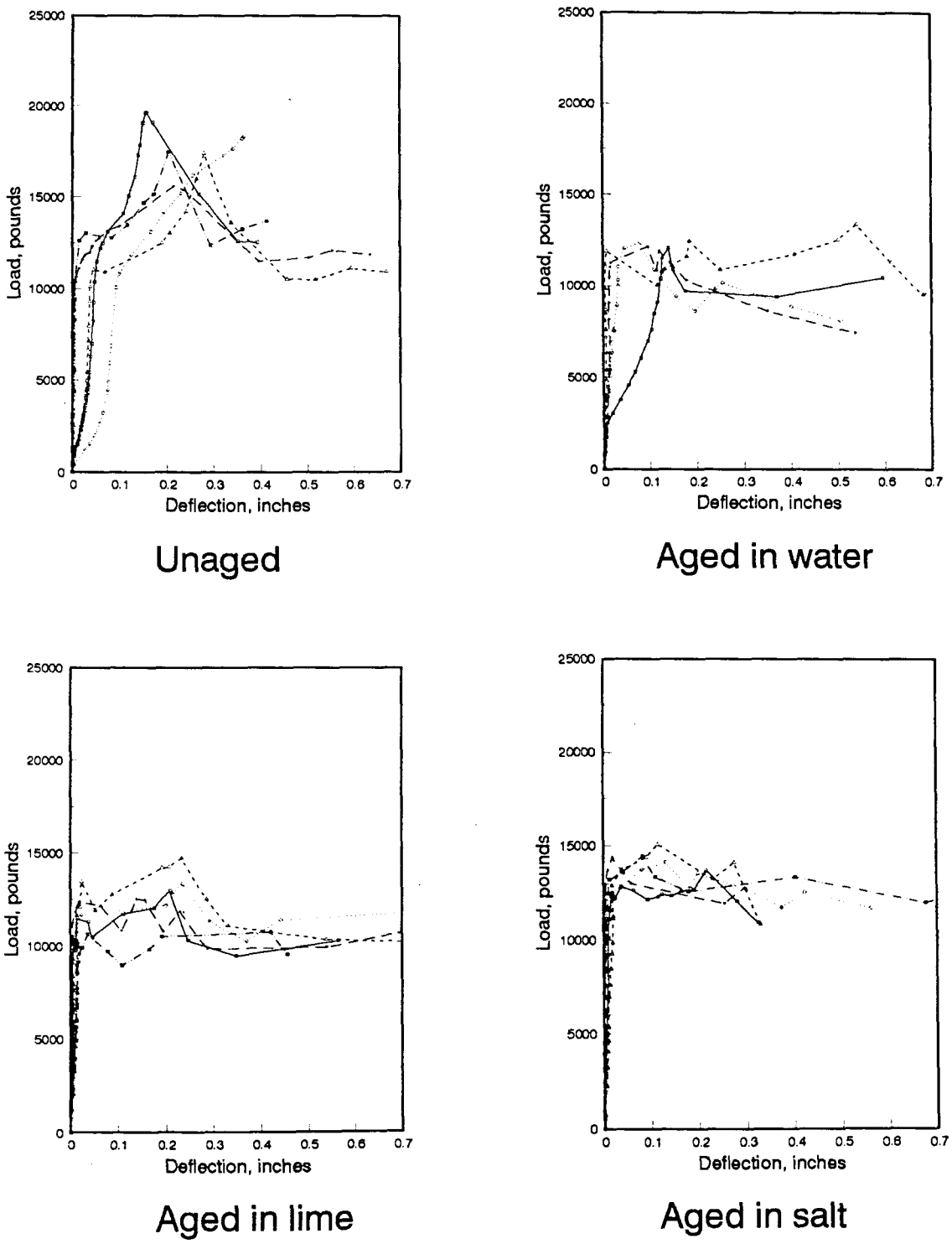

Figure 3.19. Comparison of aged and unaged A-FC-D assemblies

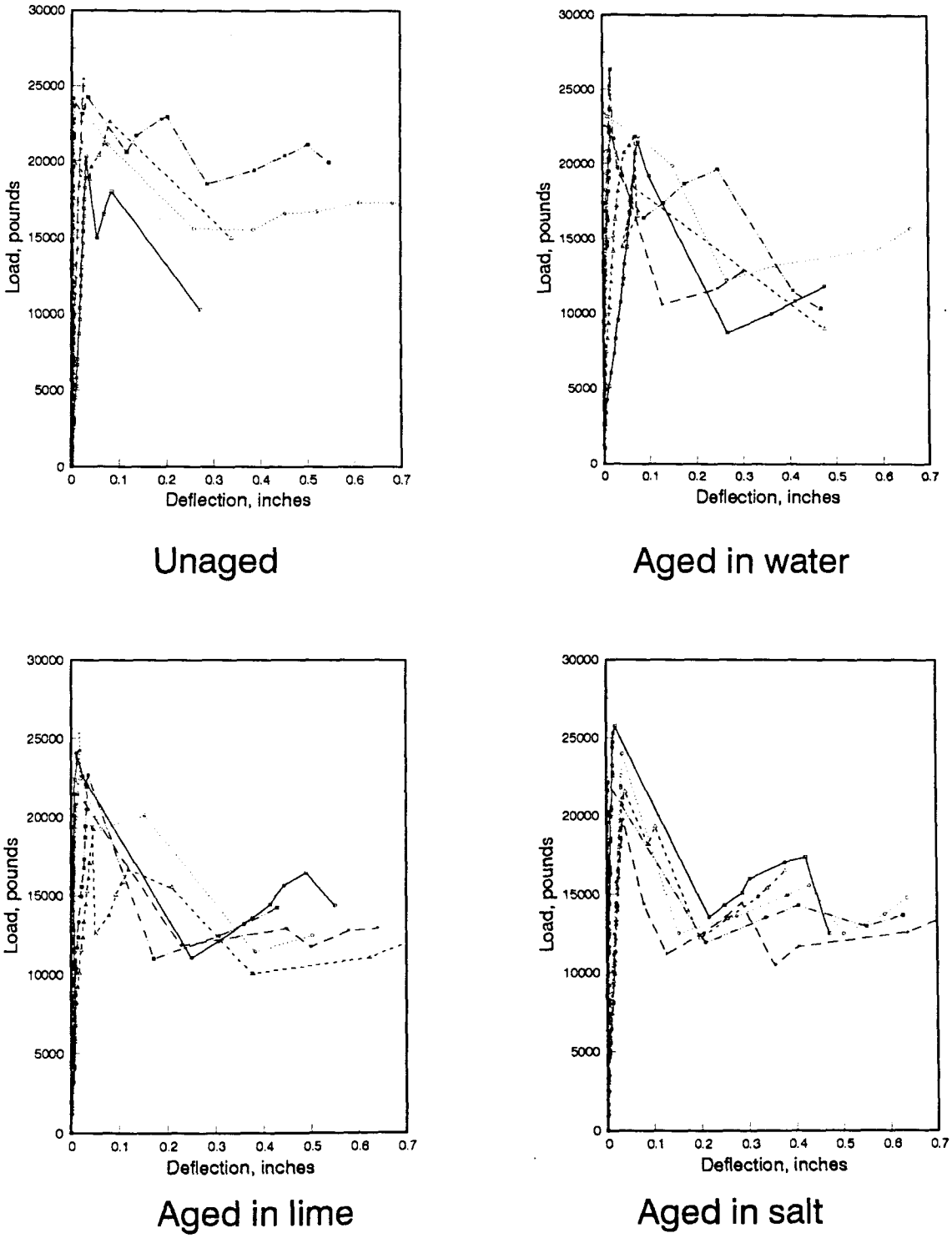

Figure 3.20. Comparison of aged and unaged O-S-D assemblies

CHAPTER 4. DEVELOPMENT OF FAILURE MECHANISMS FOR DOWEL SPECIMENS

4.1. Truncated Pyramid Concrete Failure

Figure 4.1 shows truncated failure mode mechanisms. Note in Figure 4.1, that subfigures for the isolated pyramidal surfaces have been rotated when drawn separately from the specimens for use of showing the dimensions.

The failure surface of the concrete may be in the form of a truncated pyramid as shown in Figure 4.1a. The sides of the truncated pyramid form 45-degree angles with the planar surface adjacent to the dowel bar. This failure mechanism considers that the entire length, Y for the concrete pyramidal element (see Figure 4.1a), is under uniform tension. For this case, the tensile strength exhibited by the concrete is given by Equation 4.1 [22].

$$P_c = \mu\sqrt{f'_c}(2.8A_{slope} + 4A_{flat}) \qquad \text{Eqn. 4.1}$$

where:

P_c = the nominal tensile strength of a concrete pyramidal element (lbs)

μ = factor specifying the type of concrete (ie., 1.0 for normal weight, 0.85 for sand-lightweight, and 0.75 for all-lightweight)

A_{slope} = surface area of the 45° slope sides of the truncated pyramid in Figure 4.1 (in^2)

A_{flat} = surface area of the flat part of the truncated pyramid in Figure 4.1 (in^2)

f'_c = concrete compressive strength (psi)

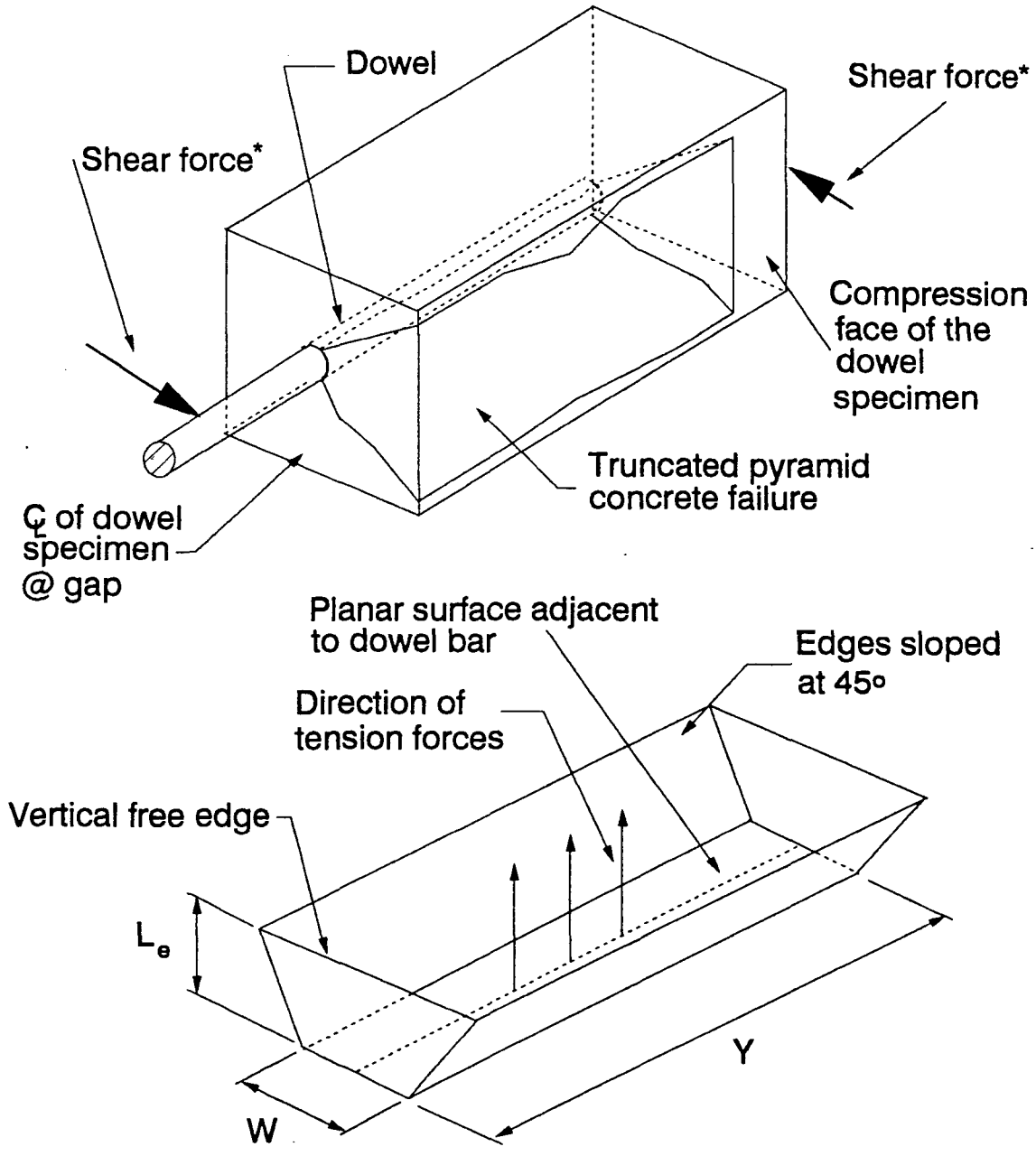

(a) Truncated pyramid concrete failure

* Only applied forces shown, equilibrium forces from test apparatus are ommitted for clarity.

Figure 4.1. Tensile-failure mechanisms for dowel bars

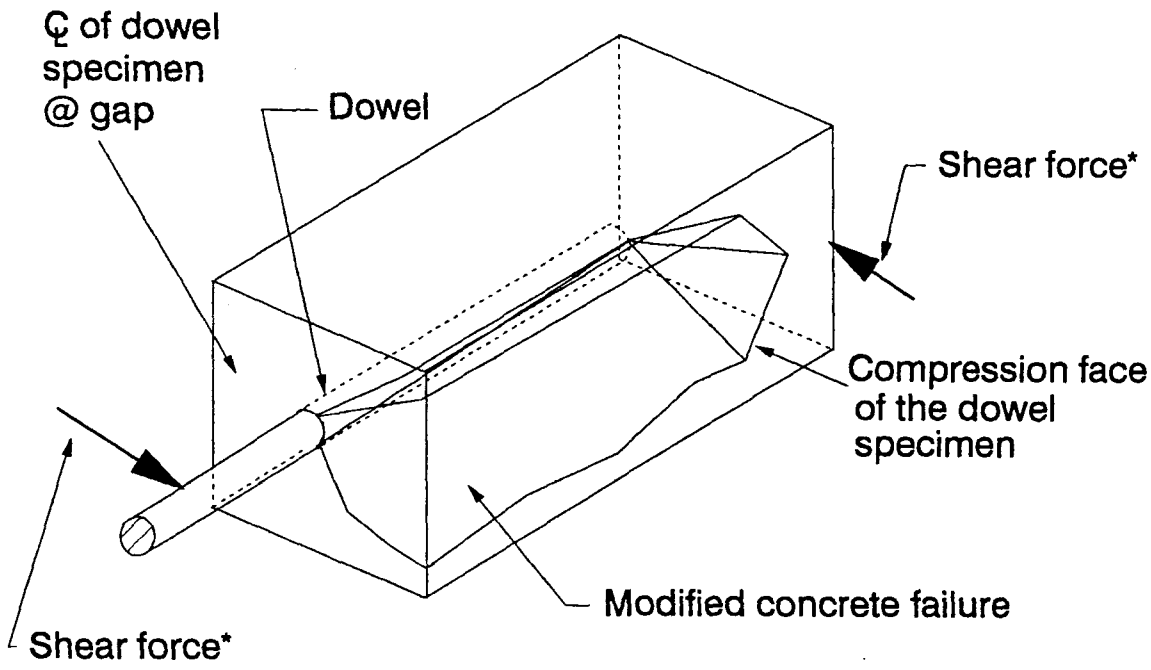

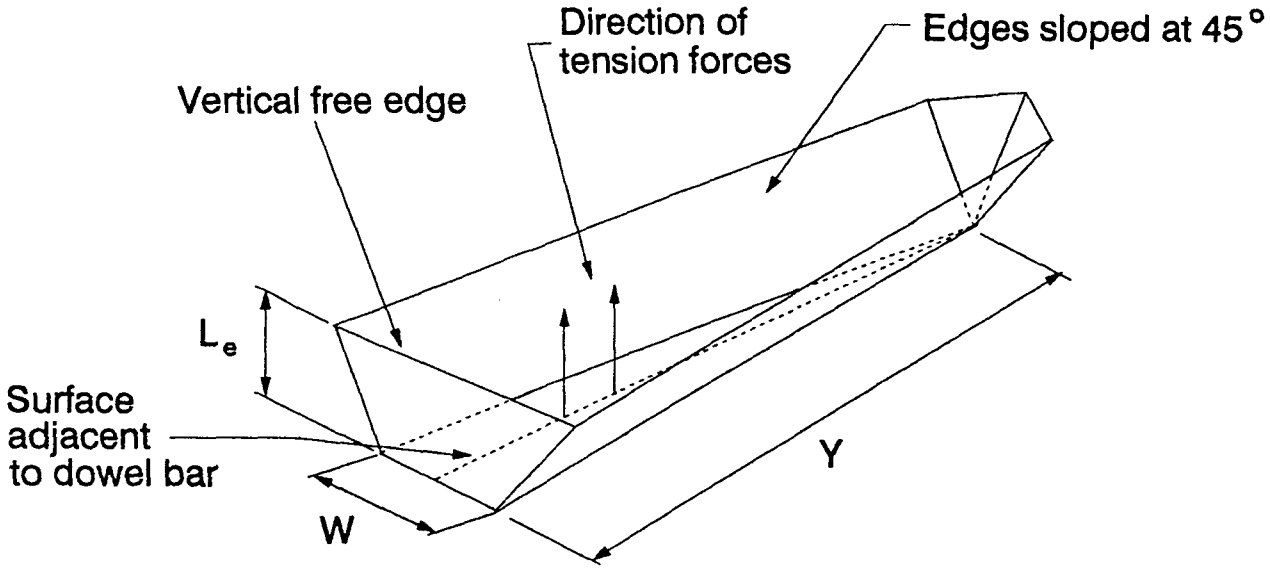

(b) Modified concrete failure

* Only applied forces shown, equilibrium forces from test apparatus are ommitted for clarity.

Figure 4.1. Continued

The area of the flat portion in Figure 4.1a is given by Equation 4.2.

$$A_{flat} = WY \qquad \text{Eqn. 4.2}$$

where:

W = width of the flat portion in Figure 4.1 (in.)
Y = length of the flat portion in Figure 4.1 (in.)

The area of the sloped portion of the truncated pyramid, excluding the vertical free edge, is given by Equation 4.3.

$$A_{slope} = 2\sqrt{2}L_eY + \sqrt{2}L_eW + 2\sqrt{2}L_e^2 \qquad \text{Eqn. 4.3}$$

where:

L_e = depth of concrete in tension (in.)

By substituting Equations 4.2 and 4.3 (A_{flat} and A_{slope}, respectively) into Equation 4.1, the concrete wedge element's strength based upon a tensile force (for dowel loading) can be shown in Equation 4.4 [22].

$$P_c = 4\mu\sqrt{f'_c}[WY + L_e(2Y+W) + 2L_e^2] \qquad \text{Eqn. 4.4}$$

The value of A_{flat} assumes that tensile forces are being developed across the flat portion of the truncated pyramid. The dowel bar (due to its presence across the flat portion) does not allow for tensile forces to develop. Therefore, the A_{flat} term in Equation 4.4 will be omitted as shown in Equation

$$P_c = 4\mu\sqrt{f'_c}\,[L_e(2Y+W)+2L_e^2] \qquad \text{Eqn. 4.5}$$

4.2. Modified Concrete Failures

The development of Equations 4.4 and 4.5 (except across the curved dowel portion) considered uniform tension across the length, Y. The loading seen by the dowel bars is given in Part 1 of this report and is a maximum at the face of the joint (vertical free edge in Figure 4.1). The load decreases as the distance from the face of the joint increases. The resulting rotation by the dowel bar allows the dowel to fully push out the pyramid as a mechanism, as shown in Figure 4.1b.

The development of the concrete tensile strength is based on Equation 4.1. A_{flat} and A_{slope} are determined from Figure 4.1b, and given in Equations 4.6 and 4.7, respectively.

$$A_{flat} = \frac{1}{2}WY \qquad \text{Eqn. 4.6}$$

$$A_{slope} = 2\sqrt{2}L_e\sqrt{\frac{1}{4}W^2 + Y^2} + \sqrt{3}L_e^2 \qquad \text{Eqn. 4.7}$$

Using the same reasoning that the tensile strength can not be developed across a circular surface then zero will be substituted for the A_{flat} term in Equation 4.1. By eliminating the A_{flat} term and substituting Equation 4.7 for A_{slope} into Equation 4.1 gives Equation 4.8.

$$P_c = 2\mu\sqrt{f'_c}\,[4L_e\sqrt{\frac{1}{4}W^2 + Y^2} + 1.4\sqrt{3}L_e^2] \qquad \text{Eqn 4.8}$$

4.2.1. FC dowel specimens

Using typical values from the unaged FC dowel specimens and applying them to Equations 4.5 and 4.8 gives a comparison between the two equations. Typical values include:

W = 1.25 in.
Y = 3 in. (same as L_c value in Figure 3.18)
L_e = 4.69 in.(distance from midheight of dowel)
μ = 1.0 (normal weight concrete)
f'_c = 7090 psi (from Table 3.2)

Applying these values to Equation 4.5 gives the following results:

$$P_c = 4(1)\sqrt{7090}\,[4.69(2(3) + 1.25) + 2(4.69)^2]$$

$$P_c = 26271\ lbs$$

Applying these values to Equation 4.8:

$$P_c = 2(1)\sqrt{7090}\,[4(4.69)\sqrt{\frac{1}{4}1.25^2 + 3^2} + 1.4\sqrt{3}(4.69)^2]$$

$$P_c = 18664\ lbs$$

Therefore, Equation 4.8 gives the lower value of concrete failure under a tensile load.

4.2.2. Steel dowel specimens

Using typical values for the unaged steel dowel specimens which include:

W	= 1.5 in.
Y	= 5.5 in. (same as L_c in Figure 3.18)
L_e	= 4.63 in.(distance from midheight of dowel)
μ	= 1.0 (normal weight concrete)
f'_c	= 7090 psi (from Table 3.2)

Applying these values to Equation 4.5 gives the following results:

$$P_c = 4(1)\sqrt{7090}\,[4.63(2(5.5) + 1.5) + 2(4.63)^2]$$

$$P_c = 33933\ lbs$$

Applying these values to Equation 4.8:

$$P_c = 2(1)\sqrt{7090}\,[4(4.63)\sqrt{\frac{1}{4}1.5^2 + 5.5^2} + 1.4\sqrt{3}\,(4.63)^2]$$

$$P_c = 26066\ lbs$$

Therefore, Equation 4.8 gives the lower value of concrete failure under a tensile load for the steel dowel specimens. Using the 9-inch length for Y in Equations 4.5 and 4.8 does not cause the results to vary significantly between steel and FC dowel specimens. Therefore, the author believes that the length Y must be adjusted according to dowel type (steel or FC) to accommodate the slightly different failure modes as observed during experimental testing. The value of L_c as shown in Figure 3.1 was different for both steel and FC dowel specimens.

4.3. Split Cylinder Test

The split cylinder test (ASTM C496 [29]) is used commonly to determine the splitting tensile strength of concrete. Figure 4.2 illustrates the split cylinder test setup. The failure of the concrete in the dowel specimens during testing is considered to occur similar to that of the split cylinder test.

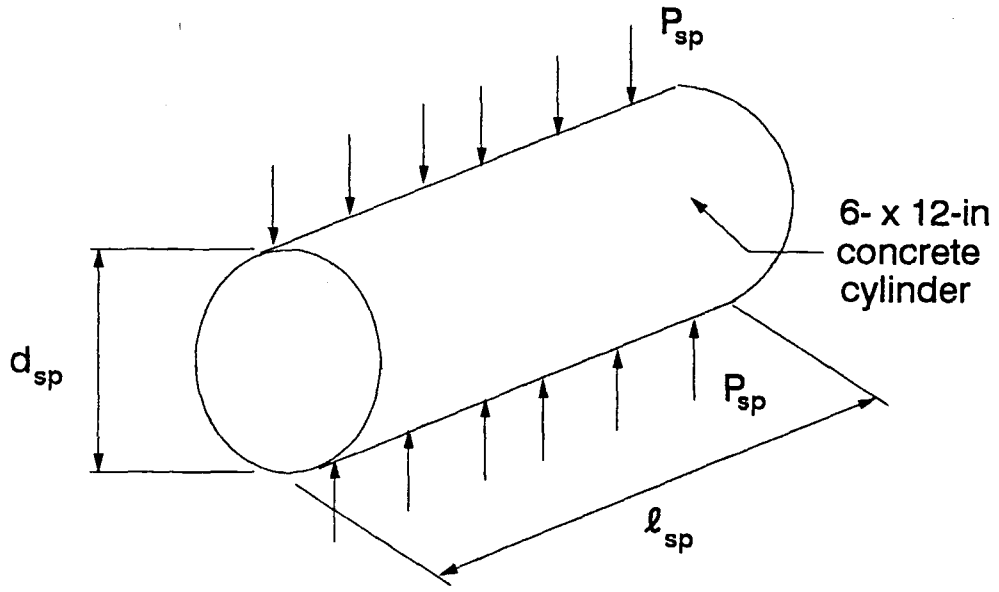

Figure 4.2. Split cylinder test [21]

The splitting tensile strength of concrete, f_{sp}, from a split cylinder test is given by Equation 4.9 [21].

$$f_{sp} = \frac{2P_{sp}}{\pi \ell_{sp} d_{sp}} \qquad \text{Eqn. 4.9}$$

where:

P_{sp} = maximum load applied in the split cylinder test (lbs)
ℓ_{sp} = length of test specimen in the split cylinder test (in.)
d_{sp} = diameter of specimen in the split cylinder test (in.)

A relationship has been given in Reference 21 between the concrete compressive strength and splitting tensile strength as shown by Equation 4.10.

$$f_{sp} = 6.4\sqrt{f'_c} \qquad \text{Eqn. 4.10}$$

Split cylinder tests, to determine the concrete tensile strength, were performed according to ASTM C496 [26] on at least three cylinders from each aging bath as well as unaged cylinders. These results are presented in Table 4.1. The estimated concrete tensile strengths are presented in Table 4.1 using the empirical formula, Equation 4.10. The values for the concrete compressive strengths, f'_c were taken from Table 3.2. Results presented in Columns 3 and 4 of Table 4.1 give good correlation between these experimental and those previously derived empirical values [21] of the concrete tensile strength.

The split cylinder tensile strength was used as a value of tensile strength in developing a failure mode mechanism designated as the "splitting failure mode". The failure mode

Table 4.1. Concrete tensile strengths for dowel specimens

Aging solution	f'_c (psi)	Split cylinder test, f_{sp} (psi)	Equation 4.10, f_{sp} (psi)
Unaged (air)	7090	508	539
Aged in water	7856	568	567
Aged in lime	7943	546	570
Aged in salt	7660	562	560

exhibited by the dowel specimens is shown in Figure 4.3. This failure mode was typical of both steel and FC dowel specimens. Different values of L_c, as shown in Figure 4.3, were observed for steel and FC dowel specimens.

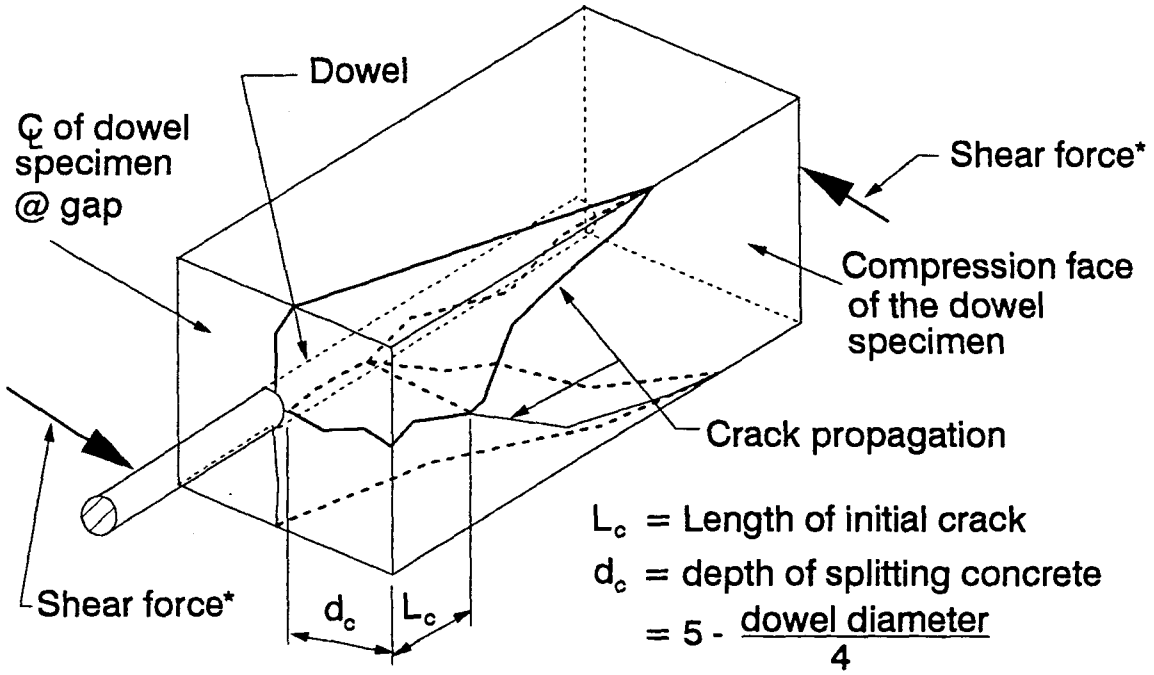

* Only applied forces shown, equilibrium forces from test apparatus are ommitted for clarity.

Figure 4.3. Splitting failure mode for the dowel specimens

4.3.1. FC dowel specimens

Solving Equation 4.9 for P_{sp} (and substituting P_d, L_c, and d_c for P_{sp}, ℓ_{sp}, and d_{sp}, respectively) gives Equation 4.11. Where the following typical values for the FC dowel specimens

$$P_d = \frac{f_{sp}\pi L_c d_c}{2} \qquad \text{Eqn. 4.11}$$

are:

P_d = load causing a splitting failure mode in dowel specimens (lbs)
f_{sp} = split cylinder test results presented in Table 4.1 (psi)
L_c = 3 in. (length of crack as shown in Figure 4.3 as measured on the FC dowel specimens)
d_c = 5 - (d_d/4) = 4.69 in.
d_d = diameter of the dowel (in.)

Utilizing the aforementioned values in Equation 4.11 gives the values of P_d as shown in Table 4.2.

The values in Table 4.2 for P_d correspond very close to the average REEL loads given in Table 3.14 for the A-FC-D assemblies, which are presented again in Table 4.2 for comparison.

Table 4.2. Comparison between FC dowel specimen's REEL loads and concrete tensile strength

Aging solution	f_{sp} (psi)	Avg. REEL load (lbs)	P_d (lbs)
Unaged (air)	508	12185	11227
Aged in water	568	11819	12553
Aged in lime	546	11916	12067
Aged in salt	562	13139	12421

4.3.2. Steel dowel specimens

Substituting the following typical values for steel dowel specimens

f_{sp} = split cylinder test results presented in Table 4.1 (psi)
L_c = 5.5 in. (length of crack as shown in Figure 4.3 as measured on the steel dowel specimens)
d_c = 5 - (d_d/4) = 4.63 in.

into Equation 4.11 gives the values of P_d as shown in Table 4.3. The load, given by Equation 4.8, that would produce a modified truncated pyramid concrete failure is greater than the load given by Equation 4.11 that produced a splitting tensile failure. Therefore, the splitting tensile failure mode is considered that appropriate theoretical mode for the dowel specimens.

Table 4.3. Comparison between steel dowel specimen's REEL loads and concrete tensile strength

Aging solution	f_{sp} (psi)	Avg. REEL load (lbs)	P_d (lbs)
Unaged (air)	508	22691	20320
Aged in water	568	22903	22720
Aged in lime	546	22352	21840
Aged in salt	562	22459	22480

4.3.3. Model for the dowel bars

The average value (aged and unaged) of REEL loads in all baths for the FC dowel specimens is 12,000 pounds and that for steel is 22,000 pounds. The value of L_c was given previously as 3.0 inches and 5.5 inches for FC and steel dowels, respectively. Dividing the REEL loads by the corresponding L_c value gives a load distribution in pounds per inch along the dowel bar. This load distribution at first failure is 4000 lbs/in. Substituting Equation 4.10 into Equation 4.11 gives Equation 4.12.

$$P_d = \frac{6.4\sqrt{f'_c}\pi L_c d_c}{2} \qquad \text{Eqn. 4.12}$$

Substituting concrete strengths for unaged dowel specimens (7090 psi) and typical values of d_c for FC and steel dowel specimens (4.69 for FC and 4.63 for steel) into Equation 4.12 gives Equations 4.13 and 4.14, respectively.

$$P_d = \frac{6.4\sqrt{7090}\pi(4.69)L_c}{2} = 3970L_c \qquad \text{Eqn. 4.13}$$

$$P_d = \frac{6.4\sqrt{7090}\,\pi(4.63)L_c}{2} = 3920L_c \qquad \text{Eqn. 4.14}$$

The results of Equations 4.13 and 4.14 are very similar to the value of 4000 lbs/in obtained by taking the peak load and dividing by the observed L_c. That is, the 12,000 divided by 3.0 and the 22,000 divided by 5.5 is equal to 4000 lb/in agreeing with Equations 4.13 and 4.14.

The bearing strength for the dowel bars can be approximated by Equation 4.15 [21].

$$0.85f'_c A_1\sqrt{\frac{A_2}{A_1}} \qquad \text{Eqn. 4.15}$$

where:

A_1 = area of the bearing contact surface (in^2)
A_2 = area of the lower base of a right pyramid or cone formed by extending the sides of the bearing area at a 2 to 1 slope (in^2)

Multiplying Equation 4.12 by the ratio of different bearing strengths (Equation 4.15) to account for different strength concretes is shown in Equation 4.16.

$$P_d = \frac{6.4\sqrt{f'_{cd}}\pi L_c d_c}{2}\left(\frac{0.85 f'_c A_1\sqrt{\frac{A_2}{A_1}}}{0.85 f'_{cd} A_1\sqrt{\frac{A_2}{A_1}}}\right) \qquad \text{Eqn. 4.16}$$

where:

f'_{cd} = concrete strength used to develop the dowel model (psi) (equal to the 7090 psi for the unaged dowel specimens)

By substituting values of d_c, L_c, and f'_{cd} into Equation 4.16 and canceling like terms in the numerator and denominator gives Equation 4.17 and 4.18 for FC and steel dowel specimens, respectively.

$$P_d = \frac{6.4\sqrt{7090}\pi(3.0)(4.69)}{2}\left(\frac{f'_c}{7090}\right) \qquad \text{Eqn 4.17}$$

$$P_d = \frac{6.4\sqrt{7090}\pi(5.5)(4.63)}{2}\left(\frac{f'_c}{7090}\right) \qquad \text{Eqn. 4.18}$$

Equations 4.17 and 4.18 reduce to give Equations 4.19 and 4.20 for 1.25-inch FC dowels and 1.50-inch steel dowels, respectively, cast in a 10-inch thick specimen.

For 1.25-inch FC dowel specimens:

$$P_d = 1.7\ f'_c \qquad \text{Eqn. 4.19}$$

For 1.50-inch steel dowel specimens:

$$P_d = 3.0\ f'_c \qquad \text{Eqn. 4.20}$$

Equations 4.19 and 4.20 are analyzed with respect to the appropriate error analysis in Section 4.3.5.

The approximate equations can be used to determine the maximum load applied to 1.25-inch FC and 1.50-inch steel dowel bars cast in a 10-inch thick concrete specimen. The variability of concrete strength is taken into account for both Equations 4.19 and 4.20.

The unaged 1.25-inch poly vinyl dowel specimens that were tested and results presented in Chapter 5.0 had an average compressive strength of 6100 psi. Using f'_c = 6100 psi in Equation 4.19 gives a value of P_d equal to 10370 pounds. The actual average value of dowel specimen failure is 9947 pounds. This approximates the dowel failure very well.

The use of Equation 4.19 and 4.20 is for a 1.25-inch and 1.50-inch diameter dowel, respectively, cast in a 10-inch thick concrete specimen. From the data collected thus far, the effect of pavement thickness or dowel diameter is not known. This model (for FC and steel) represents variation in concrete strength for a single diameter dowel bar.

4.3.4. Dowel model compared with f'_c versus REEL load data

The equations developed for the dowel model in Section 4.3.3 (Equations 4.19 and 4.20) are based on concrete failure modes (splitting and bearing). The equations were developed for one concrete strength (unaged) and would change slightly if one of the other concrete strengths (listed in Table 3.2) would have been used. To compare Equations 4.19 and 4.20 with actual data, f'_c (Table 3.2) was plotted against the REEL load (Table 3.16) and Equations 4.19 and 4.20 were plotted through the data as shown in Figure 4.4.

The data used to develop Figure 4.4 is presented in Table 4.4 for clarity. Curve A is for the steel dowel specimens while Curve B is for the FC dowel specimens. Equations 4.19 and 4.20 are reproduced for Section 4.3.3 for the FC and steel dowel specimens, respectively.

$$P_d = 1.7 f'_c \qquad \text{Eqn. 4.19}$$

$$P_d = 3.0 f'_c \qquad \text{Eqn. 4.20}$$

Equations 4.19 and 4.20 correlate very nicely with the data given in Table 4.4, as shown by Figure 4.4.

To show a true relationship between the equations and

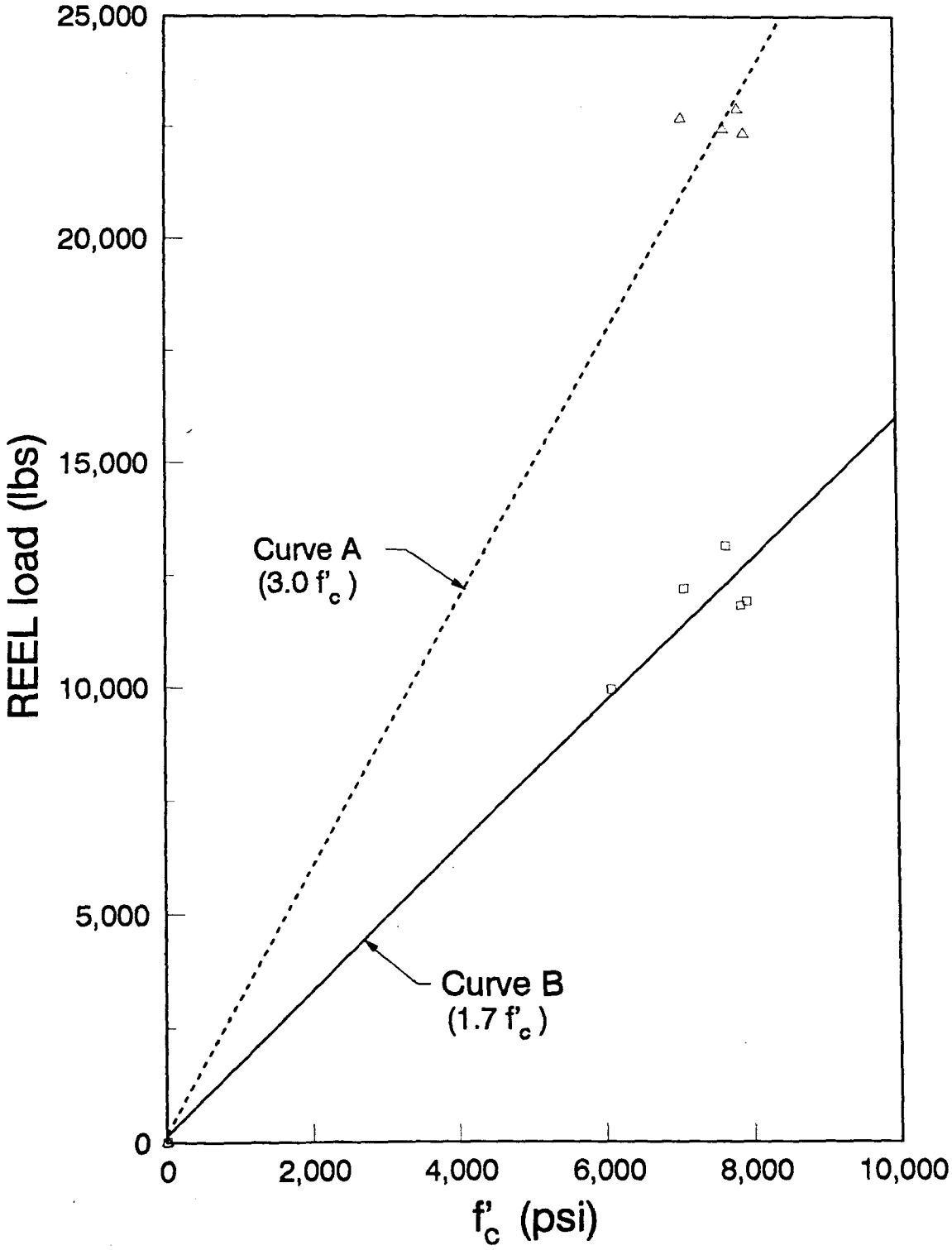

Figure 4.4. Curves based on Equations 4.19 and 4.20 plotted through f'_c versus REEL load data

Table 4.4. Data for FC and steel dowel specimens

FC dowel specimens		Steel dowel specimens	
f'_c (psi)	Avg. REEL load (lbs)	f'_c (psi)	Avg. REEL load (lbs)
6100*	9947*	-	-
7090	12185	7090	22691
7856	11819	7856	22903
7943	11916	7943	22352
7660	13139	7660	22459

* Values taken from Chapter 5

the data, a larger data sample is required for different f'_c values. The author feels that more data would plot closely to Equations 4.19 and 4.20 in Figure 4.4, thus strengthening their suitability. Equations 4.19 and 4.20 can therefore be thought of as "best fit curves" for the FC and steel dowel data.

Considering the magnitude of the load, Equations 4.19 and 4.20 developed in Section 4.3.3 represent the data both graphically and based on concrete bearing and splitting failures. This section is presented to verify Equations 4.19 and 4.20 and to show a different way to related f'_c and REEL load data. In other words, a simple linear relationship may exist.

4.3.5. Error analysis for the dowel specimen model

Equation 4.16 is rewritten as Equation 4.25 (after canceling like terms) showing the errors (e) for each corresponding term.

$$P_d = \frac{6.4\pi (L_c \pm e_1)(d_c \pm e_2) f'_c}{2 (f'_{cd} \pm e_3)^{\frac{1}{2}}} \qquad \text{Eqn. 4.25}$$

where:
e_1 = error or standard deviation for L_c
e_2 = error or standard deviation for d_c
e_3 = error or standard deviation for f'_{cd}

With all other terms defined previously, the values of e_1, e_2, and e_3 were taken as the standard deviation or error in measurement associated with each set of data. For e_1 the standard deviation was 0.5. An approximate value of 0.125 was used for e_2 and represented a casting error that could not be measured directly. Based on the concrete compressive strength of three test cylinders, the standard deviation, e_3, was calculated to be 170.6.

There are a total of eight combinations for e_1, e_2, and e_3 that can result. The "true value" of Equation 4.25 is when e_1, e_2, and e_3 are zero and gives $1.7f'_c$ for FC specimens and $3.0f'_c$ for steel specimens. The combinations of e_1, e_2, and e_3 resulting in the largest variation from the "true

value" are $+e_1$, $+e_2$, $-e_3$ and $-e_1$, $-e_2$, $+e_3$. The calculations using these combinations are shown in Equations 4.26 and 4.27 for FC specimens and Equations 4.28 and 4.29 for steel specimens.

For FC specimens:

$$P_d = \frac{6.4\pi(3 + 0.5)(4.69 + 0.125)f'_c}{2(7090 - 170.6)^{\frac{1}{2}}} = 2.0f'_c \qquad \text{Eqn. 4.26}$$

$$P_d = \frac{6.4\pi(3 - 0.5)(4.69 - 0.125)f'_c}{2(7090 + 170.6)^{\frac{1}{2}}} = 1.4f'_c \qquad \text{Eqn. 4.27}$$

For steel specimens:

$$P_d = \frac{6.4\pi(5.5 + 0.5)(4.63 + 0.125)f'_c}{2(7090 - 170.6)^{\frac{1}{2}}} = 3.4f'_c \qquad \text{Eqn. 4.28}$$

$$P_d = \frac{6.4\pi(5.5 - 0.5)(4.63 - 0.125)f'_c}{2(7090 + 170.6)^{\frac{1}{2}}} = 2.6f'_c \qquad \text{Eqn. 4.29}$$

The equations representing the failure of the dowel specimens can be given by Equations 4.30 and 4.31. The maximum values are given for FC and steel specimens as $2.0f'_c$ and $3.4f'_c$, respectively. The minimum values are given for FC and steel specimens as $1.4f'_c$ and $2.6f'_c$, respectively.

For FC specimens:

$$P_d = (1.7 \pm 0.3) f'_c \qquad \text{Eqn. 4.30}$$

For steel specimens:

$$P_d = (3.0 \pm 0.4) f'_c \qquad \text{Eqn. 4.31}$$

CHAPTER 5. MODIFIED TEST FRAME FOR DOWEL SPECIMEN TESTING

The testing procedure for the dowel specimens required clamping of each half of the dowel specimens. The author did further testing to determine whether the clamping force affected the load-deflection data obtained during testing. A modified method of gripping the dowel specimens was developed. The author felt this modified method of gripping more closely represented the Iosipescu test method.

5.1. Test Procedure

Six additional FC dowel specimens were cast as shown in Figure 3.2. Polyester dowel bars were used in place of the vinyl ester dowel bars. The polyester dowels were 1.25 inches in diameter and exhibited an average flexural modulus of 6.64×10^6 psi. The new dowel specimens had an averaged compressive of 6100 psi.

Three of the FC dowel specimens were tested using the testing procedure in Section 3.6. Figure 5.1 exhibits the corresponding clamping method. Neoprene covered the entire face of the dowel specimens to distribute the load evenly across the specimen as shown in Figure 5.1.

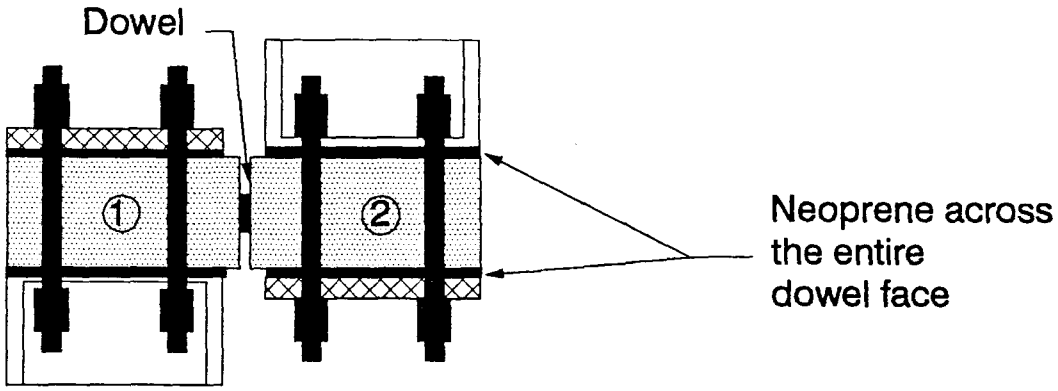

Figure 5.1. Clamping method for dowel specimens

The remaining three dowel specimens were tested using a modified clamping method as shown in Figure 5.2. Neoprene pads were placed as shown in Figure 5.2. The neoprene did not cover the entire face of the dowel specimens which may restrict the failure mode.

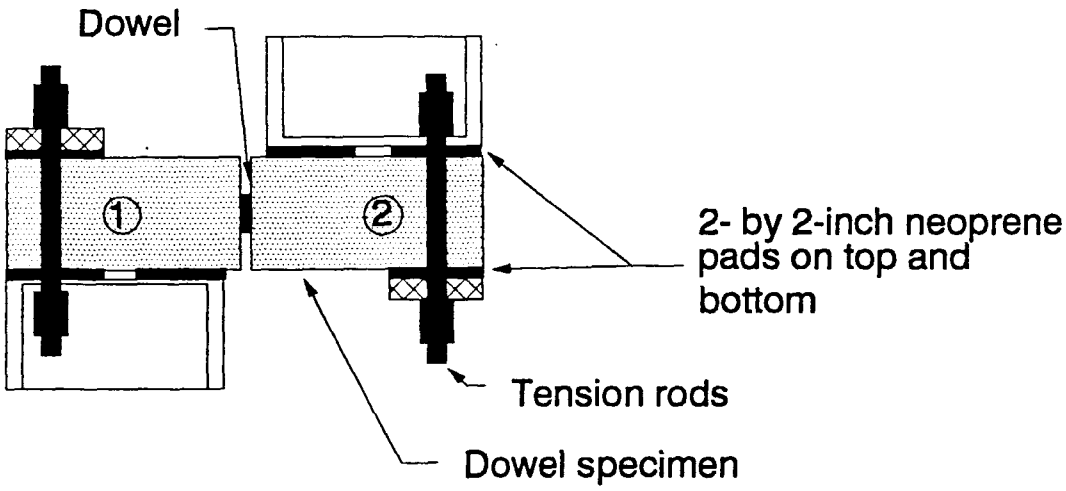

Figure 5.2. Modified clamping method for dowel testing

5.2. Results

The results of each clamping method are shown in Figures 5.3 and 5.4. The author's decision in Part 1 of the final report was to use the peak load at the first significant drop in load (presented as the REEL load in Part 1 of the final report) as shown in Figure 5.3. The load increased following this significant drop. This increase in load (see Figure 5.3) is due to the confinement of the final failure in the dowel specimens by the testing frame. This final failure would have reduced the dowel specimens load-carrying capacity to little or nothing.

Figure 5.4 shows the results of the modified clamping method. The results indicate a sudden drop in load after the REEL load was obtained. The grips did not restrict the dowel specimen's failure and there was no load increase.

The REEL loads and deflections correspond very well and were not affected by the clamping method. The average REEL load was 9947 pounds. Therefore, the author feels that the test method used in Section 3.6 is representative of the Iosipescu test method.

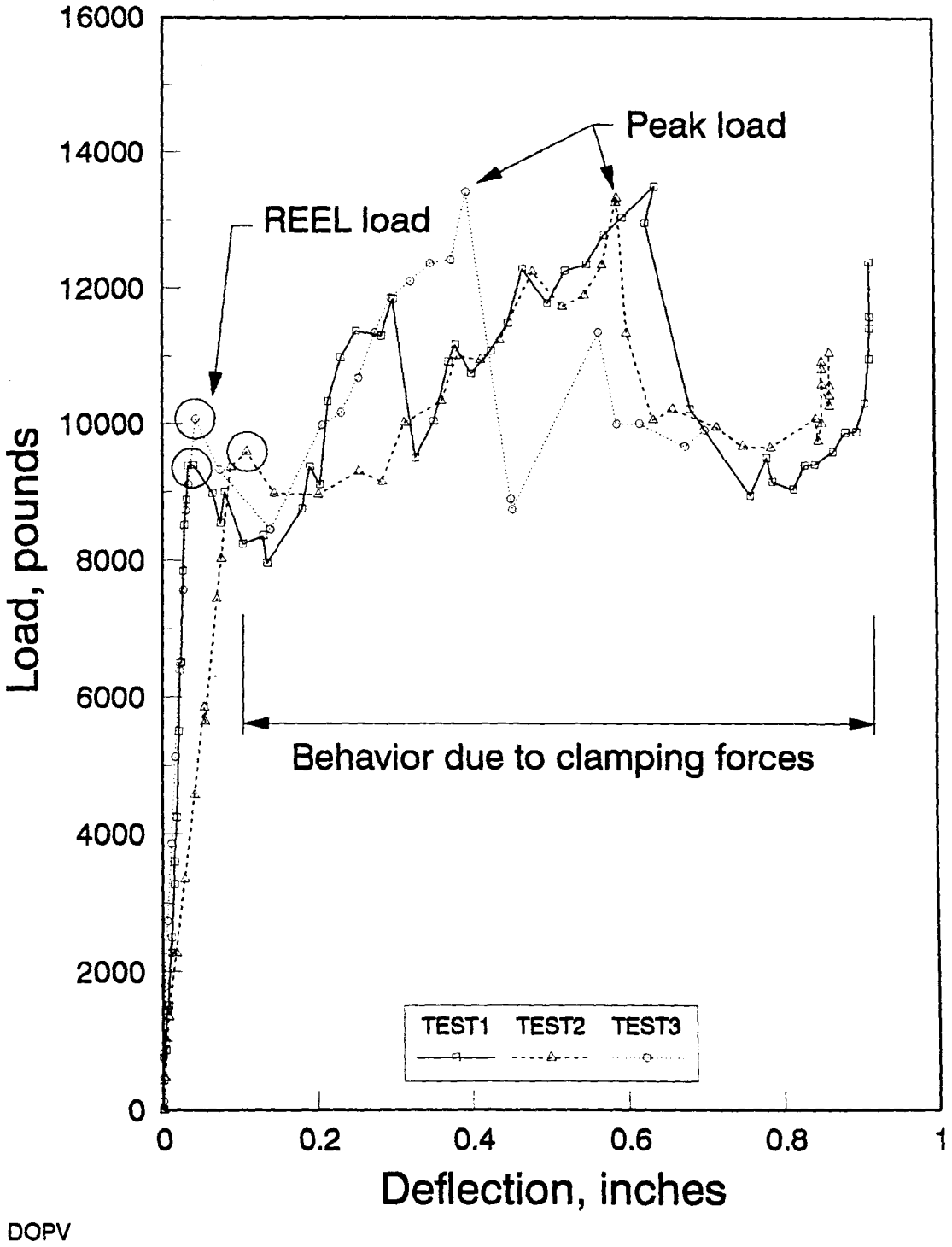

Figure 5.3. Tests on polyester dowel bars

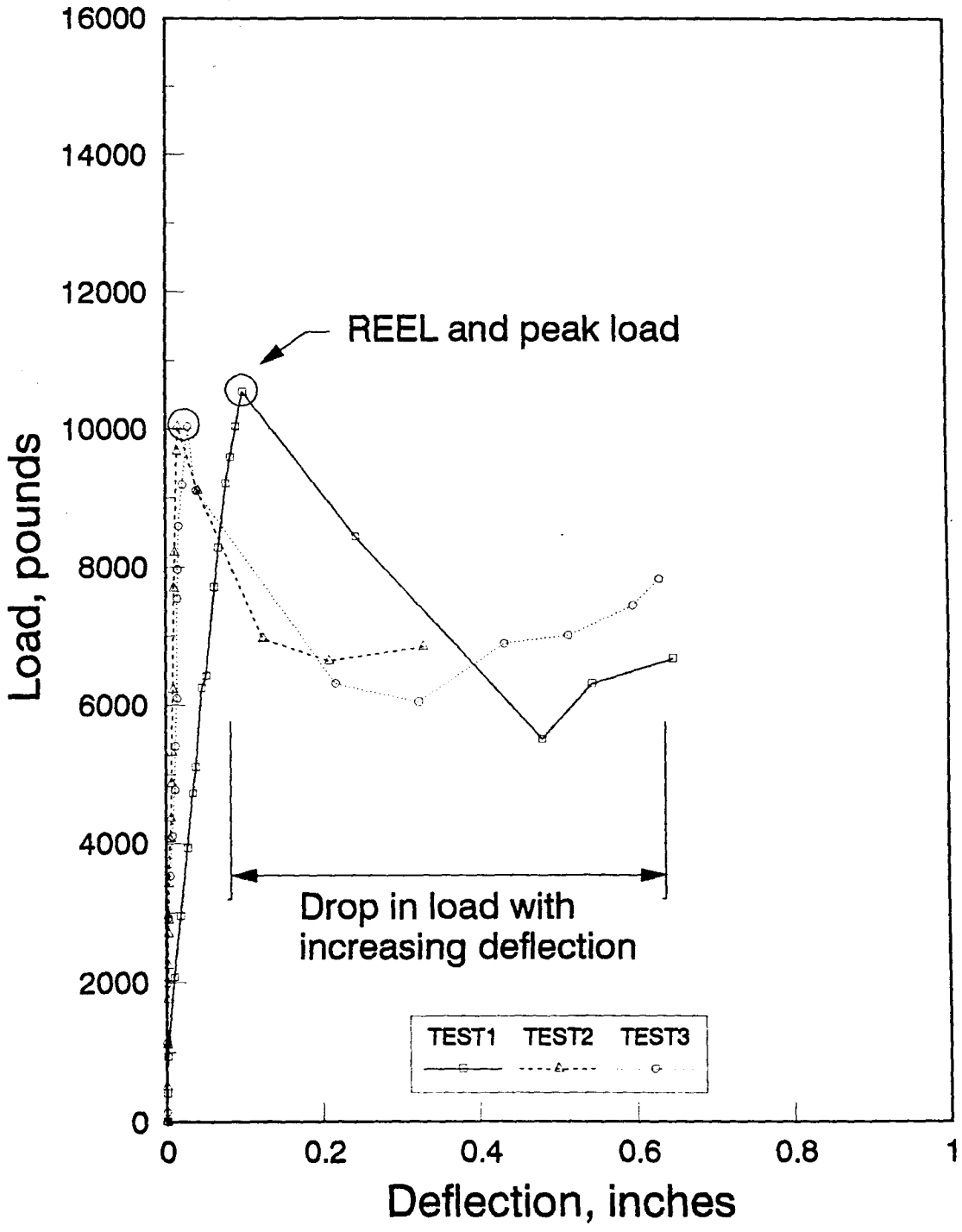

DNPV

Figure 5.4. Tests of polyester dowel bars using modified grips

CHAPTER 6. VERIFICATION OF THE THEORETICAL MOMENT MODEL

The theoretical model developed in Part 1 of the final report was based on Timoshenko's analysis of a finite beam on an elastic foundation [23,24]. The distribution of bending moment along the length of the dowel was obtained from the second differential of the deflection equation (the deflection equation is given in Part 1). The equation for the distribution of moment along the dowel is shown by Equation 6.1.

$$\frac{d^2y}{dx^2} = \beta^2 e^{\beta x}[-2A\sin\beta x + 2B\cos\beta x] + \beta^2 e^{-\beta x}[2C\sin\beta x - 2D\cos\beta x] \qquad \text{Eqn. 6.1}$$

where:

A,B,C,D	=	constants used to represent the solution for deflection of the dowel bar
x	=	distance along dowel from the face of the joint (in.)
y	=	deflection of dowel (in.)

and

$$\beta = \sqrt{\frac{k_o d}{4EI_z}}$$

where:

k_o	=	modulus of dowel support (pci)
d	=	diameter of dowel (in.)
EI_z	=	flexural rigidity of the dowel (lb-in²)

By applying the appropriate boundary conditions (given in Part 1) to Equation 6.1, a set of four simultaneous equations can be formed. These equations can be solved for the unknown constants A, B, C, and D. This equation with the known constants can be used to obtain the theoretical moment distribution along the dowel bars. This model was also used to obtain theoretical shear, deflection, and load distributions (by successive differentiation of the deflection equation given in Part 1) along the dowel bar. The theoretical moment distribution along the dowel bar is shown in Figure 6.1 (as presented in Part 1). The value of k_o used to develop Figure 6.1 was calculated as 2,139,000 pci based on a y_o (y_o is one-half the total average deflection at the face of the joint) of 0.00373 inches. The theoretical moment distribution in Figure 6.1 is a result of Timoshenko's finite beam analysis for a 1.5-inch steel dowel bar with an assumed dowel shear of 10,000 pounds.

The theoretical moment distribution in Figure 6.1 exhibits a maximum moment of 6000 in-lb at one and one-half inches from the center of the dowel, an inflection point at about five inches, and a maximum positive moment at around six and one-half inches. To verify the theoretical model, steel dowel bars were strain gaged as shown in Figure 6.2. Strain gages were located at 1.5, 5.0, and 6.5 inches from the centerline of the dowel as shown in Figure 6.2 on either

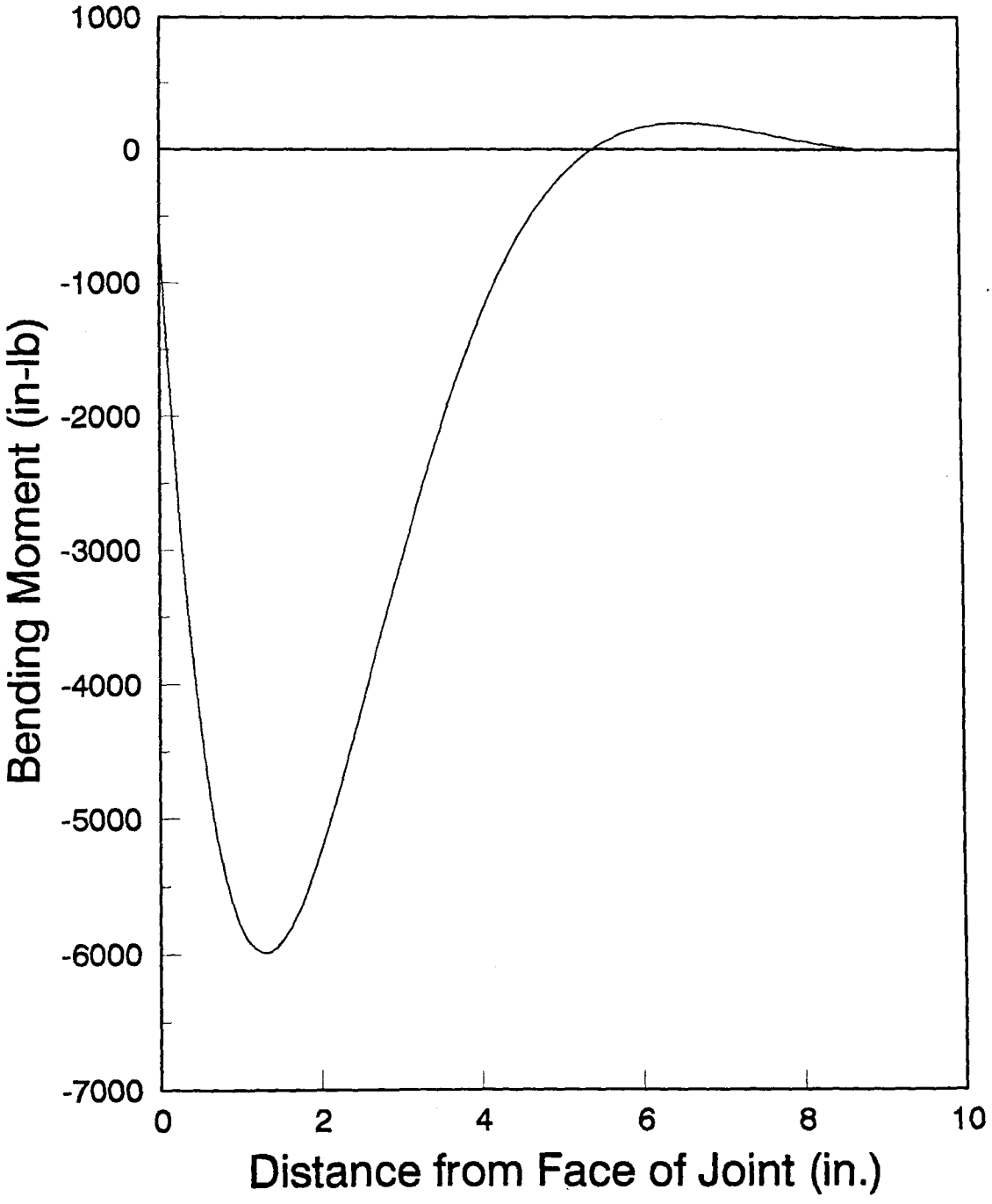

Figure 6.1. Theoretical moment distribution along the dowel bar

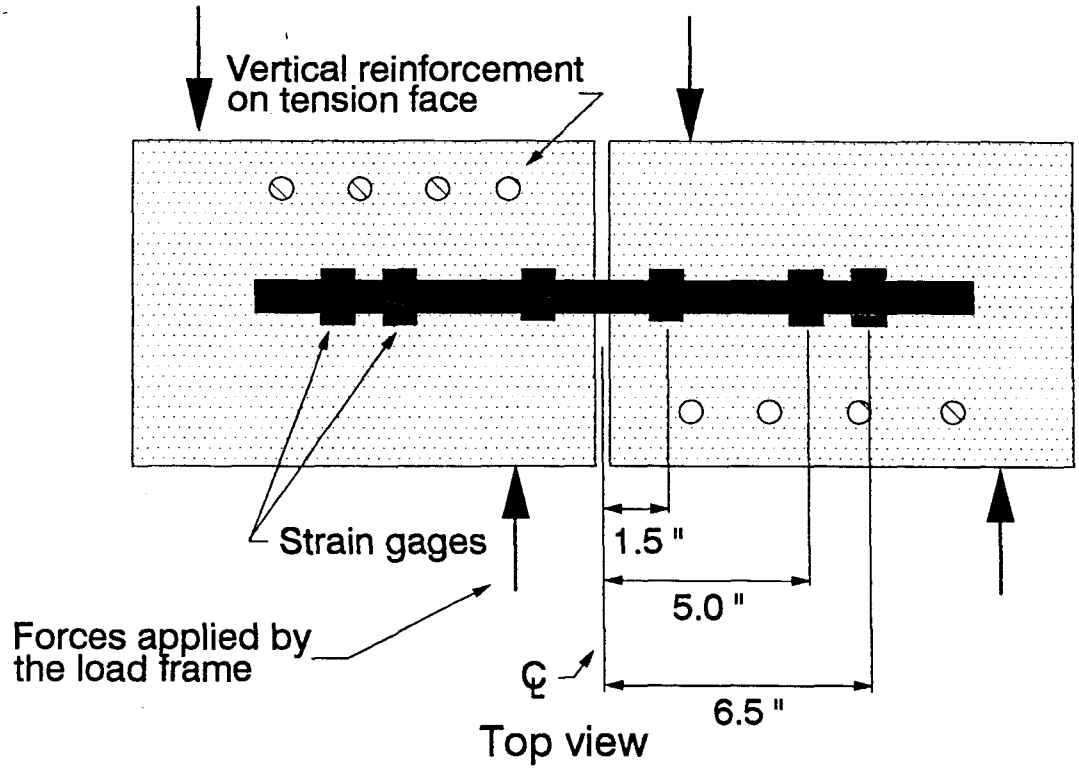

Figure 6.2. Strain gage locations on the dowel bar

side of the gap. The strain gages were mounted on opposite sides of the dowel bar (1.5 inches apart) within the plane of the shear force.

Properties of the steel dowel bars used for this part of the research project are presented in Table 6.1. The dowel specimens exhibited an average concrete strength of 7486 psi. The concrete strength was taken as the average of at least six concrete cylinders. The testing procedure was presented in Section 3.6 for the dowel-shear specimens. The strain gaged dowel specimens were tested using the same procedure. The strains were recorded along with the load and deflection

Table 6.1. Properties of the strain gaged 1.5-in. steel dowel bars

Dowel type	Supplier	Area (in^2)	Moment of inertia (in^4)	Apparent modulus of Elasticity (psi)
Steel	O	1.77	0.25	28.0×10^6

data for five different dowel specimens (the results of one dowel test specimen were considered as invalid and omitted).

The analysis of the strain gage results was completed based on Reference 25. The deformation of the dowel bar is measured by the curvature of neutral axis. The value of the curvature (the inverse of the radius of curvature) can be determined using Equation 6.2 [25].

$$\frac{1}{\phi} = \frac{\epsilon_m}{c} \qquad \text{Eqn. 6.2}$$

where:

ϕ = radius of curvature (in.)
ϵ_m = maximum normal strain (in/in)
c = distance from the neutral axis to the extreme fiber (in.)

Using the following expressions, and substituting

$$\epsilon_m = \frac{\sigma_m}{E_s} \qquad \textit{and} \qquad \sigma_m = \frac{M_s C}{I_s}$$

them into Equation 6.2 gives Equation 6.3.

$$\frac{1}{\phi} = \frac{M_s}{E_s I_s} \qquad \text{Eqn. 6.3}$$

where:

M_s = bending moment causing curvature in the dowel (in-lb)
E_s = modulus of elasticity of the dowel bar (psi)
I_s = moment of inertia for the dowel bar (in^4)

Setting Equation 6.2 equal to Equation 6.3 and solving for M_s gives Equation 6.4.

$$M_s = \frac{\epsilon_m E_s I_s}{c} \qquad \text{Eqn. 6.4}$$

Using typical properties of the steel dowels from Table 6.1 for E_s and I_s and using c equal to 0.75 inches (half the dowel diameter) the moment (M_s) could be calculated in terms of strains (ϵ_m). The measured strains were then used to determine the final moment distribution along the dowel specimens. The recorded strains at each location along the dowel were averaged and used in Equation 6.4 to determine the moment. These moments are plotted against load in Figures 6.3 through 6.5, for distances from the center of the dowel specimen equal to 1.5, 5.0, and 6.5 inches, respectively. The moments of interest (in Figures 6.3 through 6.5) occur at a load of 10,000 pounds. These moments are presented in Table 6.2 for 1.5, 5.0, and 6.5-inch distances from the centerline of the dowel specimens.

The analysis was performed again on the 1.5-inch diameter steel dowel bar for a average deflection value

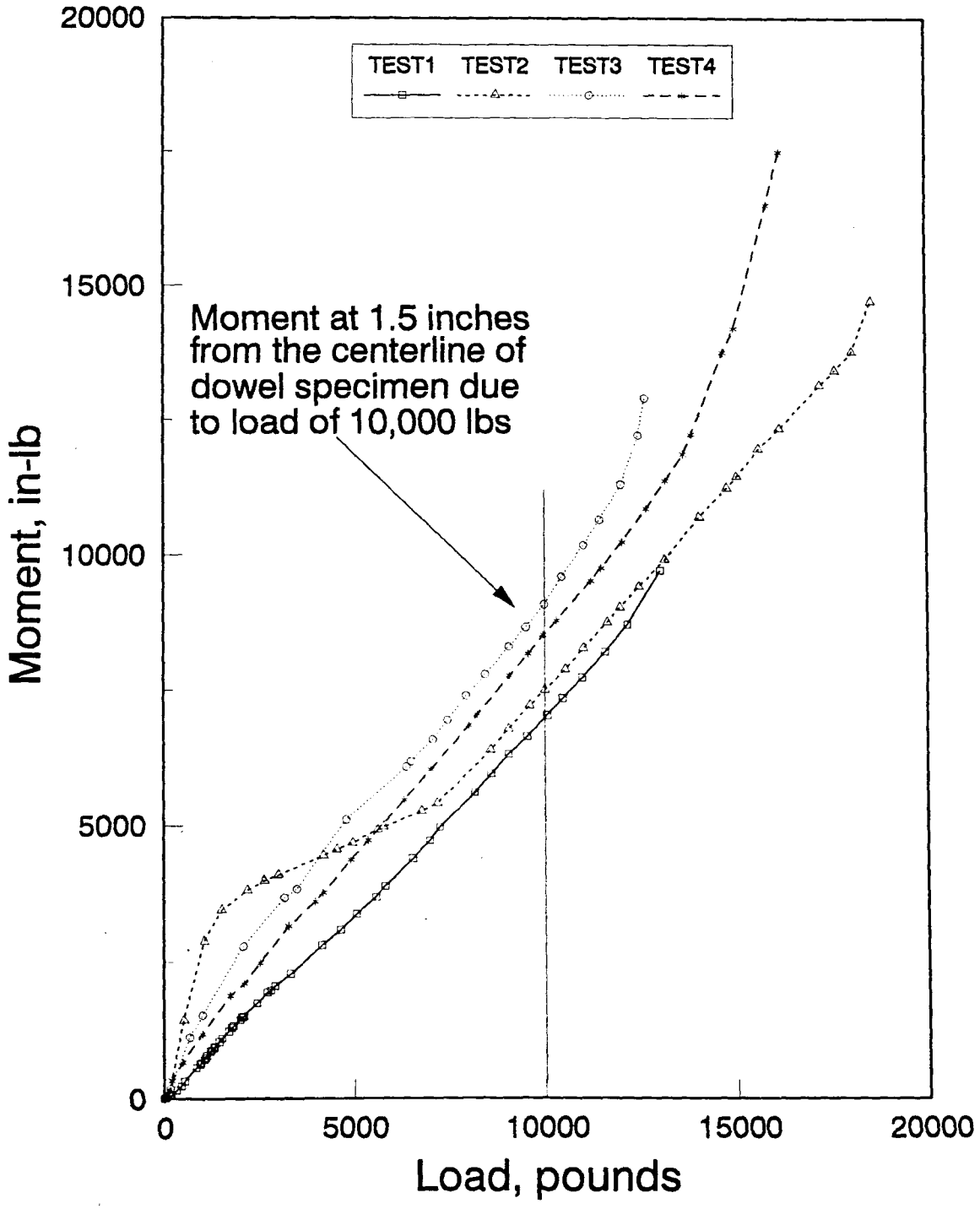

Figure 6.3. Load versus moment diagram at 1.5 inches from the centerline of dowel bar

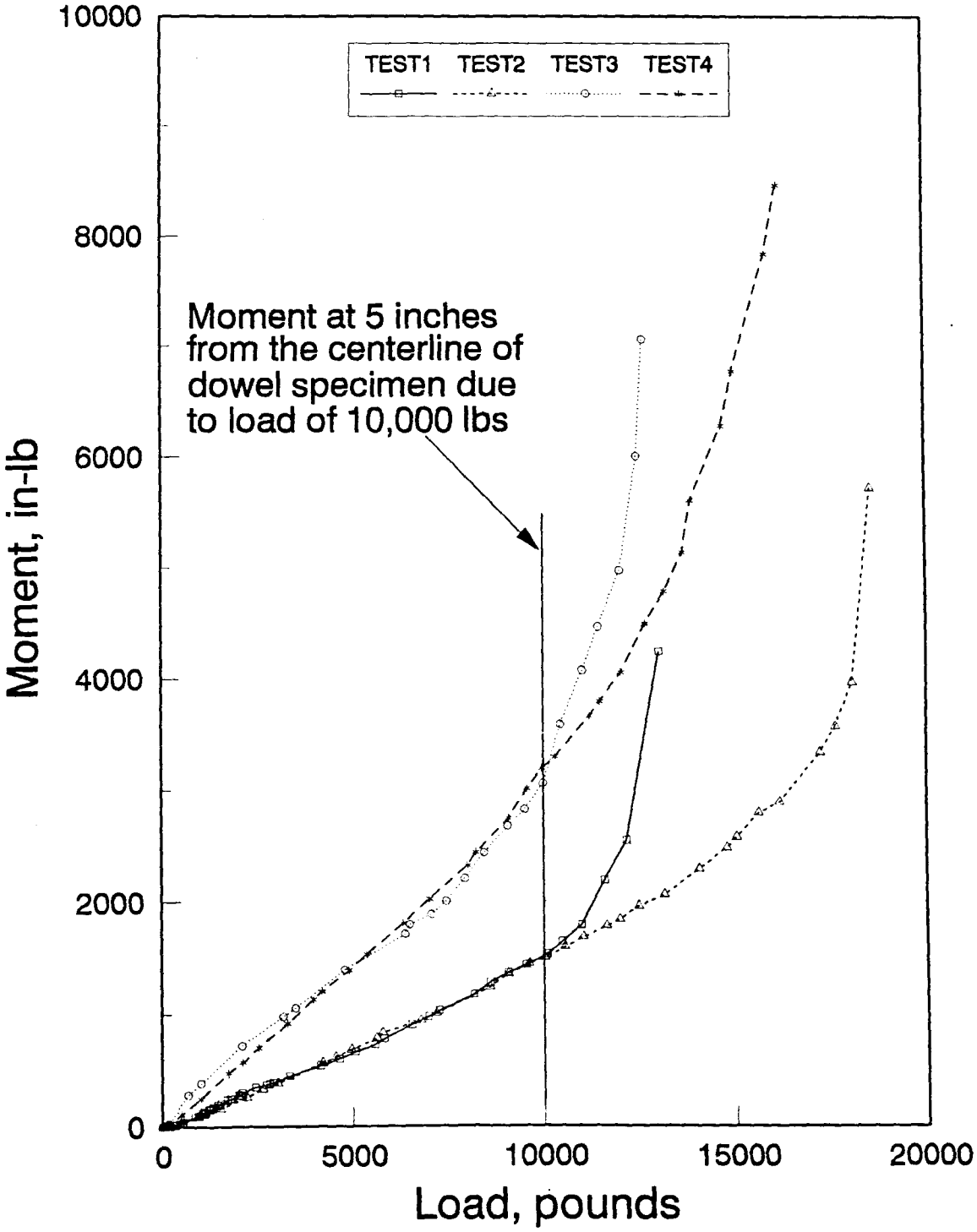

Figure 6.4. Load versus moment diagram at 5.0 inches from the centerline of dowel bar

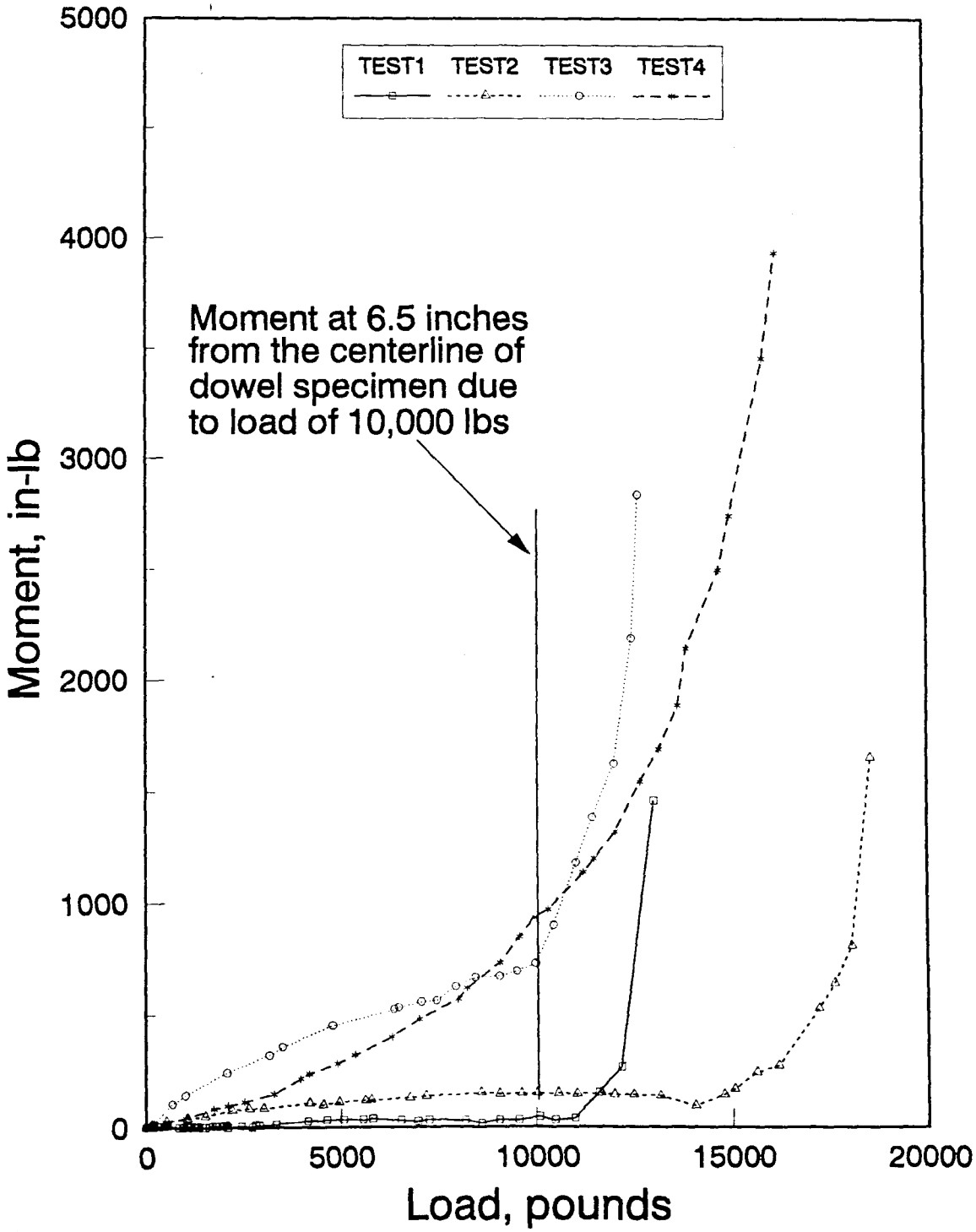

Figure 6.5. Load versus moment diagram at 6.5 inches from the centerline of dowel bar

obtained during testing. An average value of y_o (dowel deflection at the face of the joint) equal to 0.009 inches gave an approximate k_o (modulus of dowel support) for the 1.5-inch dowels equal to 650,000 pci. The results of the analysis are plotted in Figure 6.6 (theoretical moment distribution). The deflection, moment, shear, and load distribution are plotted in Figure 6.7.

The values presented in Table 6.2 are plotted in Figure 6.6 as the experimental moment distribution curve. The strain gage results indicate that the dowel has no zero point in the moment distribution curve. The experimental moment curve indicates approximately the same moment values as the theoretical distribution.

Table 6.2. Experimental moments at 10,000 lbs.

Trial	Moment at 1.5 inches from center (in-lbs)	Moment at 5.0 inches from center (in-lbs)	Moment at 6.5 inches from center (in-lbs)
1	7025	1528	46
2	7489	1500	150
3	9065	3055	728
4	8498	3193	932
Average	8019	2319	464

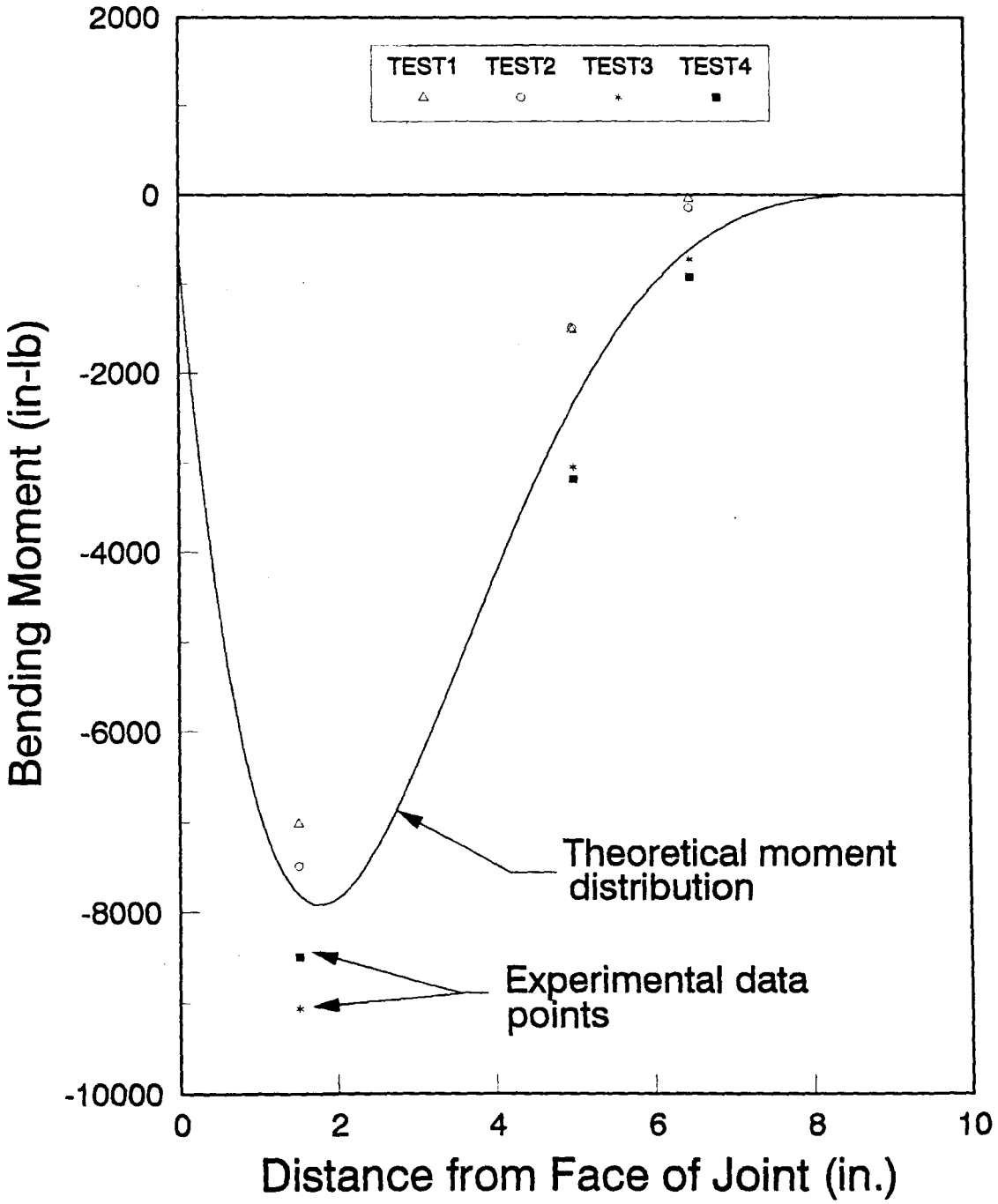

Figure 6.6. Theoretical versus experimental moment distribution along the dowel bar

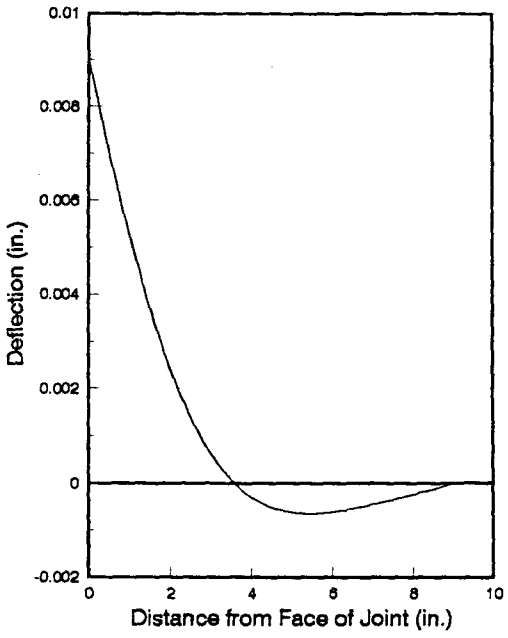

a) Deflection

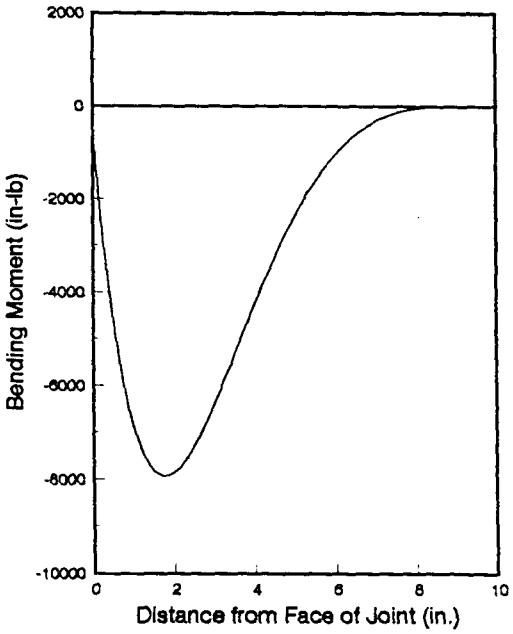

b) Bending moment

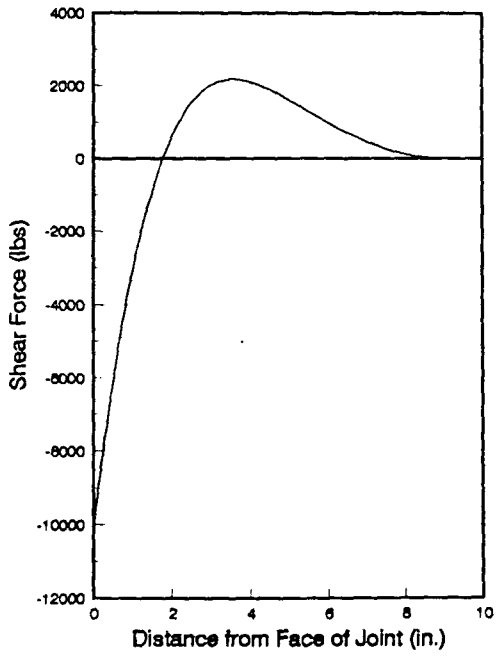

c) Shear force

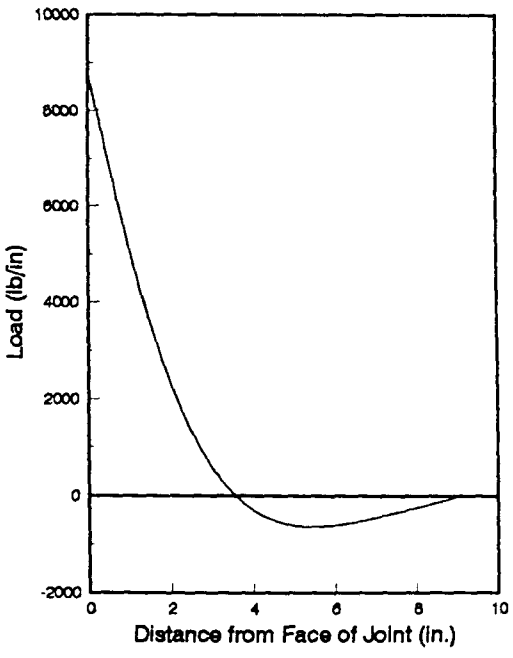

d) Load

Figure 6.7. Results of analysis of 1.5-in. dia. steel dowel

CHAPTER 7. LOAD DISTRIBUTION ON THE DOWEL SPECIMENS

Chapter 5 illustrated two clamping methods (Figures 5.1 and 5.2) that appeared different but had little effect on the failure mode or the load at concrete failure (@ REEL load). Using Figure 5.2 and assuming that both sides (Sides 1 and 2 in Figure 5.2) were loaded the same, a simplified load (assumption of point loads on the dowel specimens) distribution can be drawn on the dowel specimen as shown in Figure 7.1.

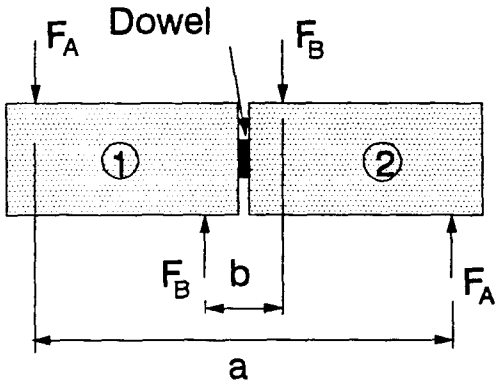

Figure 7.1. Load distribution on the dowel specimen

The corresponding shear and moment diagrams for the simplified load distribution in Figure 7.1 are shown in Figure 7.2. These shear and moment diagrams shown in Figure 7.2 assume that F_B is greater than F_A. The force couple exerted by F_B must be equal to the force couple exerted by F_A. The two force couples can be set equal and solved for F_B in terms of F_A as shown by Equation 7.1. The terms in Equation 7.1 are shown in Figure 7.1.

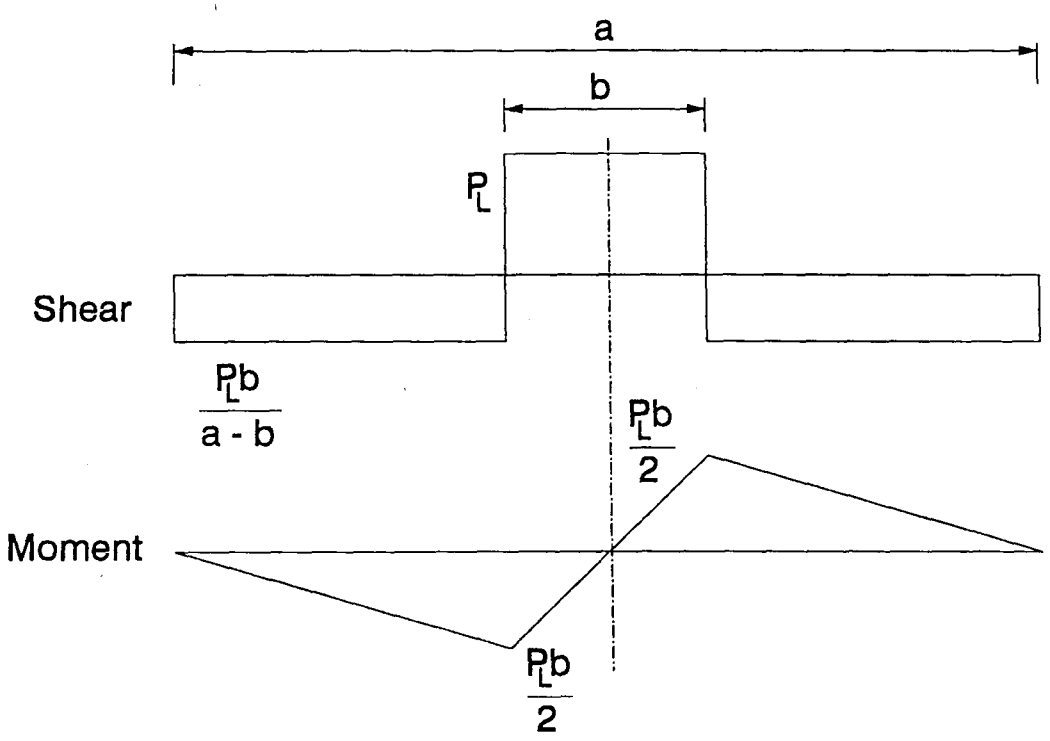

Figure 7.2. Shear and moment diagrams for the dowel specimens

$$F_B = \frac{a}{b} F_A \qquad \text{Eqn. 7.1}$$

where:

a = the distance between the outer tension rods (in.)
b = the distance between the inner tension rods (in.)
F_A = force on the outer tension rods (lbs)
F_B = force on the inner tension rods (lbs)

The shear and moment diagrams given in Figure 7.2 are based on the Iosipescu shear test method [20]. This method assumes zero moment at the centerline of the dowel specimens resulting in "pure" shear. The value of F_A and F_B are given

by Equation 7.2.

$$F_A = \frac{P_L b}{a-b} \quad and \quad F_B = \frac{P_L a}{a-b} \qquad \text{Eqn. 7.2}$$

where:

P_L = load applied to the dowel specimen (lbs)

F_A and F_B can be easily determined for any load P_L applied to the dowel specimens.

Using a value of P_L as 10,000 lbs, with a and b equal to 21 inches and 5 inches, respectively, F_A is equal to 3,125 lbs and F_B is equal to 13,125 lbs. The corresponding shear and moment diagrams for a load of 10,000 lbs are given in Figure 7.3.

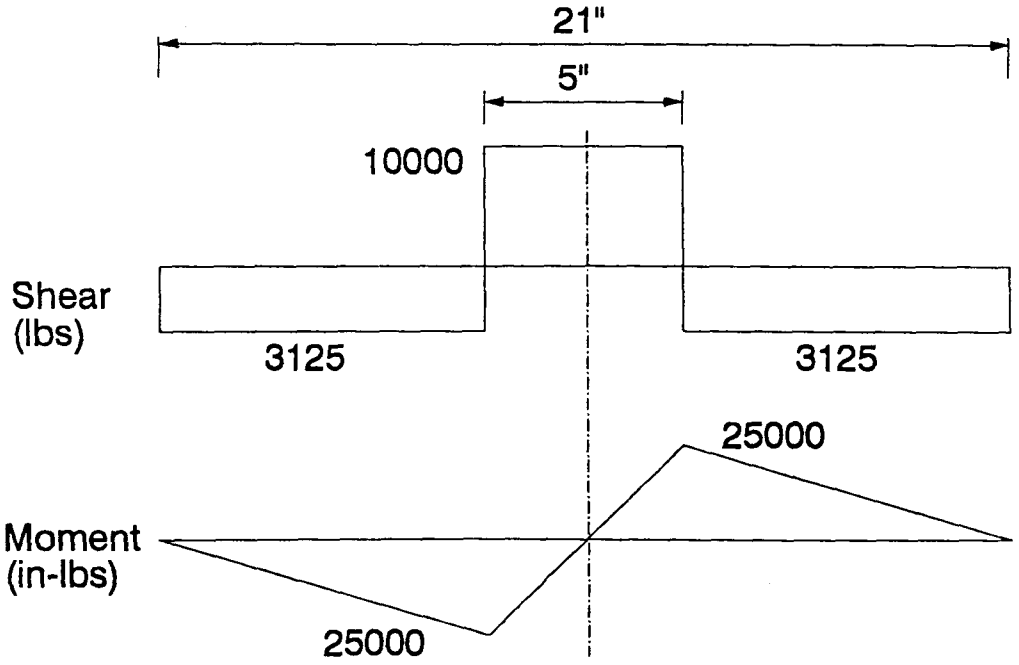

Figure 7.3. Shear and moment diagram for P_L of 10,000 lbs

CHAPTER 8. CONCLUSIONS

8.1. Accelerated Aging

A very good approximate model was developed for accelerated aging of FC materials that will approximate real weather aging. Two equations were developed for accelerated aging in central Iowa (Ames). The first equation (Equation 7.1) relates the temperature of the aging bath to the number of days aged per day. The second, the acceleration factor (AF) equation (Equation 7.2) adjusts the number of days aged per day to account for a mean annual temperature (MAT), that is different than the United Kingdom (UK) where the accelerated aging process was developed.

$$Age\left(\frac{days}{day}\right) = 0.200e^{0.052 * T} \qquad \text{Eqn. 8.1}$$

$$AF = 2.986E\text{-}19e^{13.783X} \qquad \text{Eqn. 8.2}$$

The E-glass fibers encapsulated in a vinyl ester resin matrix has proven in this research to be very resistant to accelerated aging effects. From the data collected, on the average, FC materials have been shown in this research project to be very resistant to corrosive environments.

Also, this research showed that a reduction in strength or stiffness did not occur due to accelerated aging.

8.2. Pullout Specimens

The pullout specimens for Supplier B exhibited a slight increase in peak load for all three aging solutions. Pullout specimens from Supplier C exhibited a slight decrease in peak load with exception of those specimens aged in water.

A theoretical model was developed to approximate the mechanical bond degradation in the pullout specimens. Using Equation 7.3, the tensile elongation could be approximated using a varying length L_b, that took into account the mechanical bond failure.

$$\delta = \frac{P_t L_b}{E A_{FC}} \qquad \text{Eqn. 8.3}$$

This model indicated that a slight increase in mechanical bond was exhibited by Supplier B's rebar cast in concrete, due to accelerated aging. Also, Supplier C's rebar exhibited a slight decrease in mechanical bond due to accelerated aging.

8.3. Dowel Specimens

Overall, the accelerated aging solutions of water, lime, and salt apparently had little or no affect on the shear strength behavior of any of the dowel bar series.

Approximate equations were developed for FC and steel dowels and accounted for both concrete splitting and concrete bearing type failure modes. These equations were developed for unaged dowel specimens and approximated the dowel specimens failure very close. Equation 7.4 is for a 1.25-inch diameter FC dowel cast in a 10-thick concrete specimen. Equation 7.5 is for a 1.50-inch diameter steel dowel cast in a 10-inch thick concrete specimen.

For the 1.25-inch FC dowel specimens:

$$P_d = (1.7 \pm 0.3) f'_c \qquad \text{Eqn. 8.4}$$

For the 1.50-inch steel dowel specimens:

$$P_d = (3.0 \pm 0.4) f'_c \qquad \text{Eqn. 8.5}$$

Verification was made on the testing procedure (clamping method) for the dowel specimens. The authors determined that it was a representative testing procedure based upon the Iosipescu shear test. The clamping method was modified to more closely represent the Iosipescu shear test. Upon doing so, the REEL loads, deflections, and failure modes were very

consistent between the two testing procedures.

The steel dowel bars in the dowel-shear specimens were strain gaged to check the theoretical moment distribution along the dowel bar as presented in Part 1 of this report. An experimental moment distribution was developed based upon the strain gaged dowel specimens. The theoretical moment distribution was approximately equal to the experimental moment distribution. The strain gage results indicate that the dowel has no zero point in the moment distribution curve, other than that assumed to occur at the centerline or at the end of the dowel. Overall the author feels that the theoretical model developed in Part 1 is representative of the steel dowel specimens and is also representative of the FC dowel specimens.

REFERENCES

1. Proctor, B.A., Oakley, D.R., Litherland, K.L., "Developments in the Assessment and Performance of GRC Over 10 Years", Composites, April 1982, pages 173-179.

2. Aindow, A.J., Oakley, D.R., Proctor, B.A., "Comparison of the Weathering Behavior of GRC with Predictions Made from Accelerated Ageing Tests", Cement and Concrete Research, Volume 14, August 1983, pages 271-274.

3. Litherland, K.L., Oakley, D.R., Proctor, B.A., "The Use of Accelerated Ageing Procedures to Predict the Long Term Strength of GRC Composites", Cement and Concrete Research, Volume 11, February 1981, pages 455-466.

4. Majumdar, A.J., Ryder, J.F., "Glass Fibre reinforcement of Cement Products", Building Research Station, Ministry of Public Building and Works, Garston Watford, Herts, Glass Technology, Volume 9-No. 3, June 1968, pages 78-84.

5. "Glass Fiber Reinforced Concrete", Fiber Reinforced Concrete, Portland Cement Association, Skokie, Illinois, 1991, pages 11-21.

6. Oakley, D.R., Litherland, K.L., Proctor, B.A., "The Development of a Method of Predicting the Weathering Behavior of Glass Reinforced Cement Composites", Proceedings 2nd International Conference on Durability of Building Materials and Components, Gaithersburg, Maryland, USA, September 1981, pages 225-231.

7. Janninck, D.R., Venta, J.G., "An Accelerated Aging Procedure to Predict the Long-Term Strength of Poly Vinyl Chloride Coated E-Glass in Cement Composite Panels", Proceedings- Durability of Glass Fiber Reinforced Concrete Symposium, Holiday Inn Mart Plaza, Chicago, Illinois, November 12-15, 1985, pages 230-238.

8. Bentur, A. and Diamond, S., "Aging and Microstructure of Glass Fiber Cement Composites Reinforced with Different Types of Glass Fibers", Durability of Building Materials, Volume 4, pages 201-226.

9. Diamond, Sidney, "The GFRC Durability Problem: Nature, Characteristics, and Test Methods", Proceedings-Durability of Glass fiber Reinforced Concrete Symposium, Holiday Inn Mart Plaza, Chicago, Illinois, November 12-15, 1985, pages 199-209.

10. Stark, D., Handbook For The Identification Of Alkali-Silica Reactivity In Highway Structures, Strategic Highway Research Program, National Research Council, Washington, D.C., 1991, 49 pages.

11. Struble, Leslie, and Diamond, Sidney, "Influence of Cement Alkali Distribution on Expansion Due to Alkali-Silica Reaction", (Alkalies in Concrete), Symposium Sponsored by ASTM Committees C-9 on Concrete and Concrete Aggregates and C-1 on Cement, Los Angeles, California, June 1985, pages 31-45.

12. Kilareski, W.P., "Epoxy Coating for Corrosion Protection of Reinforcement Steel", Chloride Corrosion of Steel in Concrete, ASTM STP 629, D.E. Tonini and S.W. Dean, Jr.,Eds., American Society for Testing and Materials, 1977, pages 82-88.

13. Peterson, P.C., "Concrete Bridge Deck Deterioration in Pennsylvania", Chloride Corrosion of Steel in Concrete, ASTM STP 629, D.E. Tonini and S.W. Dean, Jr., Eds., American Society for Testing and Materials, 1977, pages 61-68.

14. Performance of Concrete; Resistance of Concrete to Sulphate and other Environmental Conditions. A Symposium in Honour of Thorbergur Thorvaldson, E.G. Swenson, Technical Editor, University of Toronto Press., Toronto, 1968., pages 45-47.

15. Harboe, E.M., "Longtime Studies and Field Experiences with Sulphate Attack", George Verbeck Symposium on Sulfate Resistance of Concrete, American Concrete Institute, Detroit, Michigan, 1982, pages 1-20.

16. DERAKANE Resins, Chemical Resistance and Engineering Guide, The Dow Chemical Company, Midland, Michigan, 1990.

17. Porter, M.L., Albertson, M.D., Barnes, B.A., "Thermoset Concrete Reinforcement: Progress Report for 1990", Iowa State University, Engineering Research Institute, Ames, IA., 1990.

18. Porter, M.L., Fish, K.E., Barnes, B.B., "Fiber-Composite Rods as Reinforcing for Concrete Structures", Thermoset and Thermoplastic Composite Reinforcement for the Concrete Industry, Center for Advanced Technology Development, Iowa State University, Ames, IA., January 1992, pages 6-11.

19. EXTREN Fiberglass Structural Shapes, Design Manual, Morrison Molded Fiber Glass Company, Bristol, VA, 1989.

20. Walrath, D.E., and Adams, D.F., "The Iosipescu Shear Test as Applied to Composite Materials", Experimental Mechanics, March 1983, pages 105-110.

21. MacGregor, J.G., Reinforced Concrete: Mechanics and Design, Prentice Hall, Englewood Cliffs, New Jersey, 1988, pages 52-53.

22. Prestressed Concrete Institute: Design Handbook, Third Edition, Chicago, Illinois, Part 6, 1985, pages 6-8.

23. Timoshenko, S., Strength of Materials - Part II, Third edition, Robert E. Krieger Publishing Company, Huntington, New York, 1976.

24. Timoshenko, S., and Lessels, J.M., Applied Elasticity, Westinghouse Technical Night School Press, Pittsburgh, Pennsylvania, 1925.

25. Beer, F.P., Johnston, Jr., E.R., Mechanics of Materials, McGraw Hill Book Company, New York, New York, 1981, page 158.

26. American Society for Testing and Materials, Annual Book of ASTM Standards, Volume 8.02, Plastics (II), Philadelphia Pennsylvania, 1991, pages 328-329.

27. Weather of U.S. Cities, Third edition, Volume 1, Gale Research Co., Detroit, Michigan, 1987, page 386.

28. The Weather Almanac, Sixth Edition, Gale Research Co., Detroit, Michigan, 1992, page 542.

29. American Society for Testing and Materials, Annual Book of ASTM Standards, Volume 4.02, Philadelphia Pennsylvania, 1991, pages 266-269.

ACKNOWLEDGEMENTS

This investigation on fiber composite rods as described herein was conducted at Iowa State University (ISU) through the auspices of the Engineering Research Institute with sponsorship provided by the Iowa Department of Transportation and the Highway Research Board. This work was conducted at the ISU Structural Engineering Research Laboratories. The author wishes to thank the sponsors and all those individuals involved in the coordination of the project at the IDOT, particularly Brian McWaters and Vernon Marks for their consultation, time, and coordination with the project. The author wishes to acknowledge and thank the following firms for donation of material as well as for consultation advice during the course of the project: Economy Forms of Des Moines, Iowa; W. G. Block of Des Moines, Iowa; Composite Technologies Corporation of Ames, Iowa; Marshal Vega of Harrison, Arkansas; and Morrison Molded Fiber Glass of Bristol, Virginia. In addition, the author wishes to thank the following individuals: Jerry Mass, Robert Long, Ed Sauter, and Phil Catsman.

The author wishes to express his sincere thanks to Dr. Max L. Porter (as major professor and project director) and Mr. Bruce A. Barnes for their continued support throughout this project. Also, the author thanks previous graduate

students, Mr. Bradley R. Lehr and Mr. Kent E. Fish, for donating their research knowledge to this project. Thanks to Mr. Kasi P. Viswanath for his help in developing the theoretical model in Chapter 6.

The work of the several undergraduate assistants (namely Brent Brubaker, Dave Neuberger, and Paul Boring) who spent many hours in preparing the specimens and collecting the data is gratefully acknowledged along with the help of the Structural Engineering Laboratory Supervisor, Mr. Douglas L. Wood.

APPENDIX

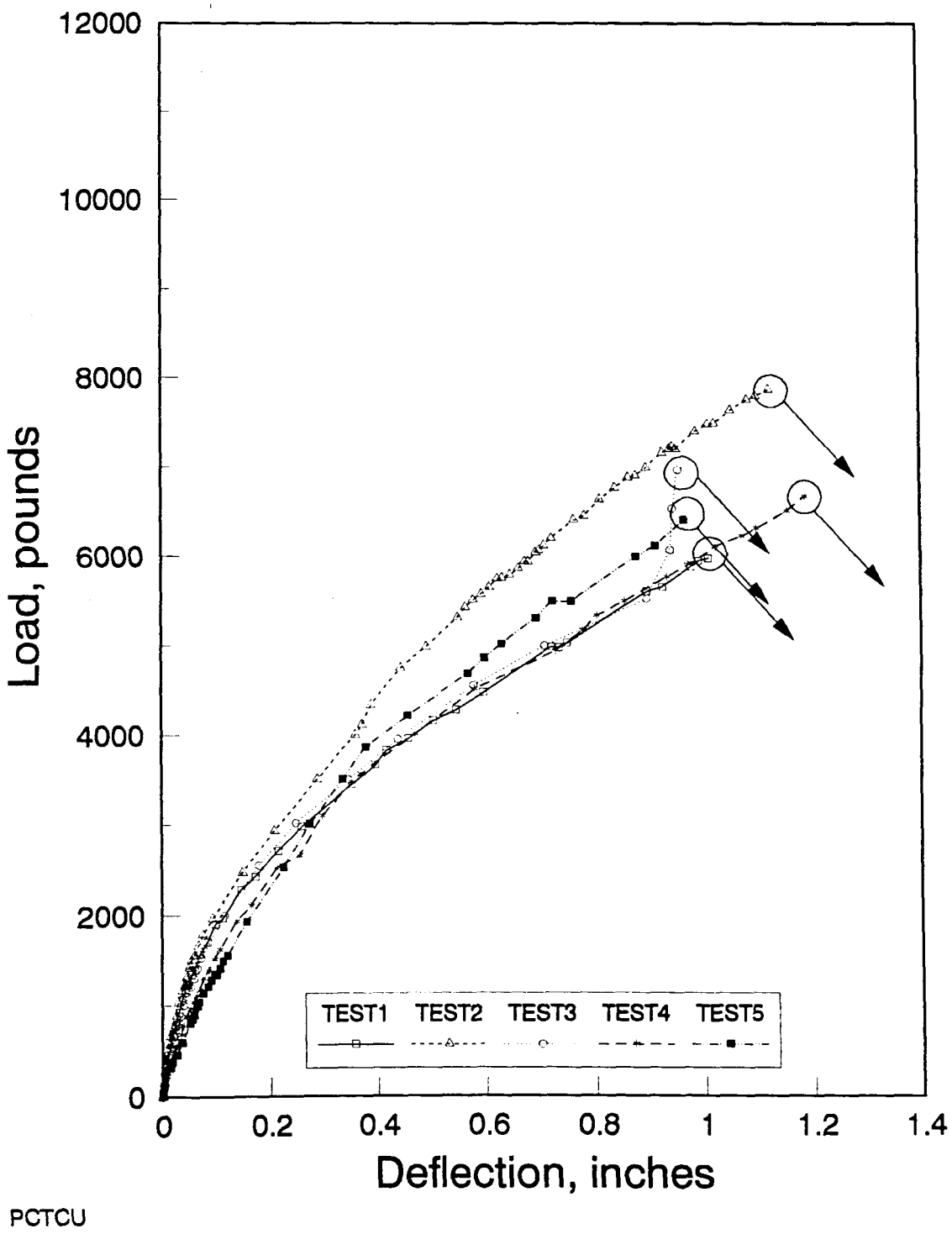

Figure A1. B-FC-P-U assembly

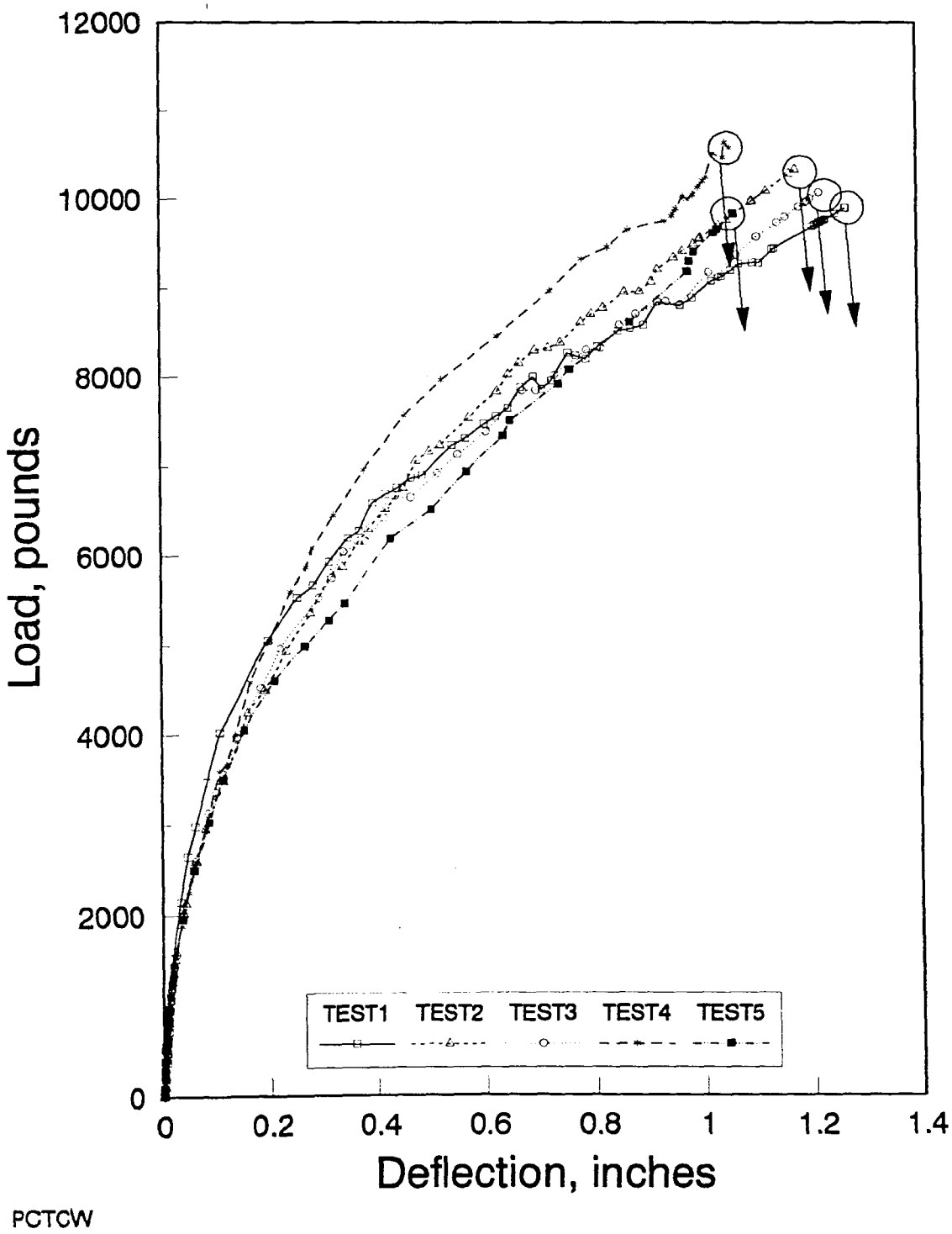

Figure A2. B-FC-P-W assembly

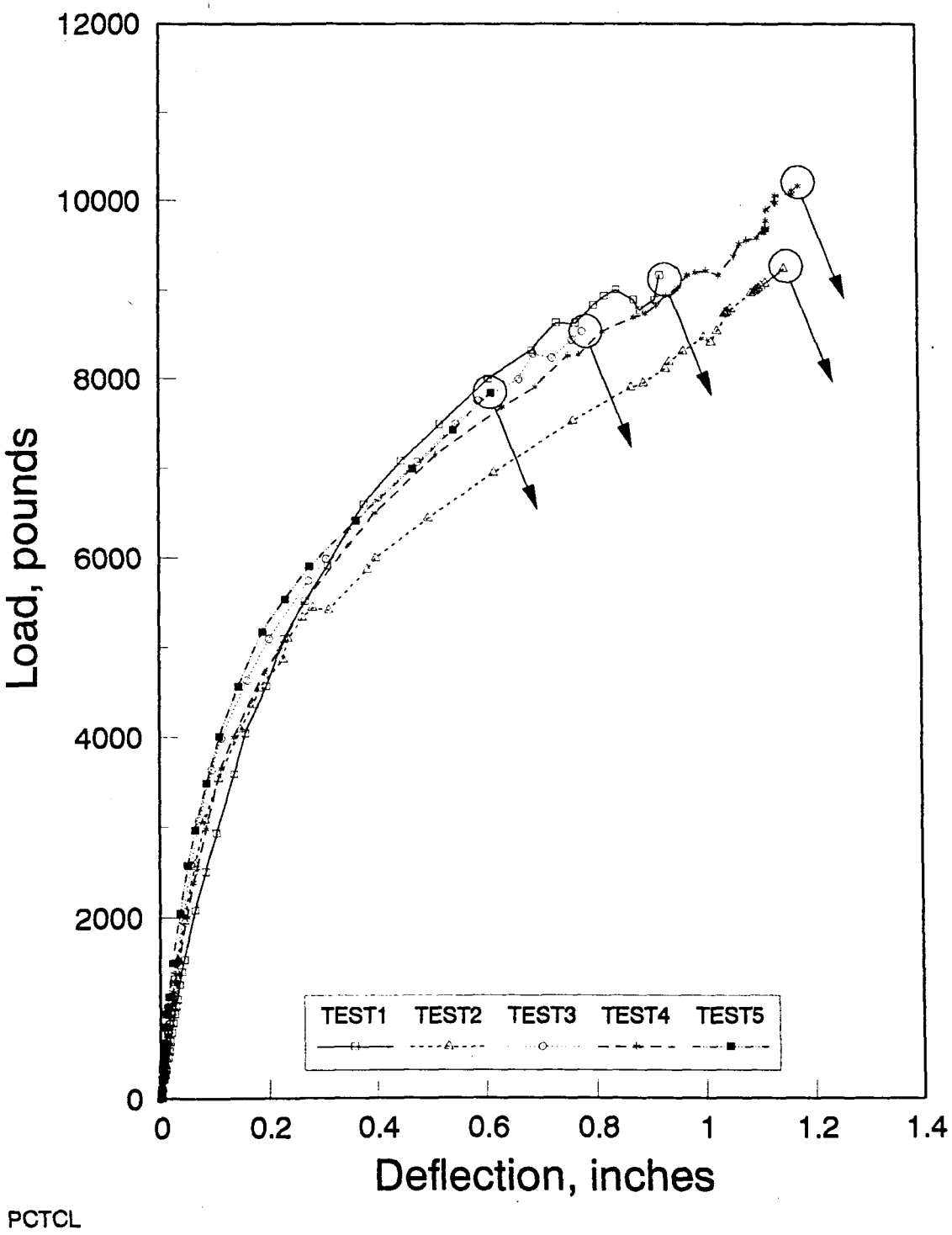

Figure A3. B-FC-P-L assembly

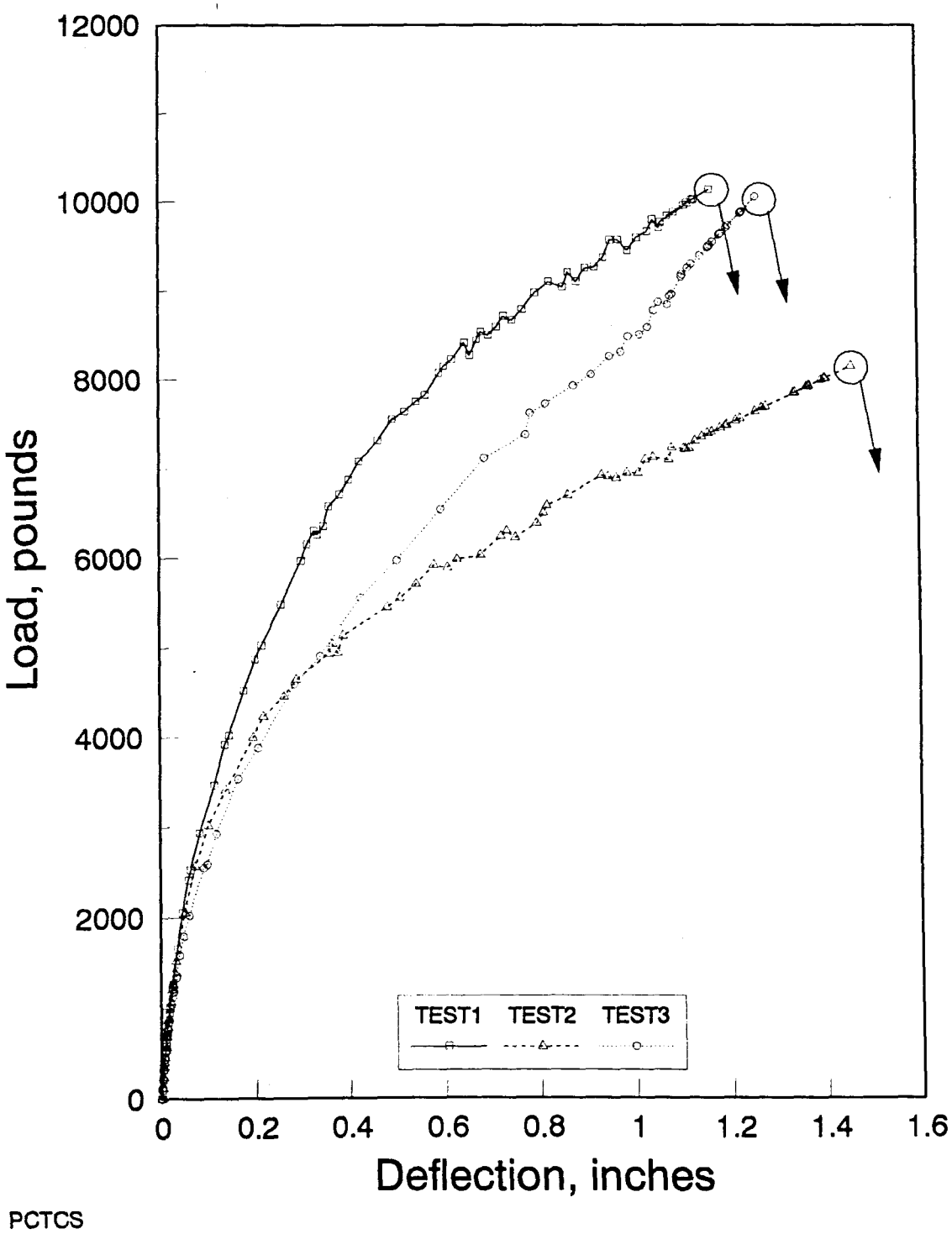

Figure A4. B-FC-P-S assembly

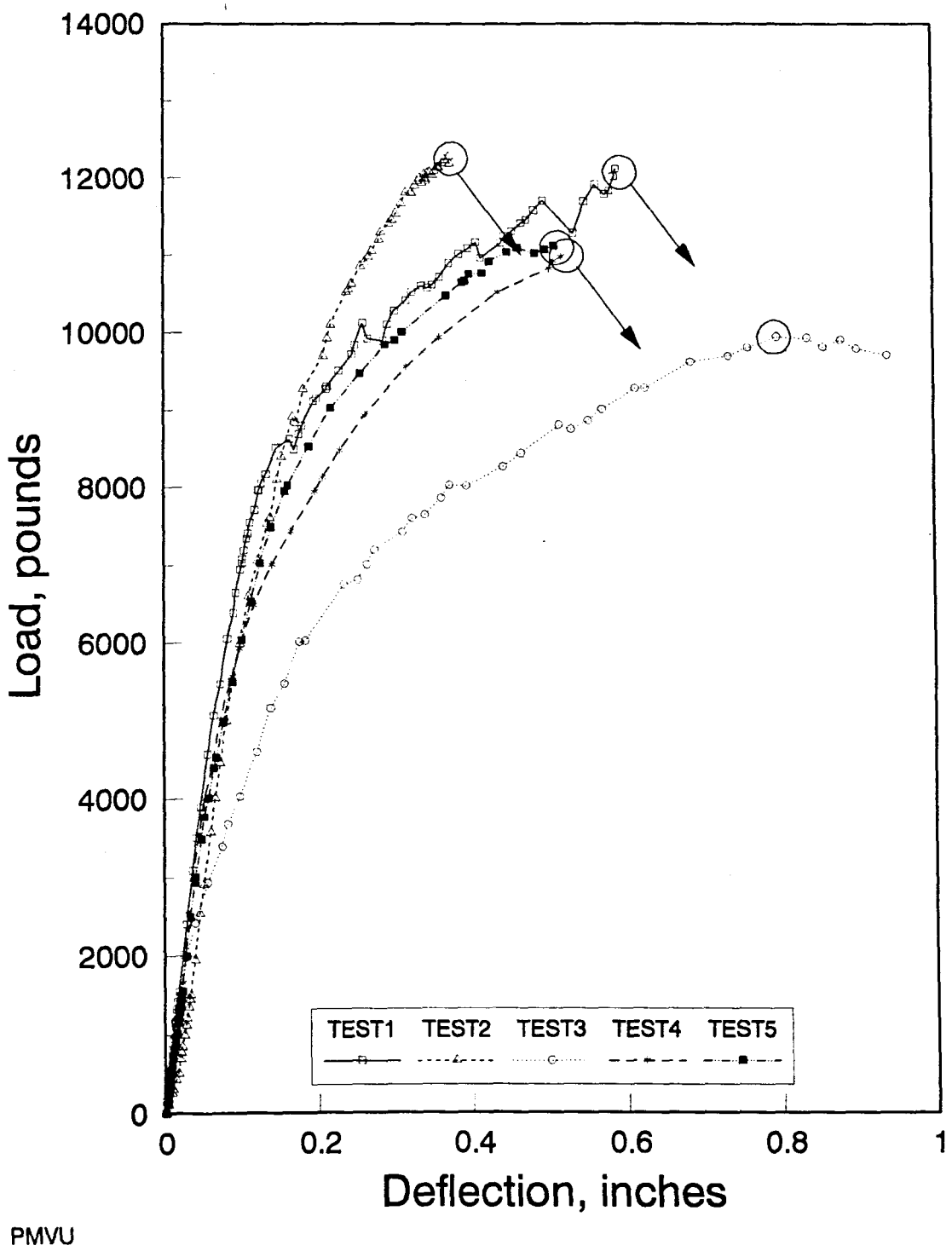

Figure A5. C-FC-P-U assembly

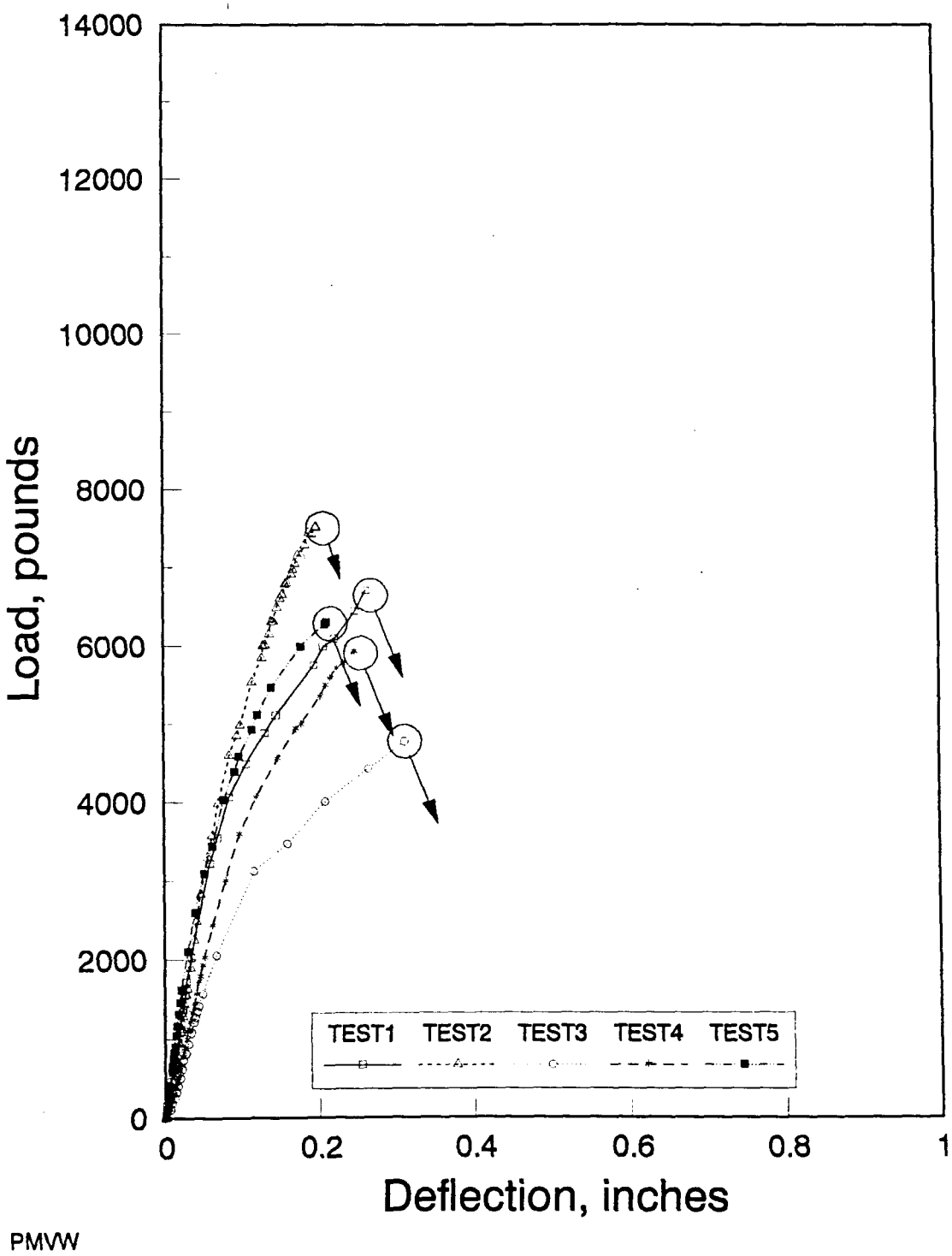

Figure A6. C-FC-P-W assembly

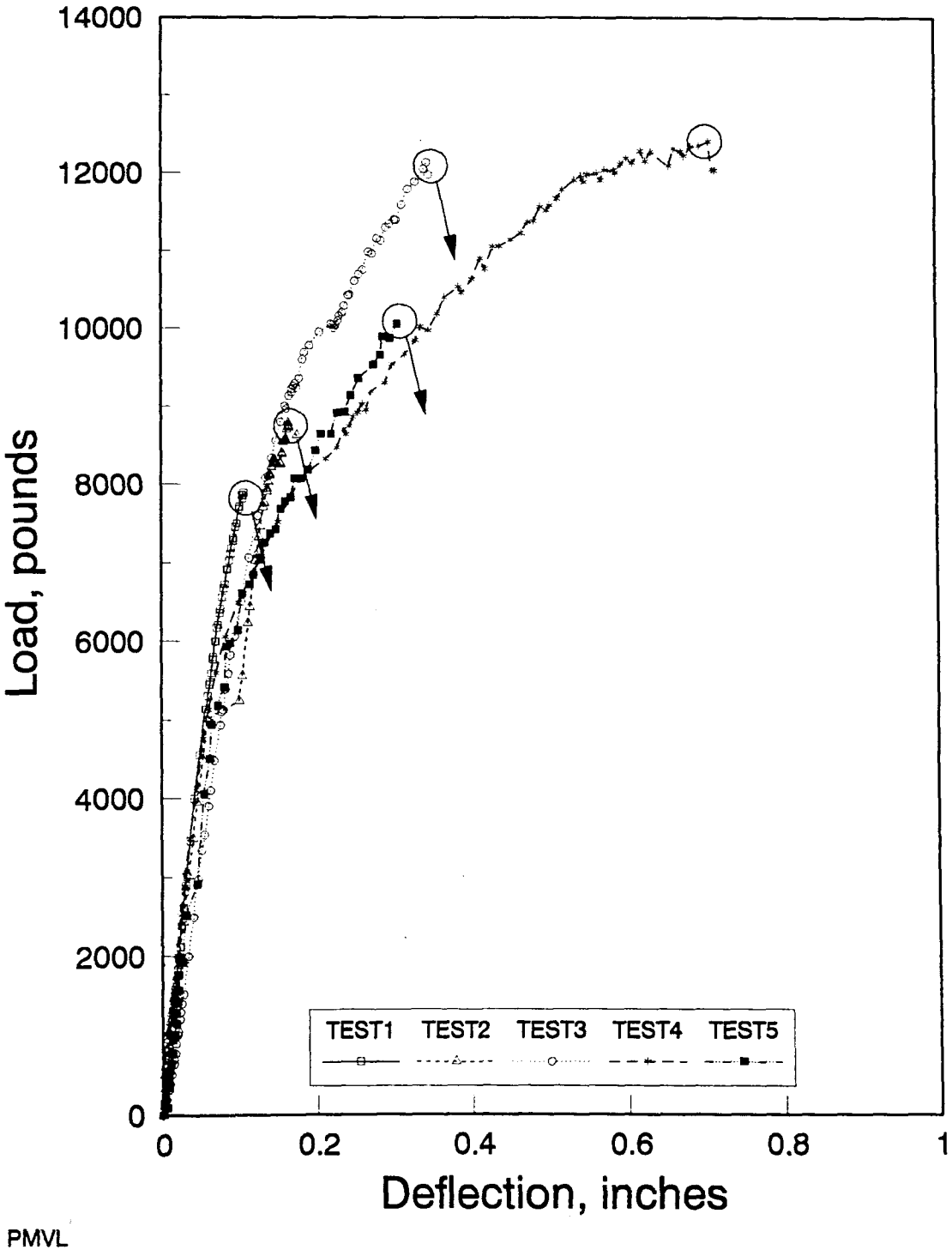

Figure A7. C-FC-P-L assembly

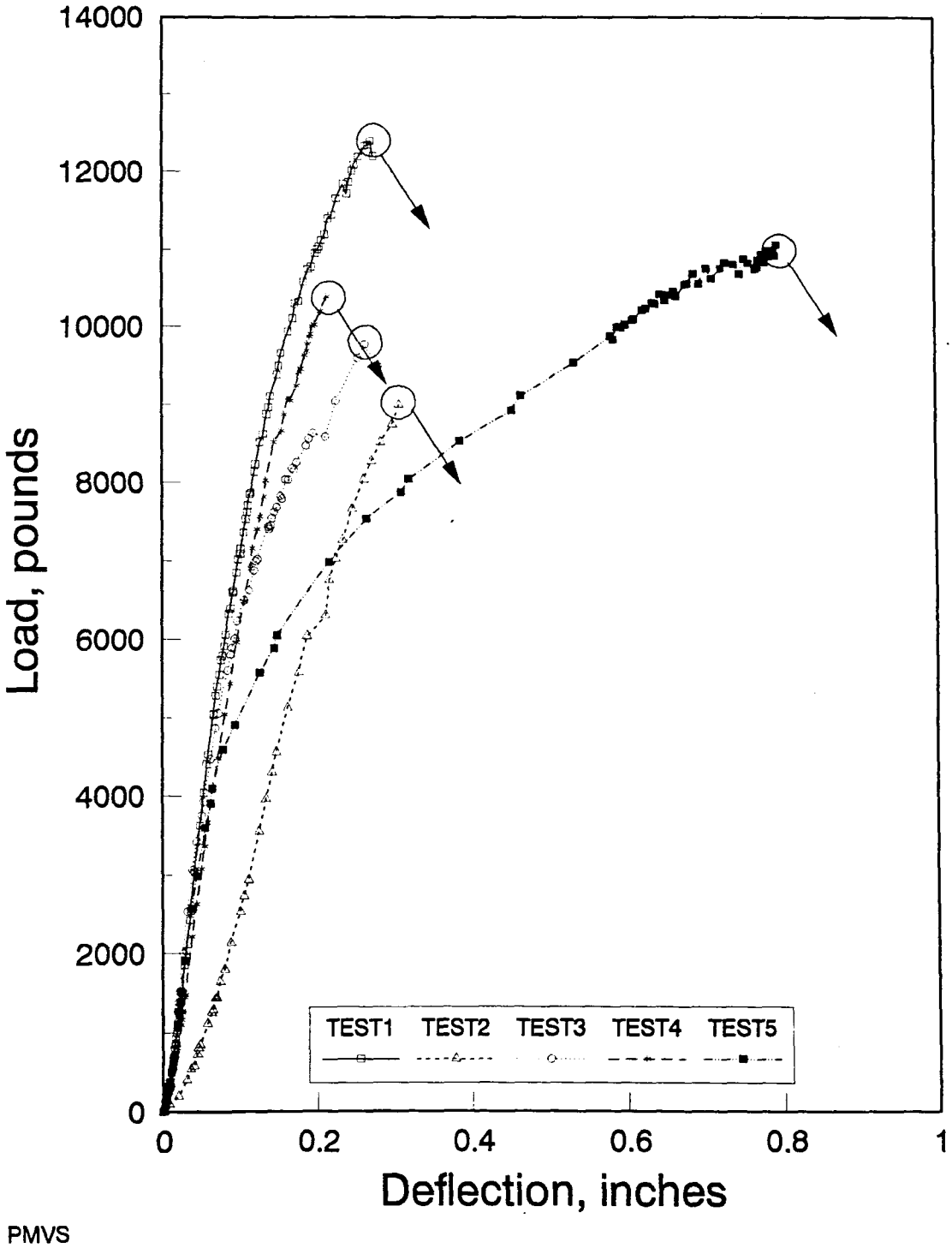

Figure A8. C-FC-P-S assembly

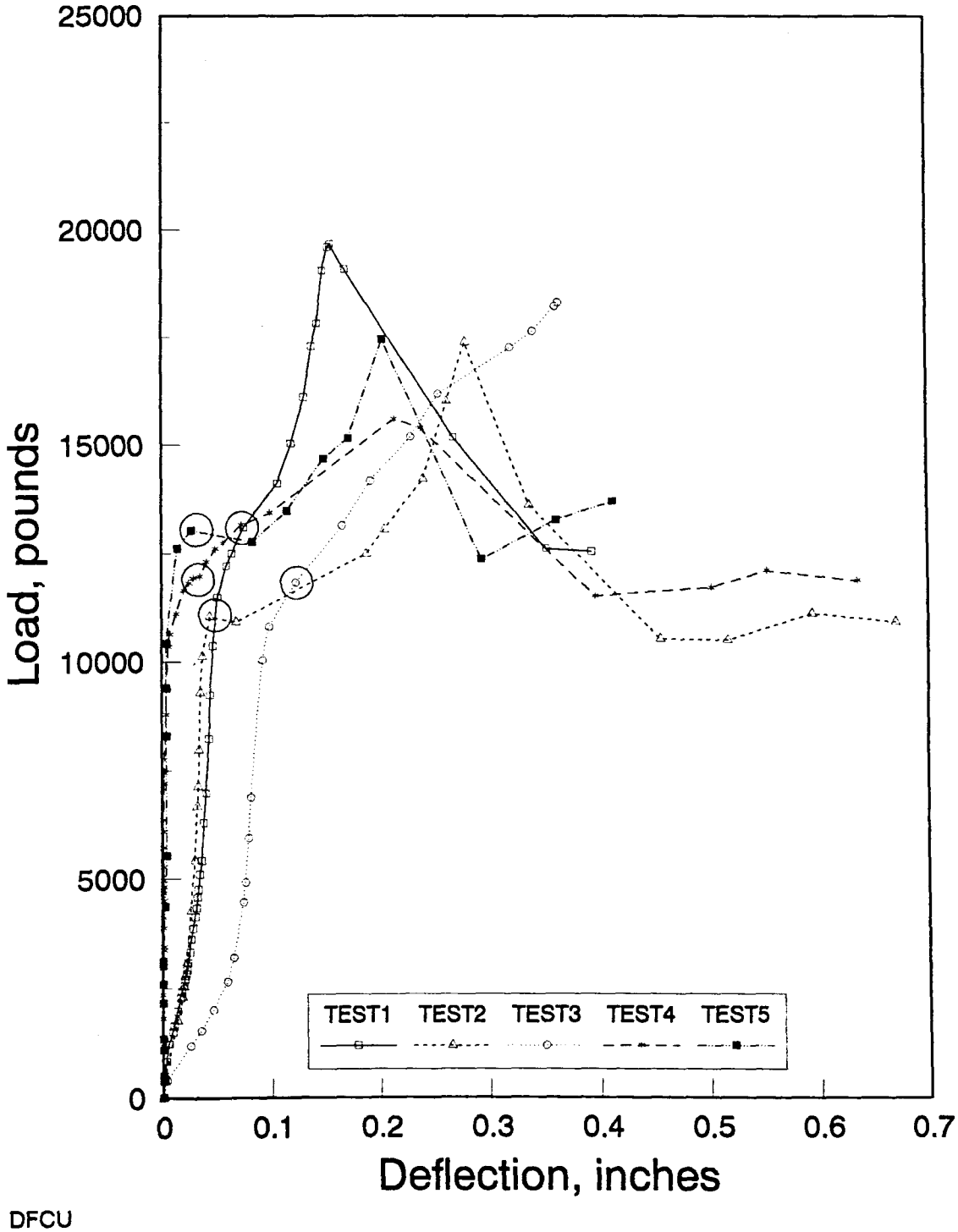

Figure A9. A-FC-D-U assembly

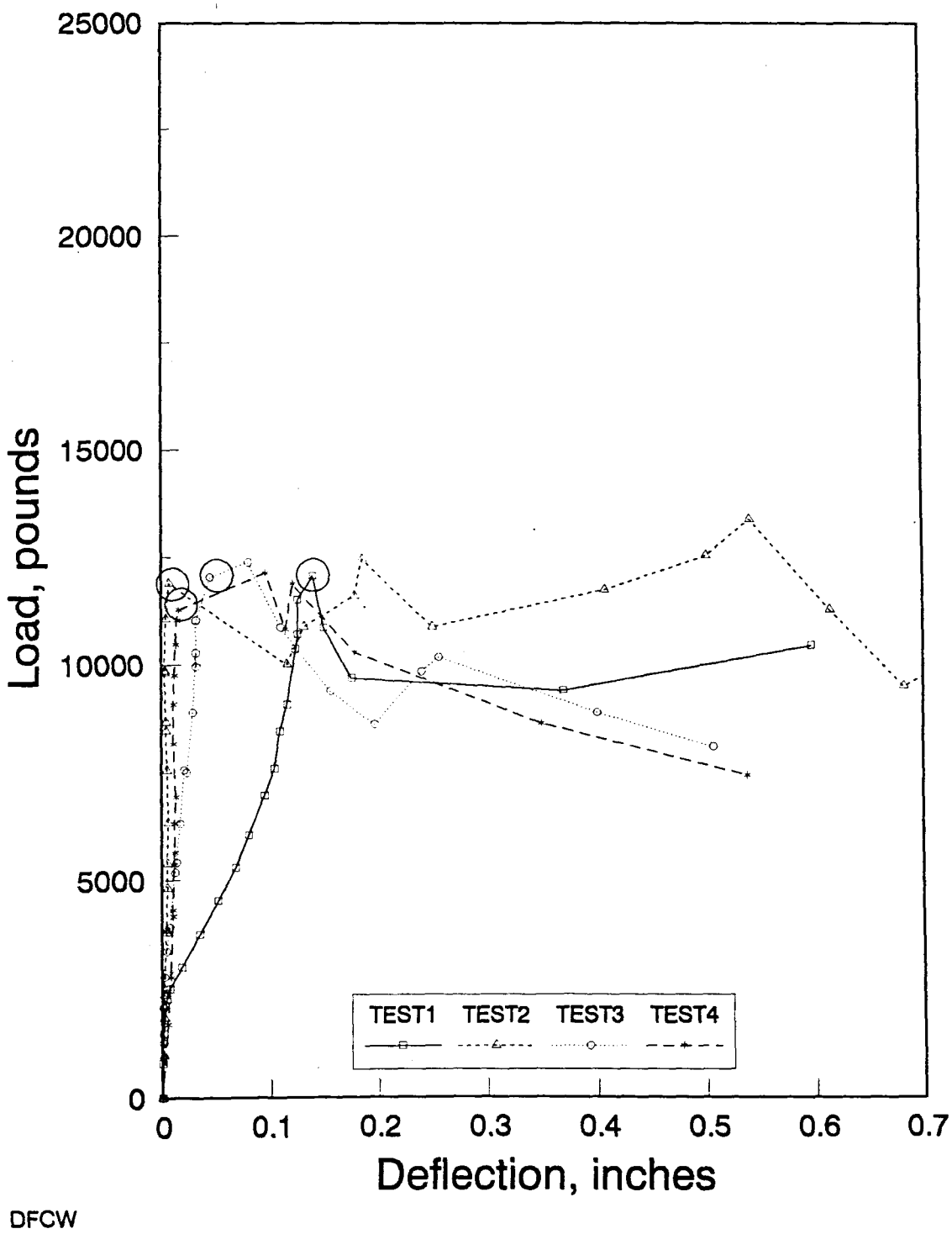

Figure A10. A-FC-D-W assembly

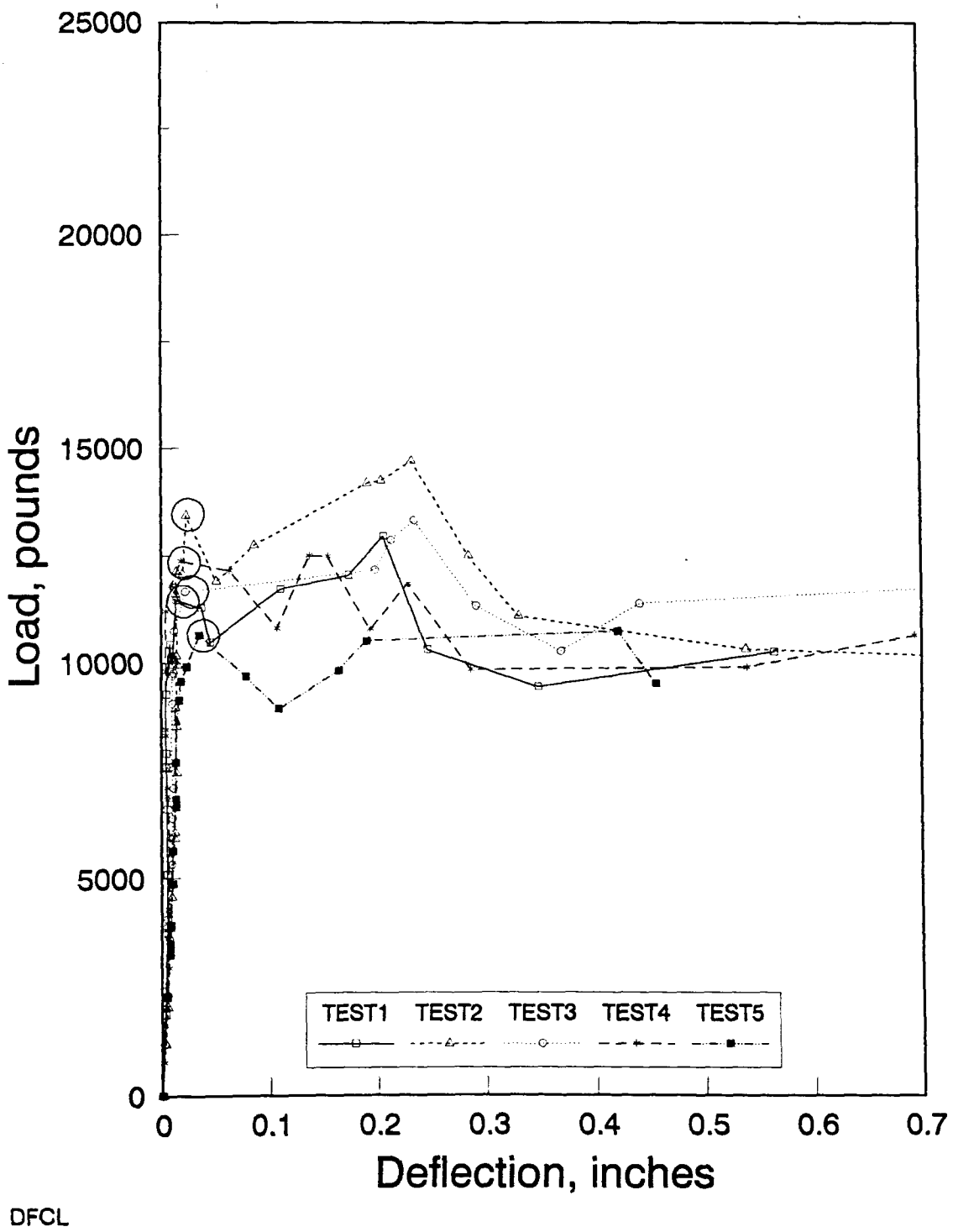

Figure A11. A-FC-D-L assembly

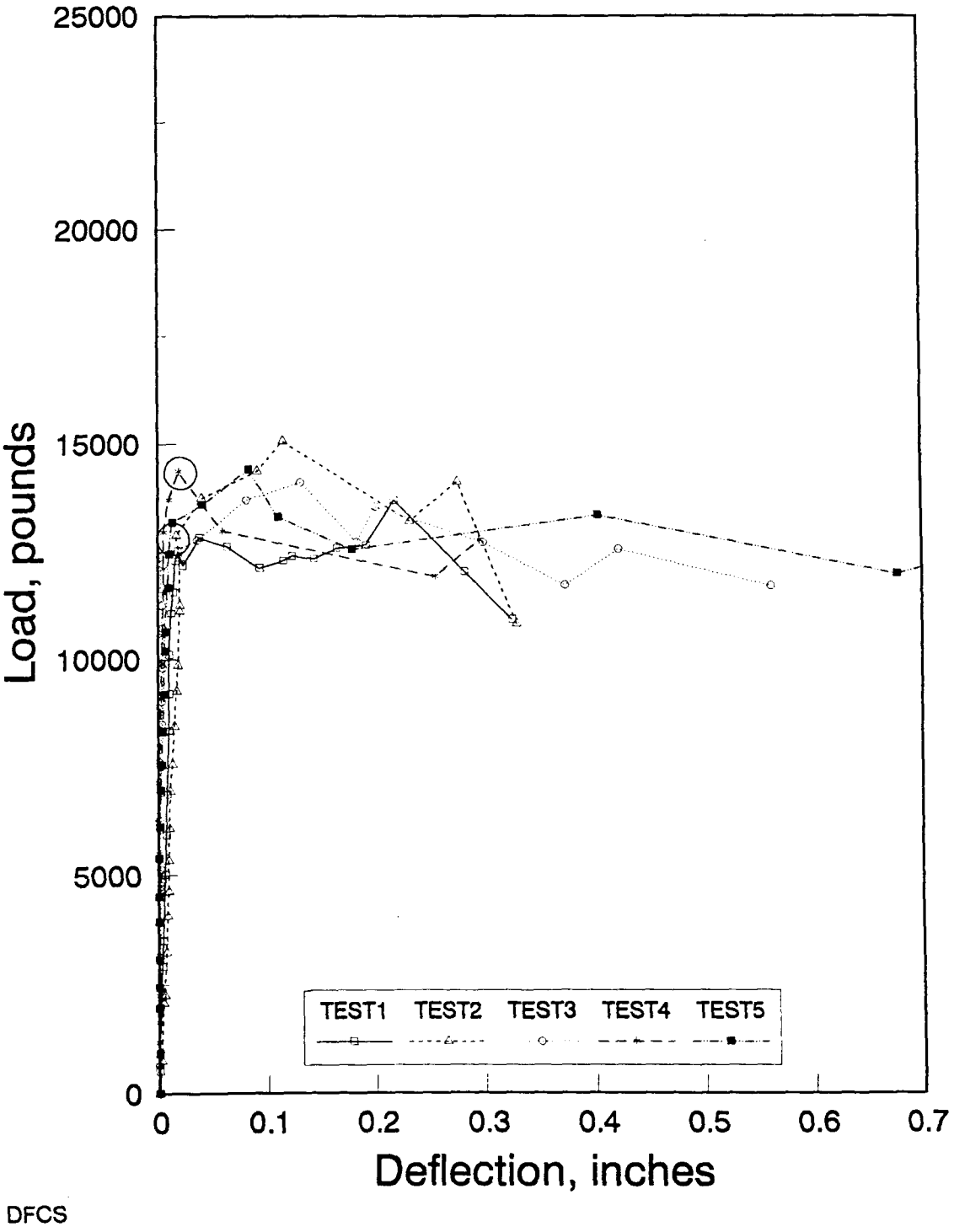

Figure A12. A-FC-D-S assembly

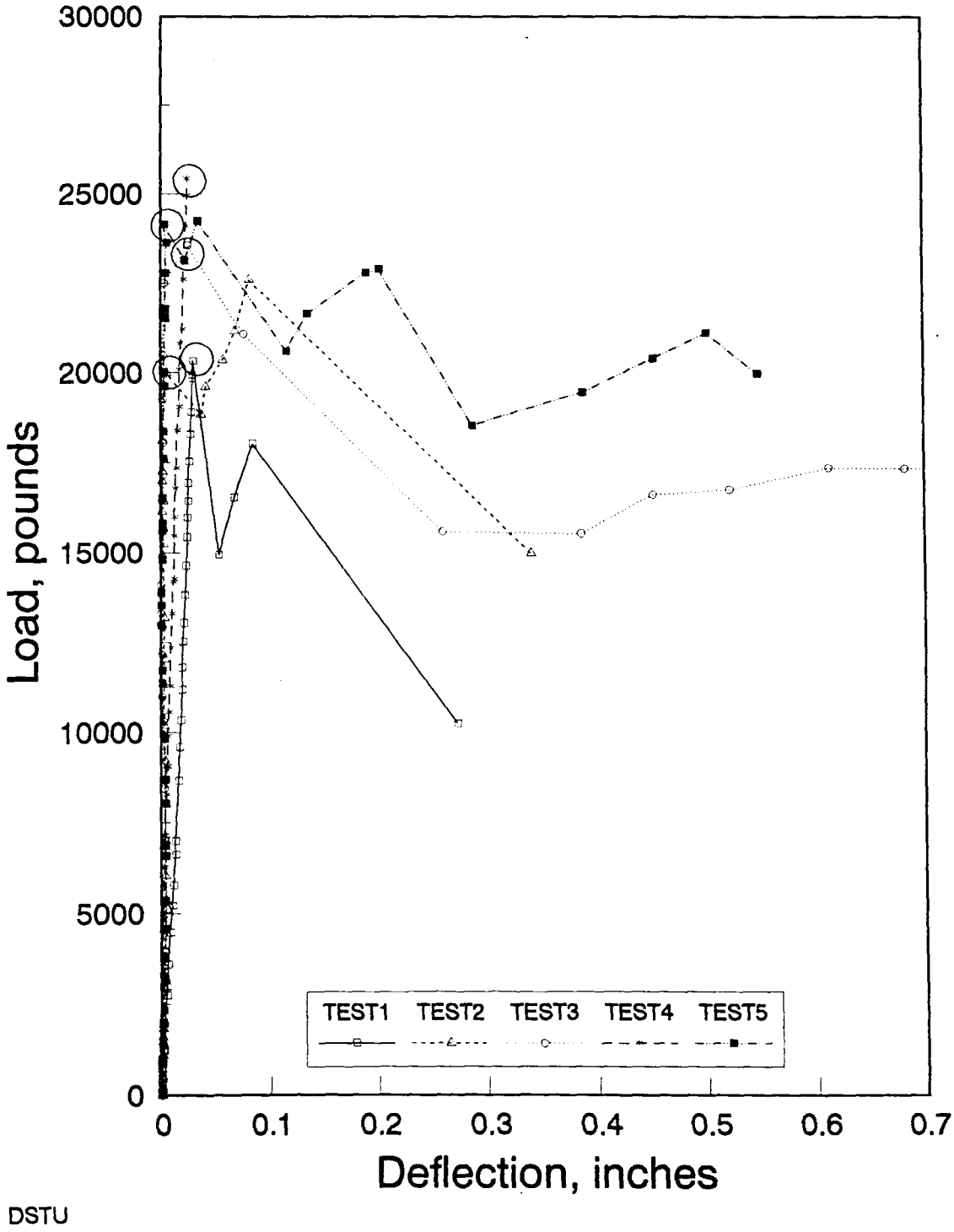

Figure A13. O-S-D-U assembly

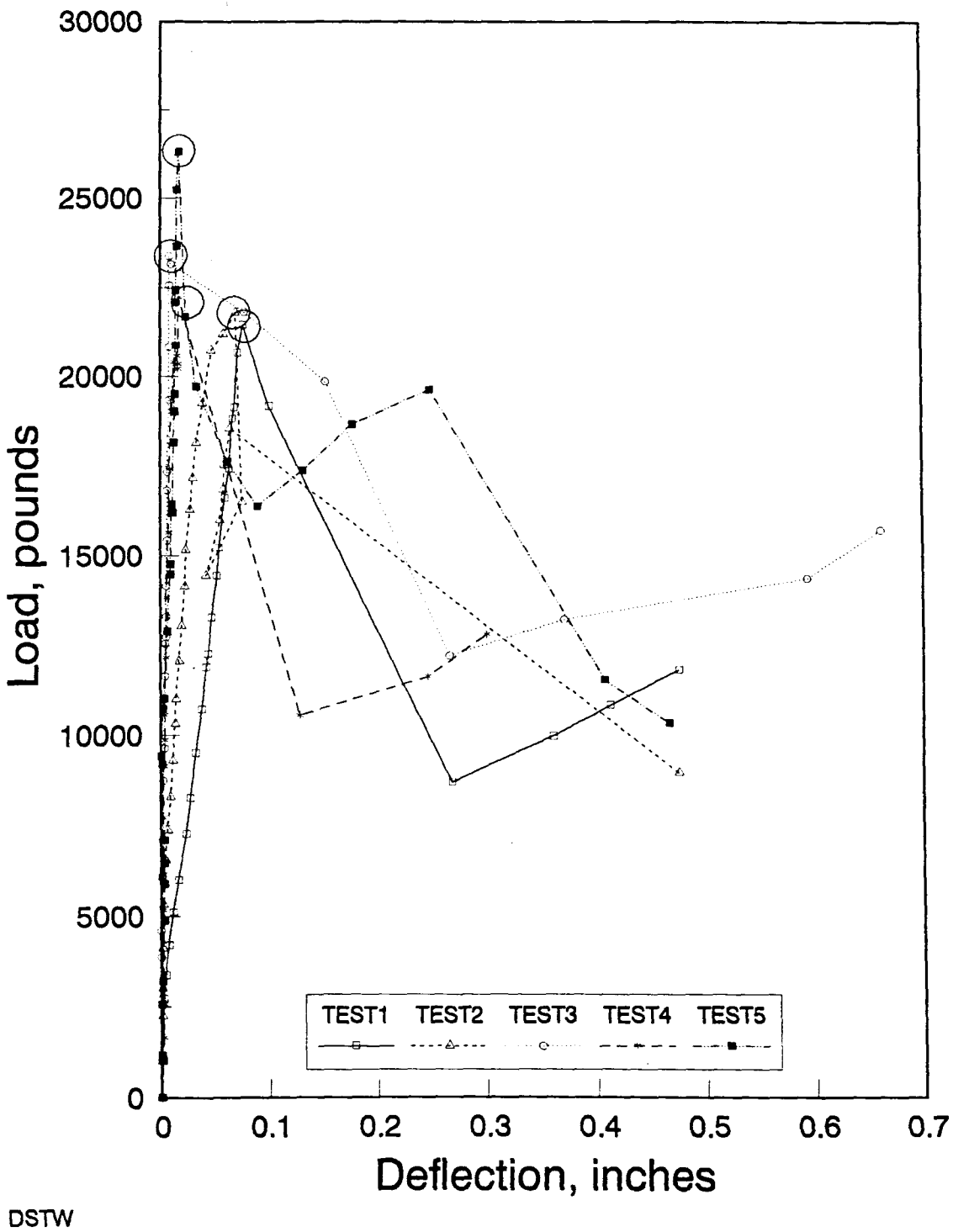

Figure A14. O-S-D-W assembly

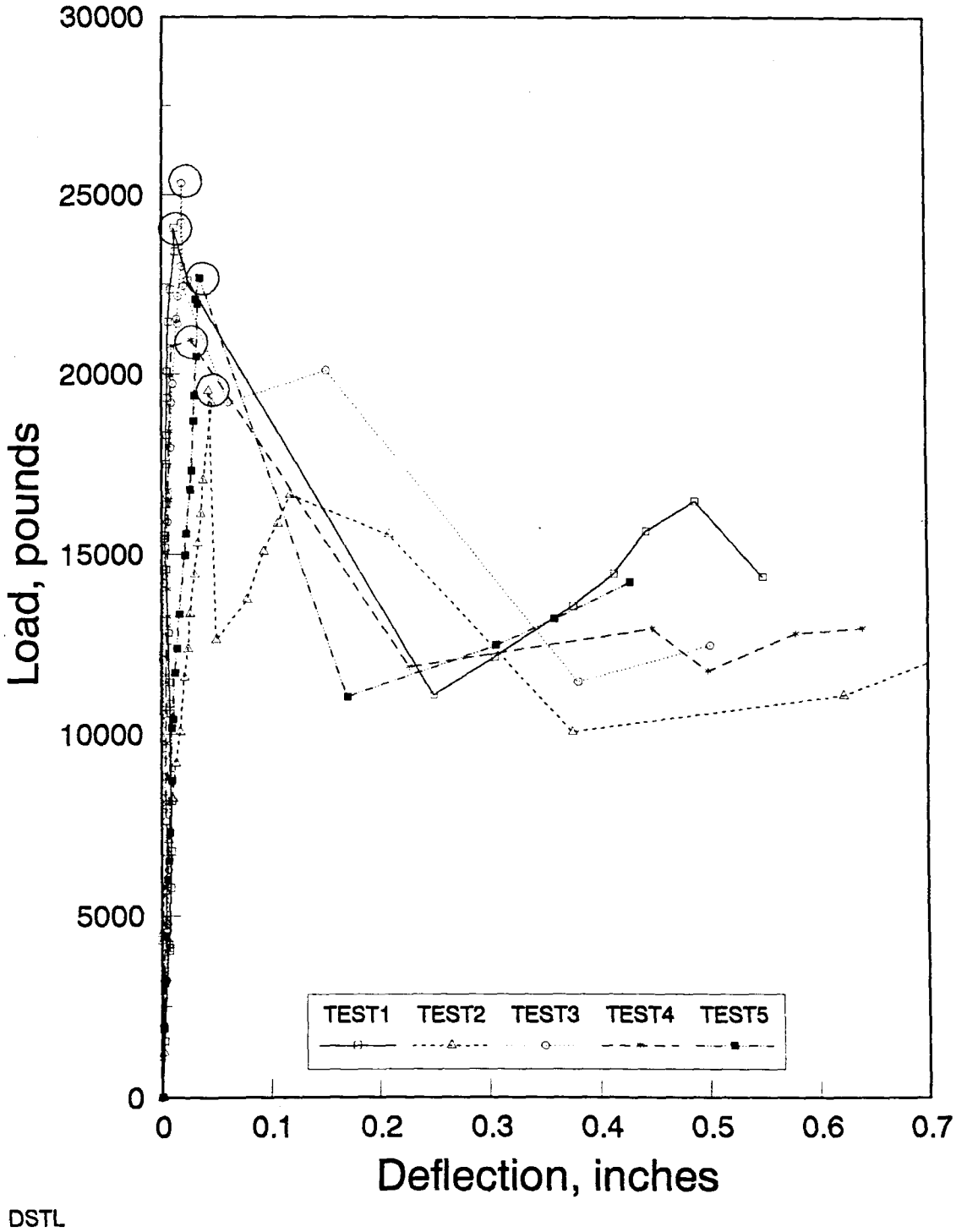

Figure A15. O-S-D-L assembly

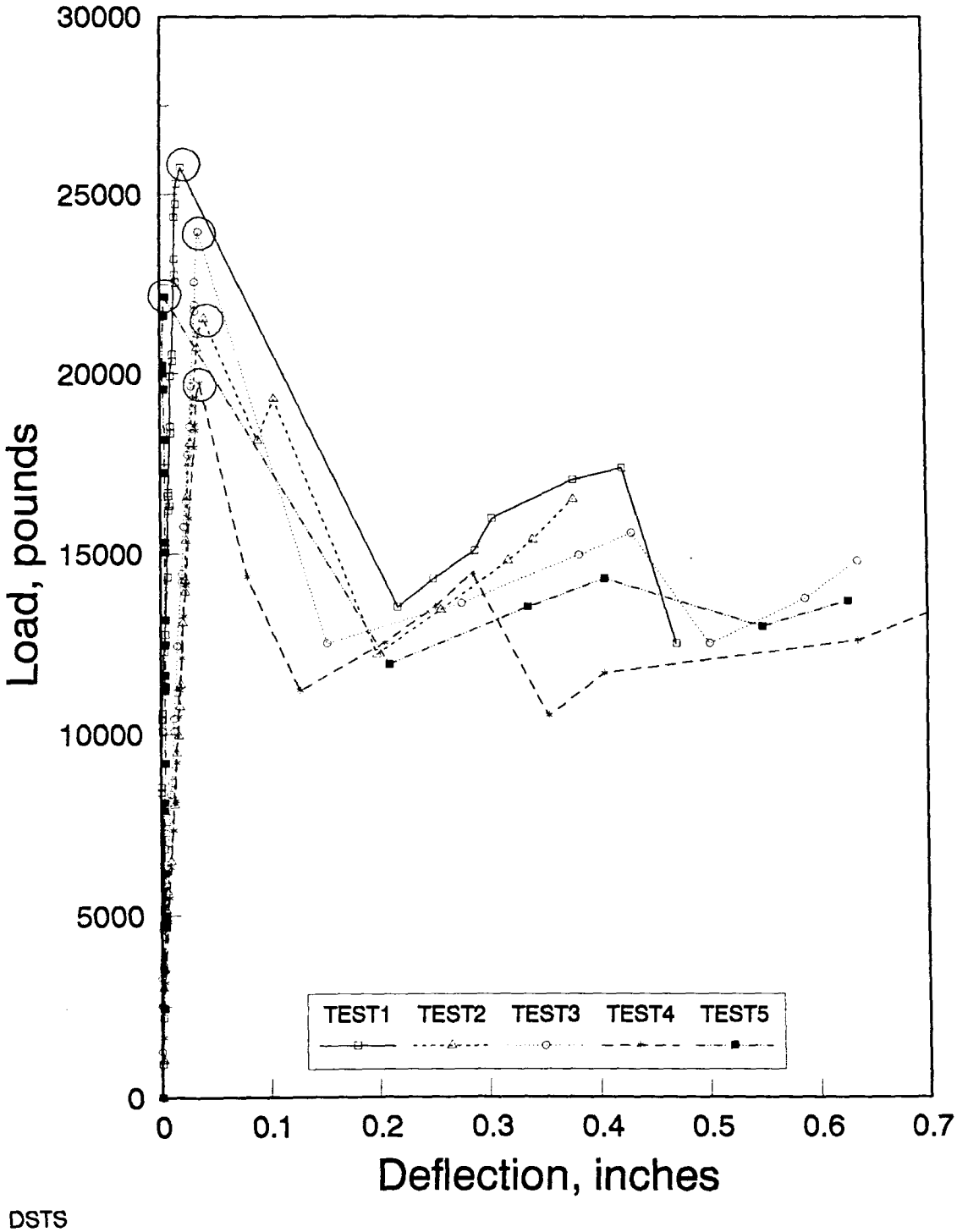

Figure A16. O-S-D-S assembly

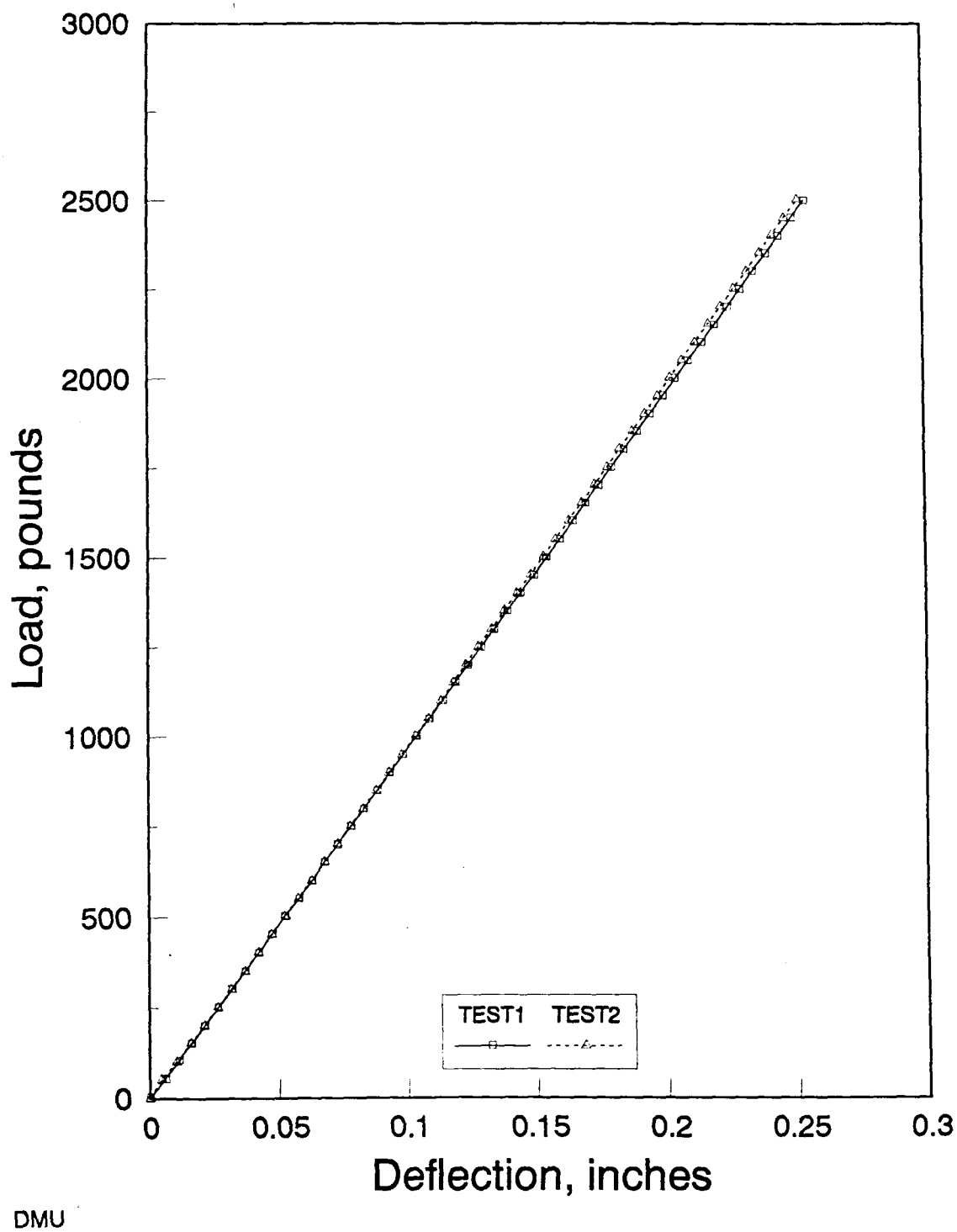

Figure A17. Modulus of elasticity curves for unaged 1.25-in. dowel

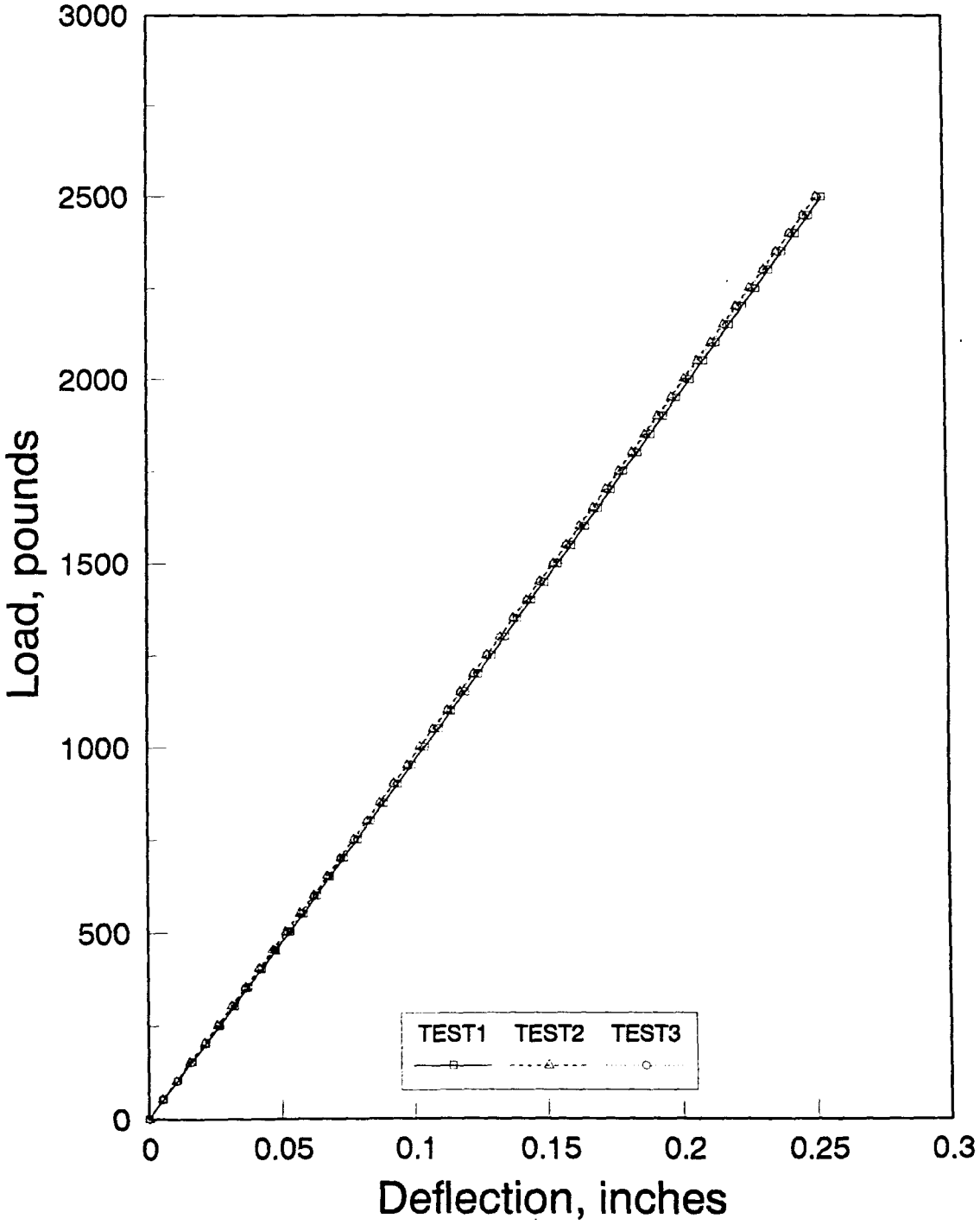

Figure A18. Modulus of elasticity curves for 1.25-in. dowel bars aged in water

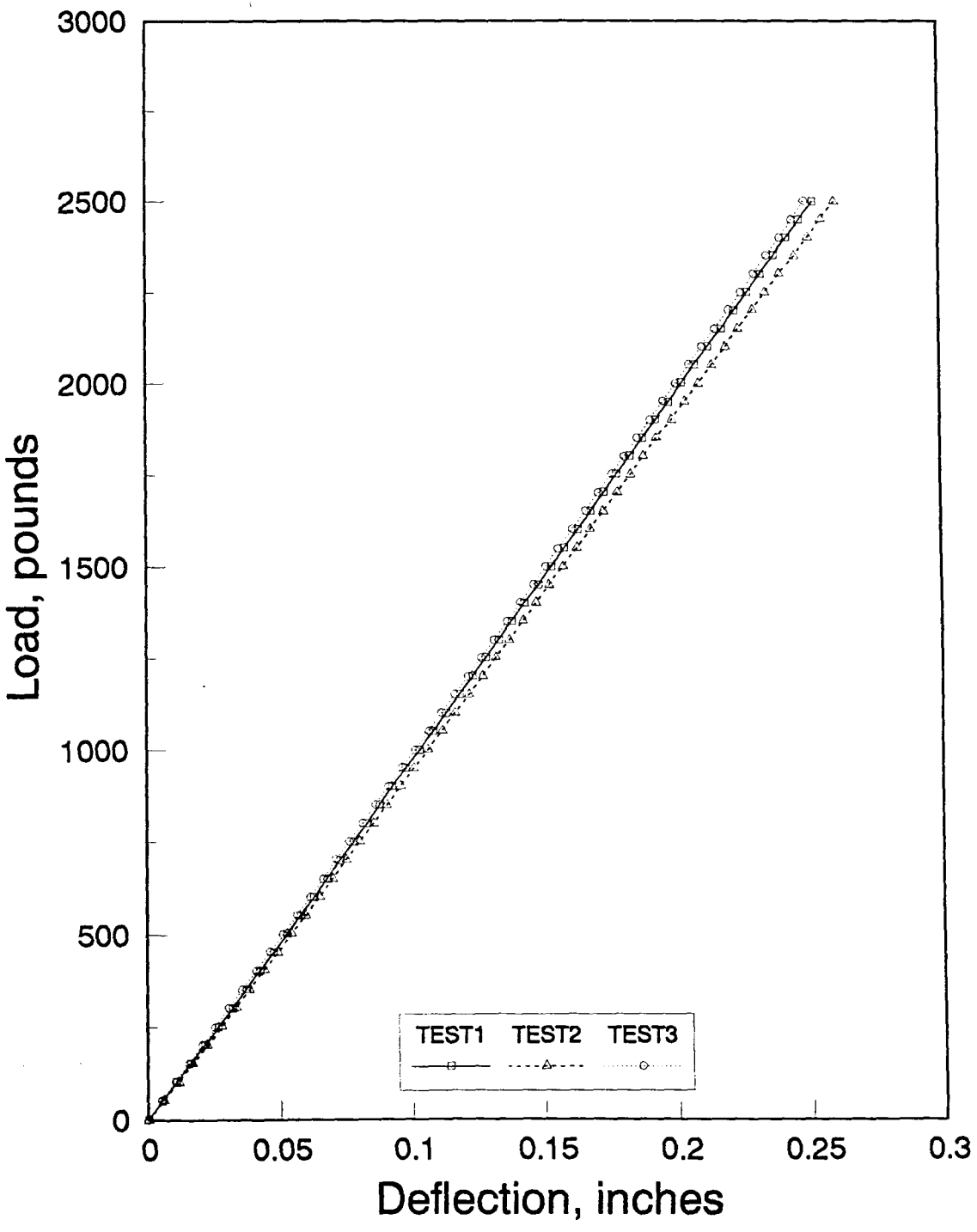

Figure A19. Modulus of elasticity curves for 1.25-in. dowel bars aged in lime

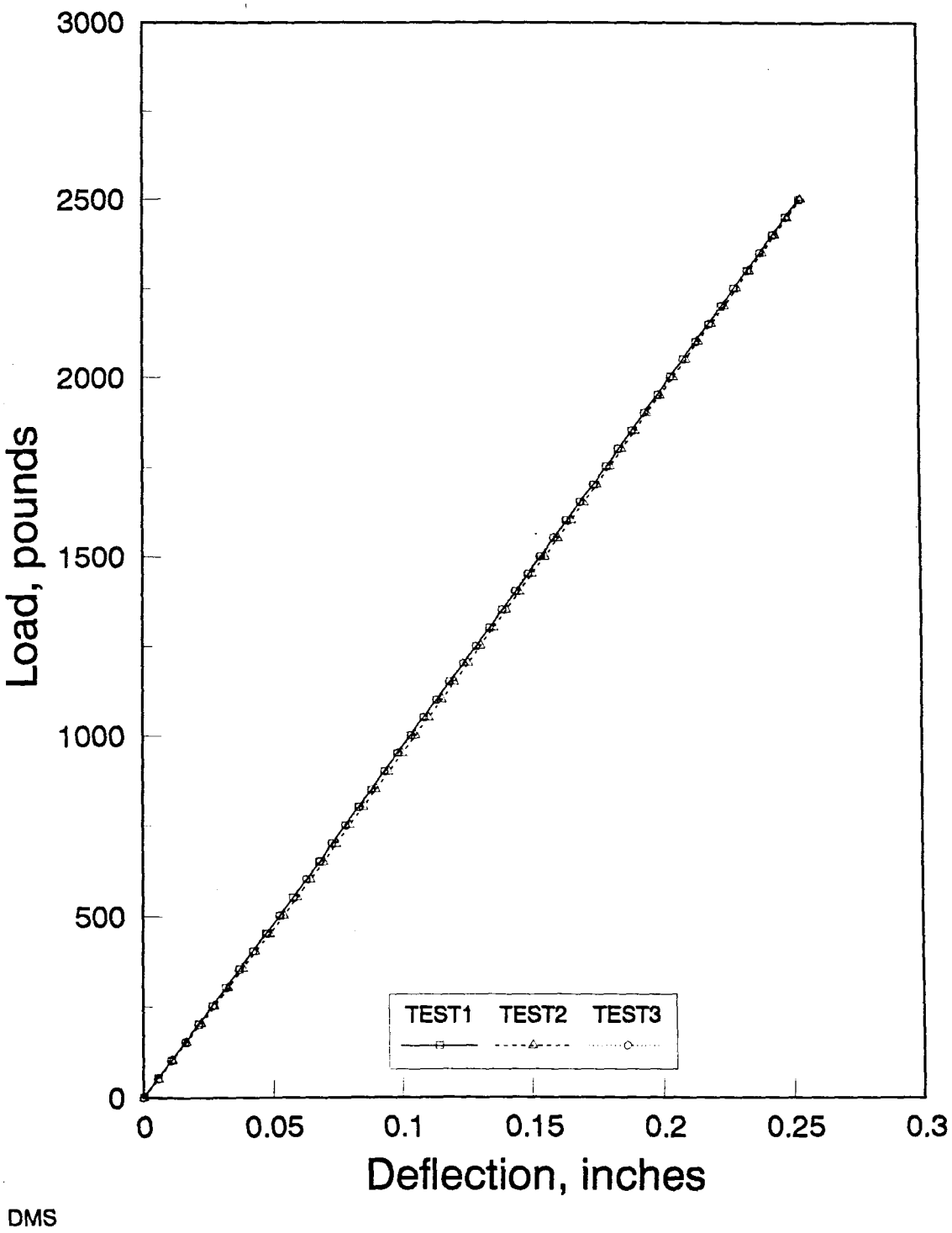

Figure A20. Modulus of elasticity curves for 1.25-in. dowel bars aged in salt

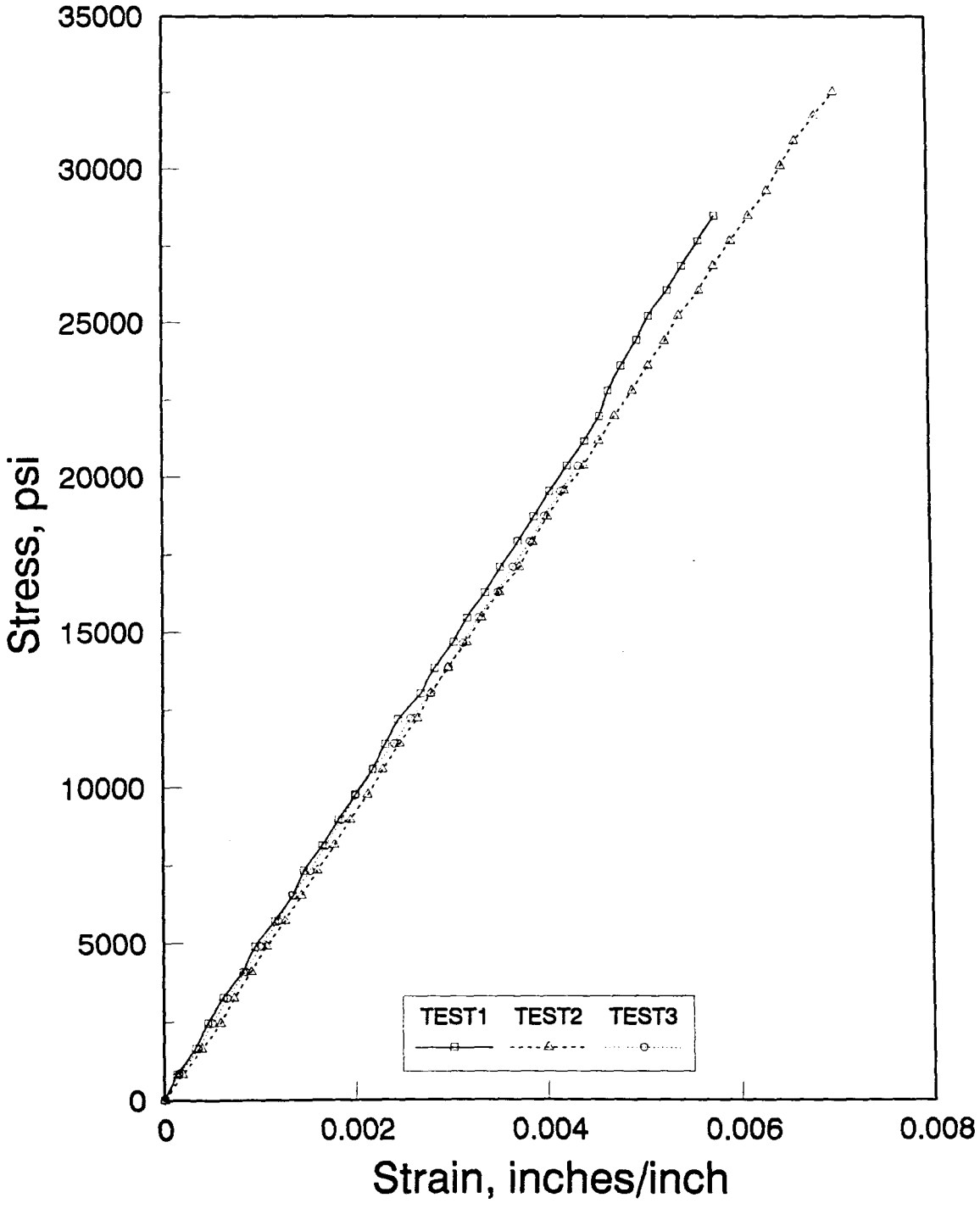

Figure A21. Tensile modulus for Supplier B three-eighths-inch FC rebar

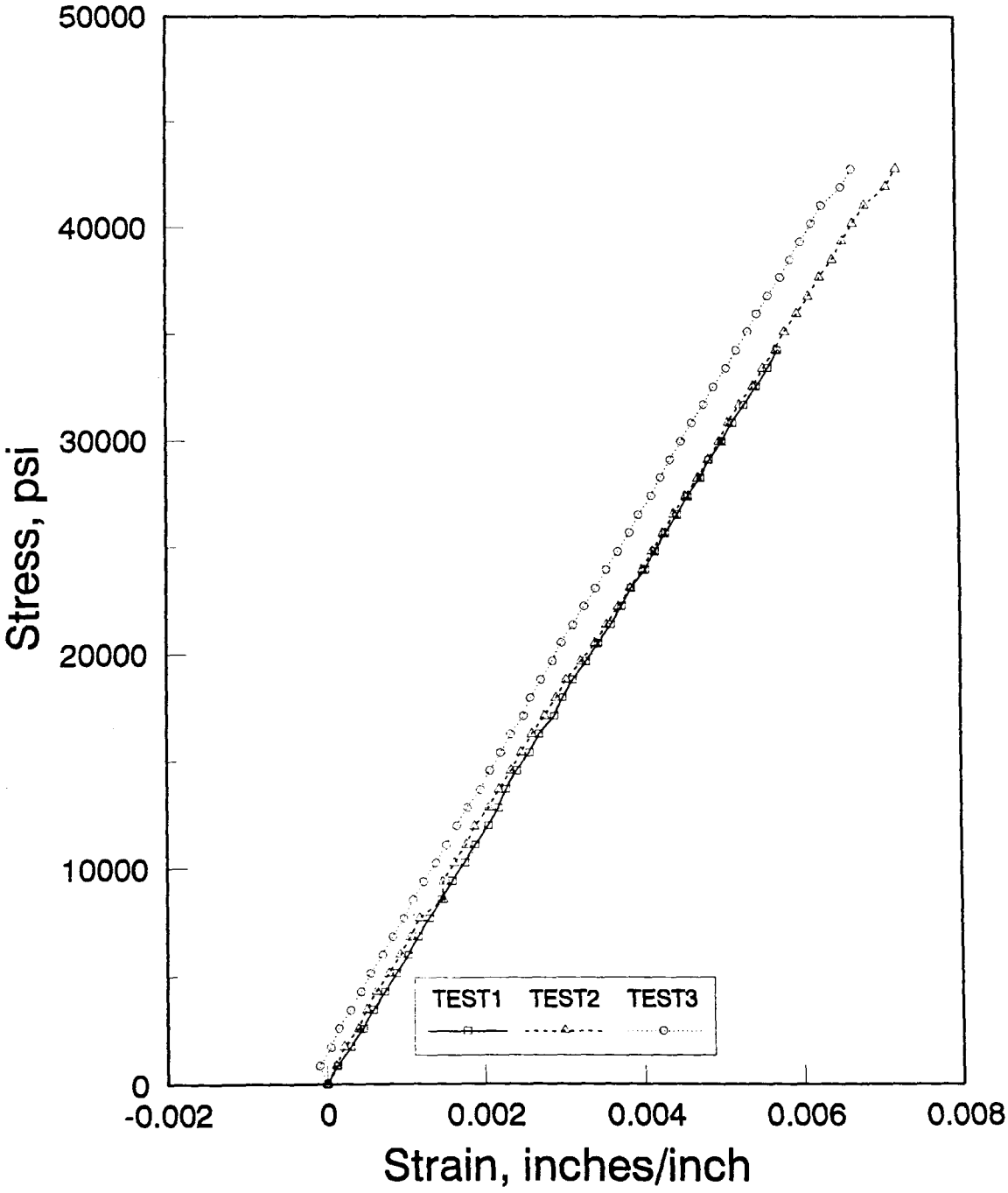

Figure A22. Tensile modulus for Supplier C three-eighths-inch FC rebar

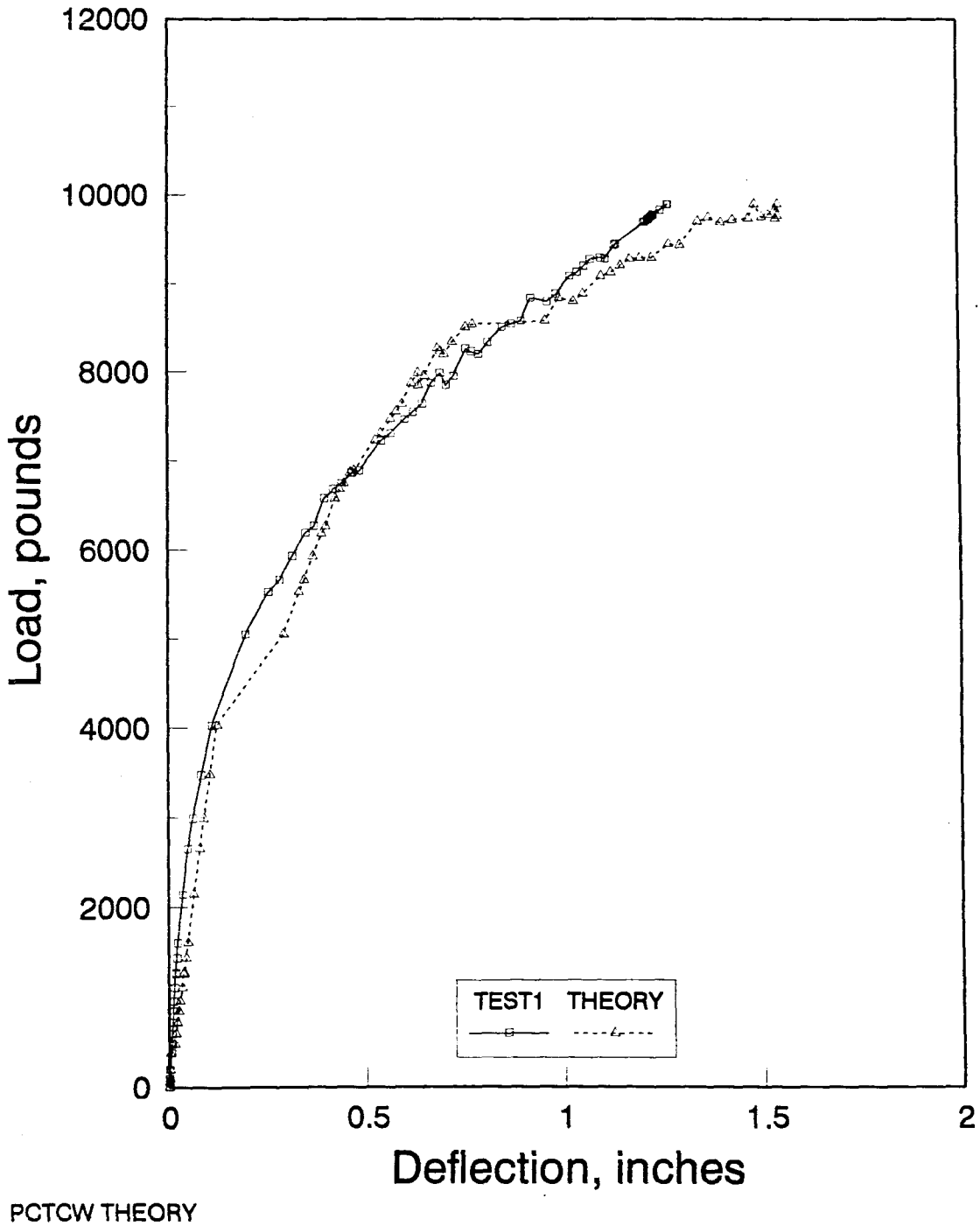

Figure A23. Comparison of approximated and experimental load-deflection curves for B-FC-P-W assembly

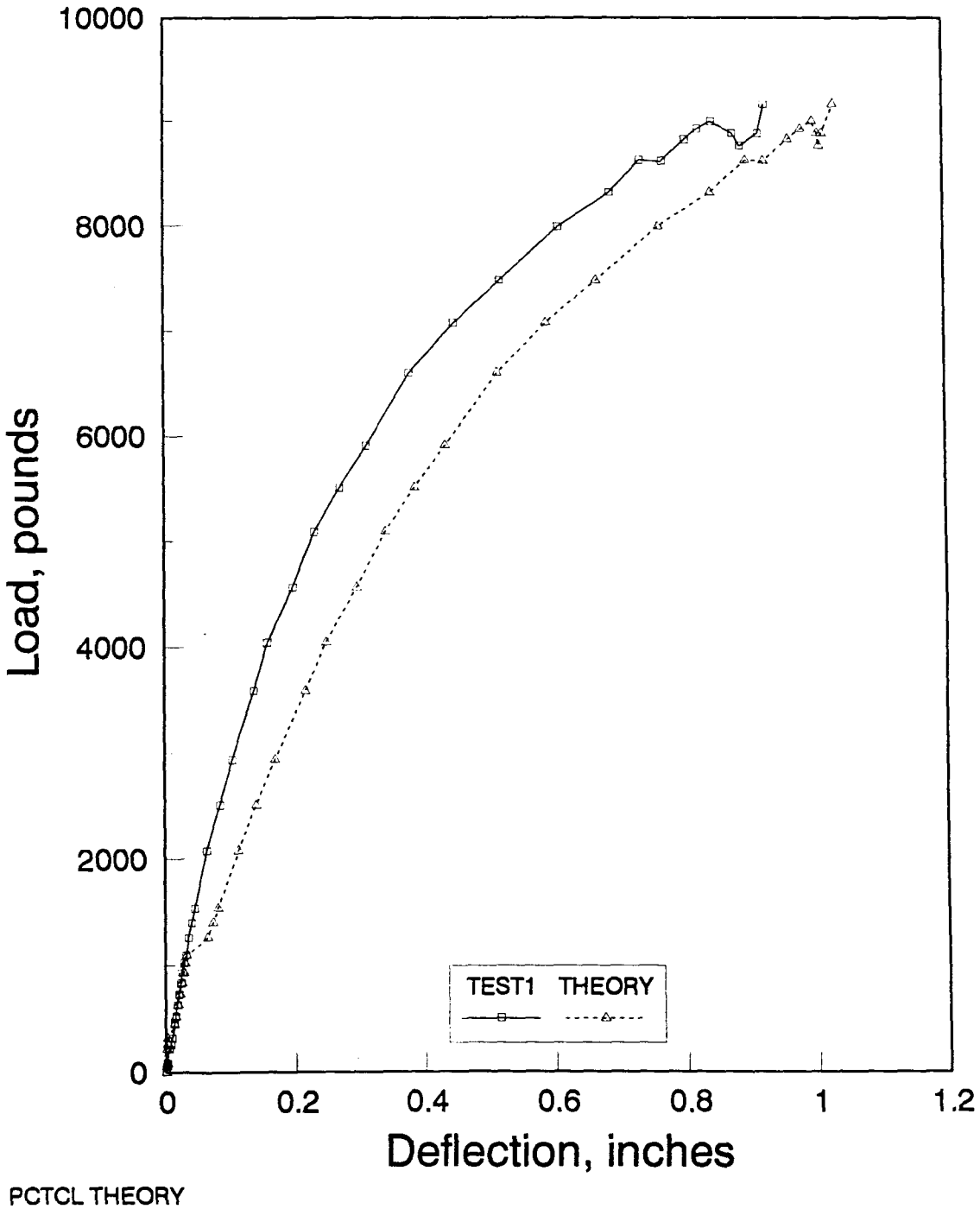

Figure A24. Comparison of approximated and experimental load-deflection curves for B-FC-P-L assembly

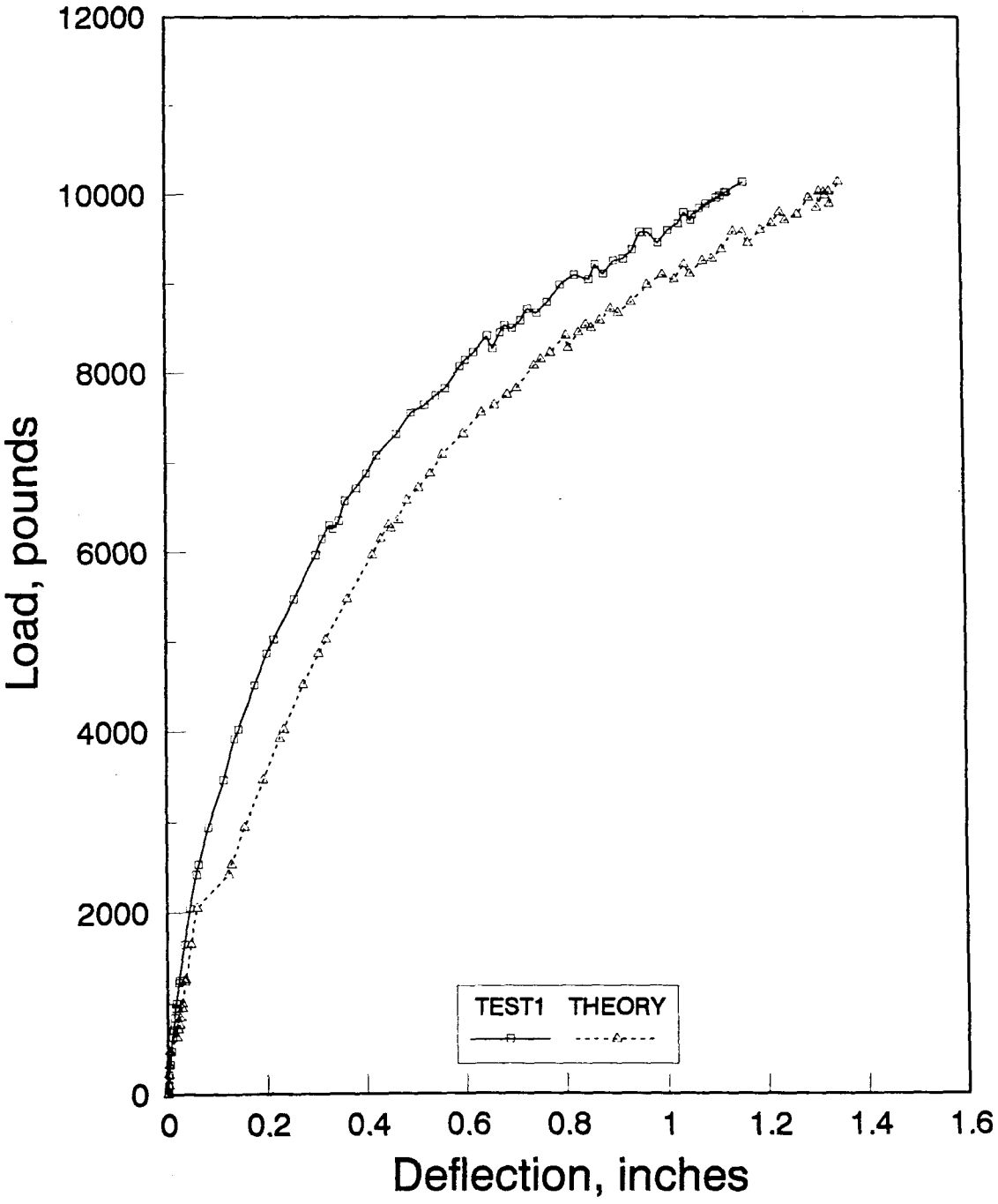

Figure A25. Comparison of approximated and experimental load-deflection curves for B-FC-P-S assembly

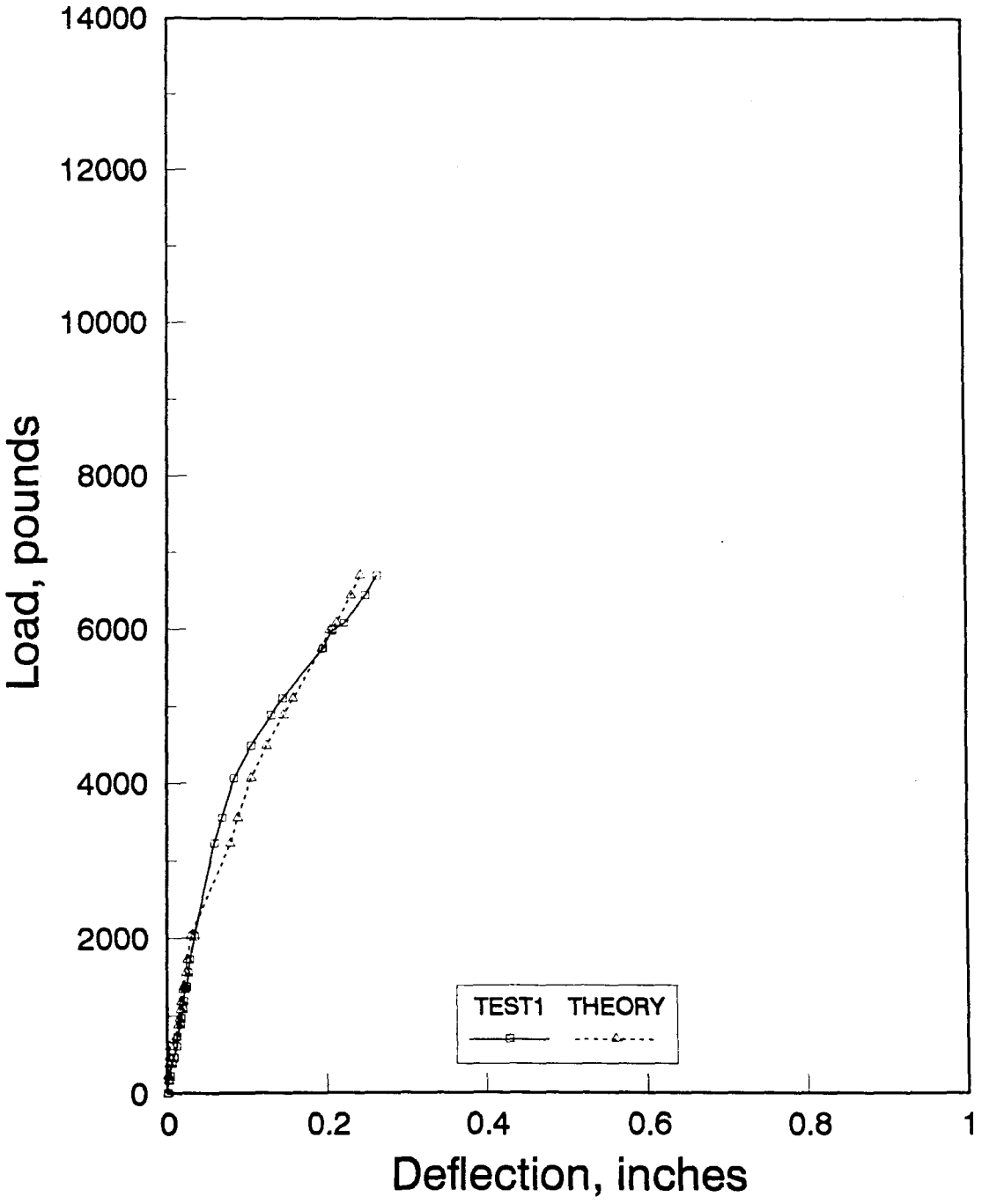

Figure A26. Comparison of approximated and experimental load-deflection curves for C-FC-P-W assembly

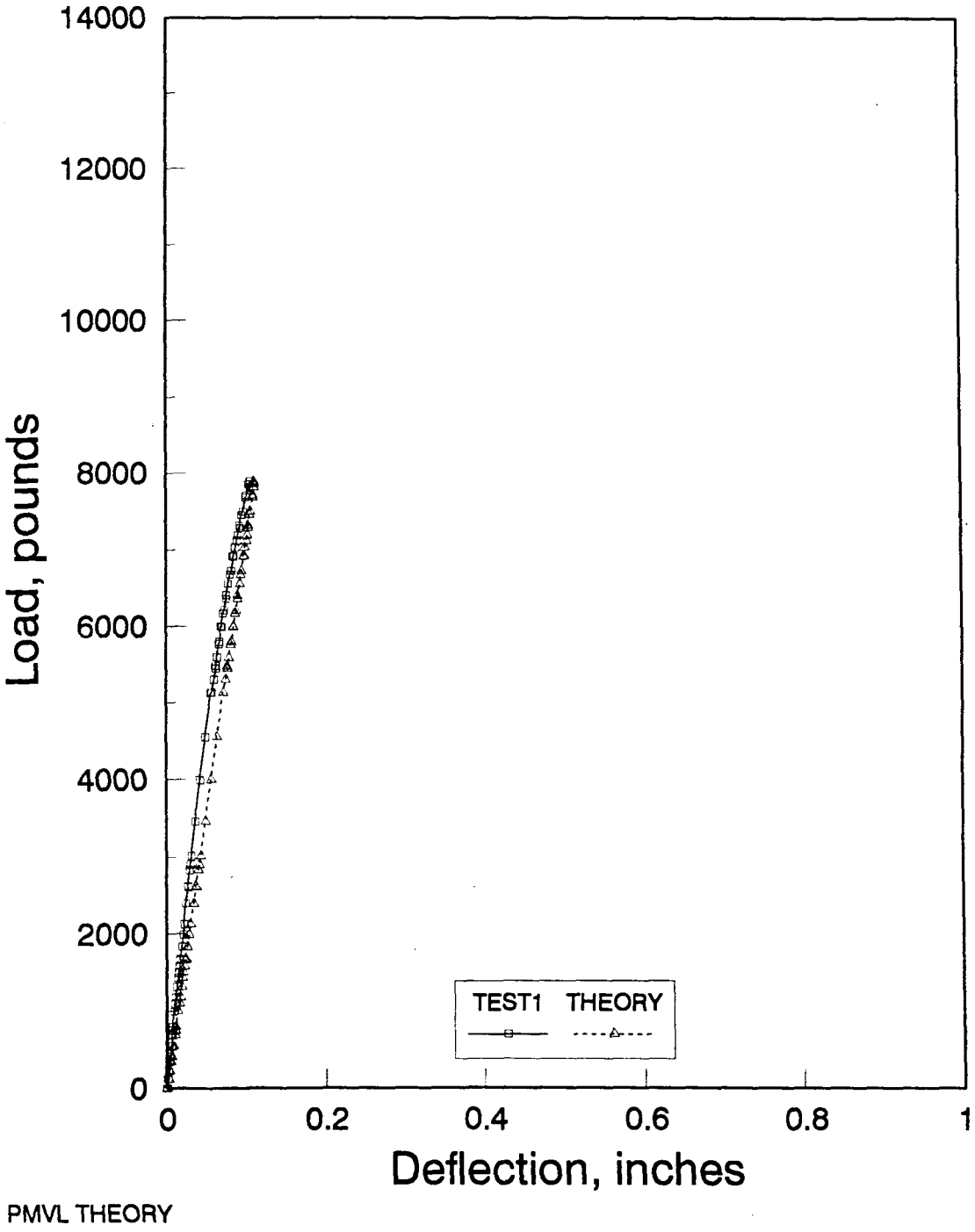

Figure A27. Comparison of approximated and experimental load-deflection curves for C-FC-P-L assembly

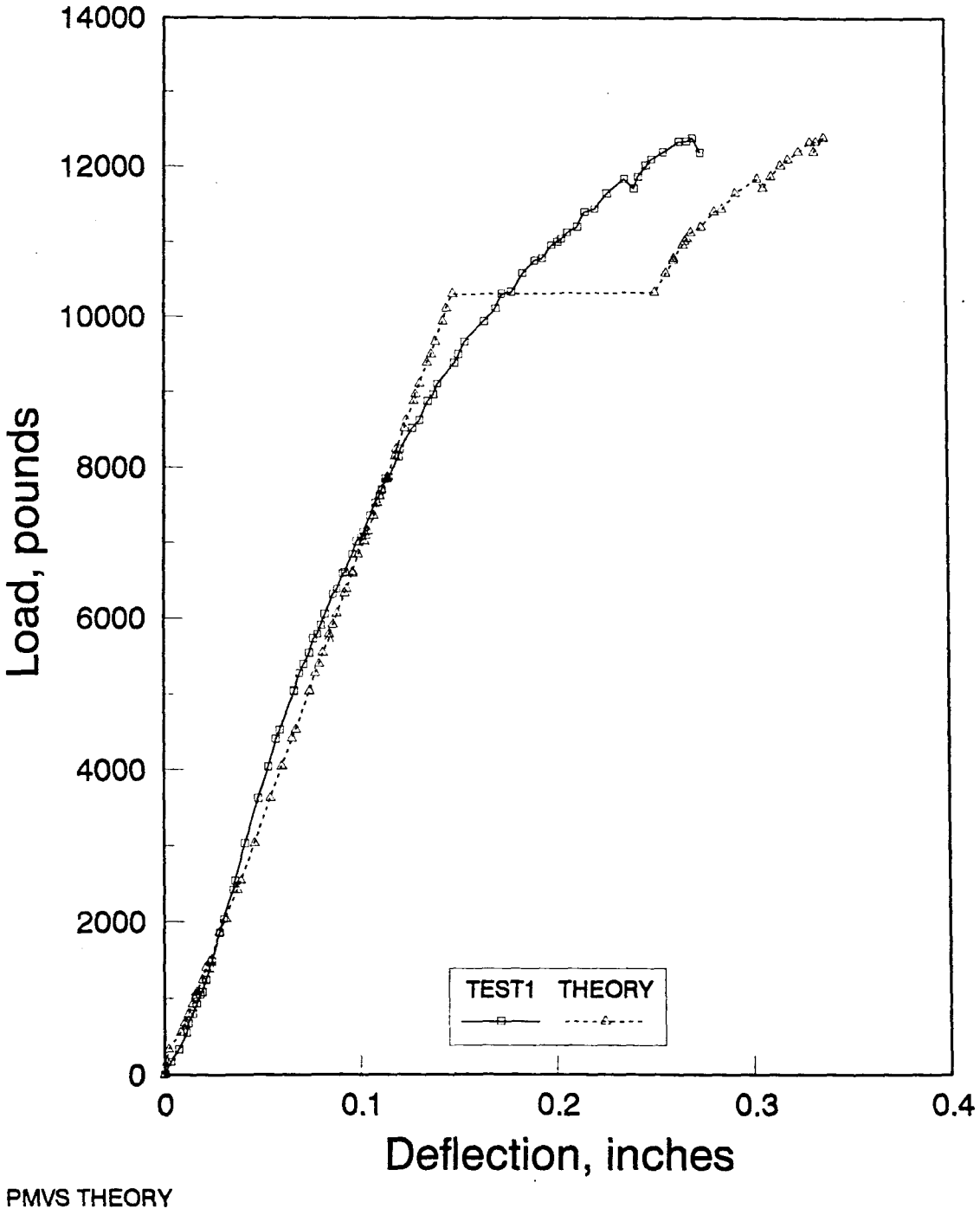

Figure A28. Comparison of approximated and experimental load-deflection curves for C-FC-P-S assembly